

ABSTRACT

Title of dissertation: QUANTUM OPTICS
IN OPTICAL NANOFIBERS

Pablo Andrés Solano Palma,
Doctor of Philosophy, 2017

Dissertation directed by: Professor Luis A. Orozco
Department of Physics

The study of atom-light interaction is a key element of quantum optics and a central part of atomic physics. Systems composed of atoms interacting with each other through the electromagnetic field can be used for studies from fundamental research to practical applications. Experimental realizations of these systems benefit from three distinct attributes: large atom-light coupling, trapping and control of atomic ensembles, and engineering and manipulation of the electromagnetic field. Optical waveguides provide a platform that achieves these three goals. In particular, optical nanofibers are an excellent candidate. They produce a high confinement of the electromagnetic field that improves atom-light coupling, guiding the field that mediates the interactions between atoms, while allowing trapping of the atoms close to it.

This thesis describes the uses of an optical nanofiber for quantum optics experiments, demonstrating its possibilities for enabling special atom-light interactions. We trap atoms near the optical nanofiber surface, and characterize the trap in a

non-destructive manner. We show how the presence of the nanofiber modifies the fundamental atomic property of spontaneous emission, by altering the electromagnetic environment of the atom. Finally, we use the nanofiber to prepare collective states of atoms around it. These states can radiate faster or slower than a single atom (superradiance and subradiance). The observation of subradiance of a few atoms, a rather elusive effect, evidences nanofibers as a strong candidate for future quantum optics experiments. Moreover, we show how the guided field mediates interaction between atoms hundreds of wavelengths apart, creating macroscopically delocalized collective states.

QUANTUM OPTICS IN OPTICAL NANOFIBERS

by

Pablo Andrés Solano Palma

Dissertation submitted to the Faculty of the Graduate School of the
University of Maryland, College Park in partial fulfillment
of the requirements for the degree of
Doctor of Philosophy
2017

Advisory Committee:

Professor Luis A. Orozco, Chair/Advisor
Professor Steven L. Rolston, Co-Advisor
Professor William D. Phillips
Professor Mohammad Hafezi
Professor Jeremy N. Munday
Professor Edo Waks

© Copyright by
Pablo A. Solano
2017

Acknowledgments

This work was supported by the National Science Foundation.

Table of Contents

1	Introduction	1
1.1	Cooperativity and optical density	2
1.2	Optical nanofiber platform	8
1.3	Cooperativity in an ONF	9
1.4	Optical density in a ONF mode	10
1.5	ONFs as interfaces for atom-light interaction	12
1.6	Outline of the thesis	14
2	Polarimetric Measurement of Trapped Atoms	16
2.1	Atomic dipole traps around an ONF	17
2.2	Transmission spectroscopy	20
2.3	Dispersive measurements	21
2.4	State-sensitive and state-insensitive traps	22
2.5	Possible heating mechanisms	25
2.6	Characterization of the trapping potential	25
2.7	Model of the atomic motion	31
3	Purcell effect of an ONF	34
3.1	Measuring the Purcell effect of ONFs	38
4	Atom-atom interaction mediated by an ONF	52
4.1	Infinite-range interactions	54
4.2	Self-Organization of atoms around an ONF	55
4.3	Single excitation collective states	55
4.4	Super- and sub-radiance mediated by an ONF	59
4.5	Comments on subradiance mediated by an ONF	68
5	Conclusions and outlook	71
A	Nanofiber electromagnetic modes	75
B	Other ONF Papers	83
	Bibliography	90

Chapter 1: Introduction

Quantum optics has followed a path to achieve the ideal limit of one single quantum of light, a photon, interacting with one single quantum of matter, an atom. The interest in this realization has theoretical and experimental implications that have illuminated and guided much of the contemporary discussion on quantum information.

The advent of cavity quantum electrodynamics (QED) [1], marked a transformative milestone in the study of atom-light interactions. Such interactions can be tailored by modifying the vacuum modes of the electromagnetic field, with cavities formed by mirrors, or other structures, while providing a preferential mode for the atom-light coupling. Cavity QED ushered in the ability to sufficiently isolate a quantum system from its environment and control nearly all of its degrees of freedom [2]. This has led, for instance, to the demonstration of the Purcell effect – increased or inhibited spontaneous emission rates [3] – and to the generation of highly nonclassical photon states [4], among other phenomena. Remarkably, these studies have been realized within many different regions of the electromagnetic spectrum, *e.g.* from the microwave [4, 5] to the optical domain [6, 7].

Motivated by the challenge of interconnecting quantum systems, recent ca-

pabilities for large coupling of atoms with propagating photons are opening a new line of research. This is possible through the use of optical waveguides that highly confine the propagating field in the transverse direction as an evanescent wave. The emerging field of waveguide QED applies the machinery of cavity QED to propagating modes in electromagnetic structures [8–11]. Our study of atom-light interactions is framed within this context. In this chapter we first introduce the concept of cooperativity from cavity-QED as the figure of merit for atom-light interaction. We then show how this concept can be extended to waveguide-QED, focusing on a particular kind of optical waveguide: optical nanofibers.

1.1 Cooperativity and optical density

Consider a two-level atom with dipole moment \vec{d} interacting with an electric field \vec{E} whose energy is equivalent to one photon. The parameter g gives the strength of the coupling in frequency units, numerically equivalent to half of the vacuum Rabi splitting [12],

$$g = \frac{\vec{d} \cdot \vec{E}}{\hbar}. \quad (1.1)$$

For an atom with spontaneous emission decay rate γ and a decay rate κ of the electric field in the cavity we define the single-atom cooperativity to be [2]

$$C_1 = \frac{g^2}{\kappa\gamma}. \quad (1.2)$$

A cooperativity of $C_1 > 1$ means that the rate that governs the interaction between the atom and the field mode is larger than the geometric mean of the atomic- and field-reservoir coupling rates. This places the system in the so-called strong

coupling regime, which was a longstanding goal within the quantum optics community that has been achieved in several systems, such as trapped ions [13], Rydberg atoms in microwave cavities [4], neutral atoms in optical cavities [6], artificial atoms such as quantum dots that give rise to excitons in semiconductor microcavities [14], optomechanical systems [15] and superconducting circuits in planar waveguides [16].

The cooperativity of a system with many atoms interacting through the same preferential electromagnetic mode scales with the number of atoms [2]

$$C = NC_1. \quad (1.3)$$

Even if the single atom cooperativity is smaller than one, for enough atoms, the coupling of the system to the mode can be larger than the coupling into the reservoir ($C > 1$).

To better understand how one can coerce a system into the strong coupling regime where a single mode of the electromagnetic field and one atom preferentially exchange an excitation, it can be useful to relate the cooperativity to the optical density (*OD*). This way of thinking comes from a predecessor of cavity QED, optical bistability [17], which is part of the more general area of dissipative systems in quantum optics [18]. We illustrate the argument by considering a high-finesse Fabry-Perot cavity with two mirrors of transmission T separated by a length L , so that its full width at half maximum (FWHM) is 2κ , with $\kappa = cT/2L$ as a frequency half-width. The electric field amplitude for a field with an energy of a single photon within this mode is given by

$$E = \sqrt{\frac{\hbar\omega}{2\varepsilon_0 V}}, \quad (1.4)$$

defining the mode volume as $V = A_{\text{mode}} \times L$. A_{mode} is the effective mode area, defined at the position of the atom (x_0, y_0) , and is given by the area that the mode would occupy if it had a constant transverse intensity profile, *i.e.*

$$\frac{c\varepsilon_0}{2} \int dA |E(x, y)|^2 = A_{\text{mode}}(x_0, y_0) I(x_0, y_0) = P, \quad (1.5)$$

where I is the electromagnetic wave intensity and P is the total optical power.

We know that the free-space decay rate of the atom in three dimensions is

$$\gamma_0 = \frac{4\omega^3}{3c^2} \frac{d^2}{4\pi\varepsilon_0\hbar c}, \quad (1.6)$$

where d is the magnitude of the dipole moment of the atom and $\omega = 2\pi c/\lambda$ is the resonant angular frequency of the decay transition associated with the wavelength λ . Typical values of d for the D2 line of alkali atoms are about $5a_0e$, where a_0 is the Bohr radius and e the electron charge [19]. Combining Eqs. (1.4) and (1.6) into Eq. (1.2) yields a single-atom cooperativity of [20]

$$C_1 = \frac{A_{\text{atom}}}{A_{\text{mode}}} \frac{1}{T}. \quad (1.7)$$

Here we have defined the “area” of the atom, A_{atom} , to be the resonant scattering cross section

$$\sigma_0 = 3\lambda^2/2\pi. \quad (1.8)$$

This motivates a geometric framework to think about the cooperativity by realizing that the *OD* for a dipole transition is:

$$OD = \frac{A_{\text{atom}}}{A_{\text{mode}}}. \quad (1.9)$$

We conclude from Eq. (1.7) that C_1 is just the product of the optical density of a single atom times the factor $1/T$, related to the cavity enhancement or finesse $F \approx \pi/T$ for $T \ll 1$.

Equation (1.7) states that the cooperativity is independent of the atomic dipole moment and the cavity length L , but depends on the ratio of the two “areas”. See Ref.[18] for a discussion not only of resonance fluorescence, but also optical bistability and superradiance and their connection through the idea of cooperativity. Efforts to increase this figure of merit have followed a few different paths, as we describe next.

For certain processes with N atoms, the total cooperativity, $C = C_1 N$, is important. Increasing N achieves an appropriate threshold of the system, *e.g.* vapor cells with high atomic densities facilitate the observation of coherent processes such as electromagnetically induced transparency (EIT) [21].

The Nobel Prize-worthy efforts of Serge Haroche focused on decreasing T with microwave cavities possessing finesse greater than 10^9 while making sure that the cavity-mode cross section significantly overlaps with the radiation pattern of the Rydberg atom capturing most of the emitted light. With this system, his group created highly nonclassical states of light and performed quantum non-demolition measurements of photon jumps [4].

Recent advances in superconducting technology have allowed the creation of nonlinear quantum circuits that behave like “artificial atoms” [22]. By coupling these effective two-level atoms to a high-quality-factor coplanar resonator, scientists have engineered an analog of cavity QED, dubbed circuit QED, that achieves couplings

far beyond what has been realized in optical systems [5, 16]. This architecture not only relies on the high finesse of the cavity to increase C , but the area of the artificial atoms (antennae, qubits) has also been increased significantly beyond that of the mode. This limit can not yet be realized with atoms in free space, but may be achievable for atoms near photonic and plasmonic structures, where the field can be confined beyond the diffraction limit.

Finally, we mention recent efforts made by some groups that have moved away from the use of a traditional cavity altogether, trying to increase the cooperativity of an atom in free space, *i.e.* $1/T = 1$ in Eq. (1.7). There are groups that use high-NA optical systems to focus light to a small spot and achieve high coupling in free space [23–25]. Another possibility is to use a parabolic mirror that focuses a laser such that the focused beam has the same structure as the dipole radiation pattern of a single atom, thereby increasing the ratio of the atomic area to the mode area [26–28].

We will consider here the coupling of atoms to one kind of nanophotonic waveguide: optical nanofibers. Nanophotonic waveguides are not like the traditional optical cavities with high finesse discussed above, but they do modify the vacuum mode structure in a nontrivial way. As a result of this modification and the appreciable increase in the ratio between the atomic and optical areas, one can appreciably couple an atom to the electric field of a photon in a single pass. In fact, there is an active area of research studying waveguides constructed via nanofabrication techniques, whose mode produces a large OD for a single atom [29–32]. Important advances have happened, for example, with hollow-core fibers: encasing

an atomic vapor in the hollow core of a photonic-crystal fiber to confine atoms and photons in the waveguide increases C , but the manipulation of the atoms is not as straightforward as if they are outside the photonic structure [33–36]. Optical nanofibers (ONFs) formed by thinning single-mode optical fibers to sub-wavelength diameters, as shown in Fig. 1.1 (not to scale), are another example of this kind of structure. It has been demonstrated that ONFs provide an excellent platform to interface trapped atoms to the evanescent field of the mode around the nanometer-size waist-region [37–42]. Next we review the platform of ONFs with atoms and its implications and applications for quantum physics.

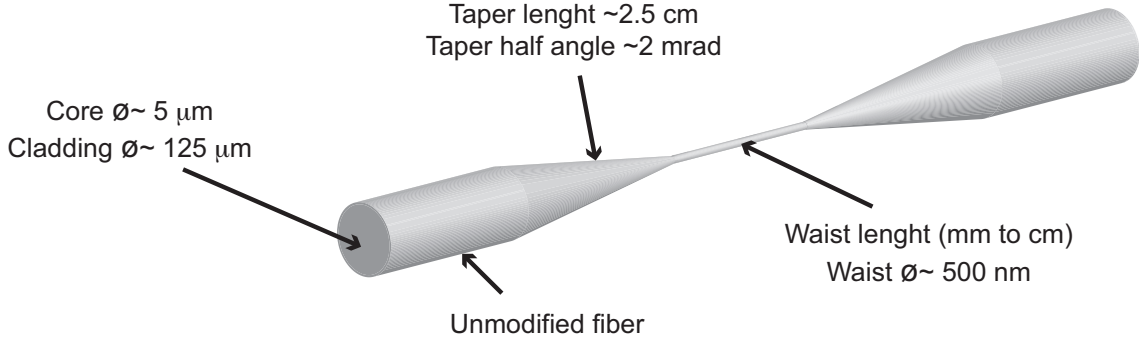


Figure 1.1: Schematic of an optical nanofiber where the transverse dimension has been greatly expanded compared to the longitudinal one. There are three distinctive sections of the ONF and the typical values are those used in our experiments. Atoms around the waist region, either free or trapped, can evanescently couple to the ONF guided mode. Fig. from Ref. [43]

1.2 Optical nanofiber platform

Before embarking on a thorough discussion of the nanofiber platform it is important to point out some advantages over other nanophotonic structures.

Nanofibers can be produced in-house, using a heat-and-pull method [44, 45]. The glass ability to flow ensures low surface roughness. The smoothness of the surface is a great asset since it leads to ultra-high transmission structures that can withstand high optical powers (almost one Watt in vacuum [44]) without damage to the fiber or degradation of the transmission.

ONFs also show great versatility in terms of connectivity to other systems. The advanced state of fiber optic technology is an enormous advantage to pursuing quantum information devices on this platform as they facilitate the interaction and communication among modular devices [46].

Moreover, ONFs have been proposed as a platform for hybrid quantum systems, with increasing importance in quantum optics and quantum information [47, 48]. The proposals rely on trapped atoms around an ONF, coupled through their magnetic dipole to a superconducting circuit in a cryogenic environment [49–51].

One of the most fascinating recent developments is the use of ONFs in quantum optics for the study of chiral quantum optics [52] and its connections with many-body physics. ONFs indeed provide a unique platform to study this nascent area.

Nanofibers are not without difficulties and challenges, the main ones being a consequence of the polarization structure of the modes and its limited control along

the waist length. However it has not been a major drawback for experiments. Also, the values of atom coupling to the nanofiber currently do not reach those recently seen in nanophotonic devices [31, 32, 53], but the entire parameter space on traps has yet to be explored, and improvements may be possible.

1.3 Cooperativity in an ONF

We now present, following closely the discussion in [54] related to waveguide QED with atoms, the connections between emission enhancement, coupling efficiency, cooperativity, and the Purcell factor. These quantities characterize in complementary ways the coupling between the nanofiber mode and a nearby atomic dipole.

The emission “enhancement” parameter α :

$$\alpha = \frac{\gamma_{1D}}{\gamma_0} \quad (1.10)$$

is the ratio between the emission rate into the quasi one-dimensional (1D) mode of the nanofiber in both possible directions combined, γ_{1D} , and the intrinsic spontaneous emission rate γ_0 of an atom in free space (see Eq. (1.6)).

The waveguide coupling efficiency β :

$$\beta = \frac{\gamma_{1D}}{\gamma_{tot}} \quad (1.11)$$

is the ratio between the emission rate into the waveguide mode in both directions combined and total emission rate into all radiative channels γ_{tot} .

The parameter α is proportional to the interaction rate of the atom and the guided mode, while β quantifies the fraction of the total rate that couples to that

mode. As an example to illustrate the two concepts consider an atom in a cavity with dimensions less than $\lambda/2$. The system has $\alpha = 0$ and $\beta = 1$, implying that there will be no decay signal despite $\beta = 1$.

The single-atom cooperativity in terms of these parameters is

$$C_1 = \frac{\beta}{(1 - \beta)} = \frac{\gamma_{1D}}{\gamma_{\text{tot}} - \gamma_{1D}}. \quad (1.12)$$

This expression relates the parameter β , often used in the microcavity literature [55], to C_1 and thus to what we have presented in Sec. 1.1. The quantity $(\gamma_{\text{tot}} - \gamma_{1D})/\gamma_{\text{tot}}$ is sometimes referred as the fraction of the decay radiated outside the ONF mode $\gamma_{\text{rad}}/\gamma_{\text{tot}}$. The meaning of Eq. (1.12) in terms of rates is equivalent to Eq. (1.2) in the sense that C_1 is the ratio of the rate of interaction between atom and field mode to the interaction to other reservoirs.

The Purcell factor, or modification of spontaneous emission, is given by the emission enhancement over the coupling efficiency

$$F_p = \frac{\alpha}{\beta} = \frac{\gamma_{\text{tot}}}{\gamma_0}. \quad (1.13)$$

A Purcell factor bigger (smaller) than one, means that the atomic spontaneous emission is enhanced (inhibited) due to the boundary condition imposed by the waveguide.

1.4 Optical density in a ONF mode

The optical density of an atomic sample in the ONF mode can be related to the spontaneous emission decay rates, in the same manner as we did with the

cooperativity in the previous section. In order to do so, we need to know first the atomic decay rate into a one-dimensional waveguide, often written as [54, 56]

$$\gamma_{1D} = \frac{4L}{v_g} g^2, \quad (1.14)$$

where L is the length of the waveguide, v_g the group velocity of the propagating mode, and g is given by Eq. (1.1). In the spirit of Fermi's golden rule, the term $4L/v_g$ comes from the density of modes where the excitation decays and g^2 comes from the atom-field coupling strength.

This equation can be written more explicitly for a infinite waveguide (independent of L) as

$$\gamma_{1D}(\vec{r}) = n_{\text{eff}} \frac{2}{\epsilon_0 \hbar} \frac{\omega}{c} \frac{d^2}{A_{\text{mode}}(\vec{r})}. \quad (1.15)$$

where n_{eff} is the effective group index of refraction of the propagating mode. We have made the equation an explicit function of the atom position \vec{r} . For a mode with a non-uniform electric field, the mode area depends on the local intensity $I(\vec{r})$ as $A_{\text{mode}}(\vec{r}) = P/I(\vec{r})$, where P is the total optical power in the mode, as defined in Eq. (1.5). For an ONF this can be calculated from the mode structure shown in Appendix A.

The ratio between the decay rate into the guided mode (see Eq. (1.15)) and the decay rate of an atom in free-space (see Eq. (1.6)) gives us the emission enhancement, which after simplification is written as

$$\alpha(\vec{r}) = n_{\text{eff}} \frac{A_{\text{atom}}}{A_{\text{mode}}(\vec{r})}, \quad (1.16)$$

where A_{atom} is the on-resonance atomic cross section in free space (see Eq. 1.8).

The effective mode area captures the modification of the vacuum electric field due to the presence of the ONF. This allows us to relate the enhancement parameter to a purely geometrical expression consisting of the ratio of two areas, the atomic cross section and the mode area. The optical density from Eq. (1.9) is then related to the spontaneous emission enhancement parameter by the effective group index of refraction of the waveguide as

$$\alpha(\vec{r}) = n_{\text{eff}} OD(\vec{r}). \quad (1.17)$$

This equation can be interpreted from a classical point of view. The enhancement parameter, given by the modification of the atomic decay rate, is related to the electromagnetic energy stored at the position of the atom. On the other hand, the optical density is related to the flux of electromagnetic energy that propagates through the waveguide and is being blocked by an object of cross section σ_0 . From classical electrodynamics we know that the electromagnetic energy stored and energy flux are related by the group velocity [57], proportional to the index of refraction of the medium. Another way to see this is noticing that the process of photon emission, related to α , is the time reversal of the absorption, related to OD . The difference between both processes is given by the density of states where the excitation ends, which increases with n_{eff} . This illuminates the physical intuition behind Eq. (1.17).

1.5 ONFs as interfaces for atom-light interaction

Fiber optics in present day telecommunications have been a game-changing technology allowing enormous bandwidth for current and future uses. It began with

the pioneering observation of the low-loss properties of glass fibers in [58]. This was recognized with the 2009 Nobel Prize awarded to Charles K. Kao. (See [59]).

More recently, ONFs have seen widespread use in science and engineering [60–62]. The tight confinement of light around ONFs [63], unique geometries provided by the fiber modes [64–66], low loss, and promise of improved atom-light interaction [37, 38, 67–69] have led to increased interest in the physics community. Optical micro- or nano-fibers are used for sensing and detection [70, 71], and coupling light to resonators [70, 72–76], NV centers [77], or photonic crystals [29, 78].

Reducing the thickness of an optical fiber to sub-wavelength diameters [79] modifies the boundary conditions of the field so that a significant fraction of the light propagates in an evanescent field outside the nanofiber. Nanofibers thus provide an excellent platform to interface light with atoms.

To confine atoms along the nanofiber, one can couple laser beams into the fiber to create an optical dipole potential around it [65]. Optical dipole trapping of atoms is a well-developed technique applied to numerous atomic species [80]. Typical trapping schemes allow trap depths of fractions of a miliKelvin located a few hundred nanometers from the fiber ([37–42]). Trapping lifetimes of tens of milliseconds and atomic ground state coherence times of $\sim 600 \mu\text{s}$ [81] have been obtained and formation of a one-dimensional lattice along the nanofiber waist has also been demonstrated [37]. In this regime, the *OD* per atom is as large as a few percent, so that a modest atom number can achieve large optical thicknesses. This confirms that ONFs are a viable platform for studying the physics of light-matter interactions, as they enable high optical density and cooperativity.

1.6 Outline of the thesis

Here I present some of the most recent works developed at the JQI and University of Maryland regarding ONFs as enablers of atom-light interactions. I focus particularly on three studies presented in three chapters, in which I was the principal experimentalist and led great part of the theoretical calculations and interpretations. Each study has culminated in an article that is included as part of the chapter. The articles are submitted or near submitted at this point (April 2017).

Chapter 2 presents the basic aspects of an ONF dipole trap. We explore the implementation of a non-destructive technique to characterize the trapping potential. We use a propagating probe beam that changes its polarization when dispersively couples to trapped atoms. The trapping frequencies can be observed through polarimetric measurements of the probe beam as a function of time. This technique could be part of a toolbox for the characterization and control of trapped atoms coupled to waveguides.

Chapter 3 discusses the effects of an ONF on a single atom close to its surface. In particular, we focused on the modification of the spontaneous emission rate of the atom, *i.e.* the Purcell effect. In particular, the atomic lifetime depends on the state in which the atoms are prepared. We perform measurements of this effect and present a theoretical model to capture some of the complex aspects of this fundamental problem.

Finally, in Chap. 4 we present ONFs as a platform that allows infinite-range interaction among distant atoms. The guided mode of the nanofiber acts as a bus

for the interaction-mediating electromagnetic field. We focus on the preparation of collective states, observing superradiant behavior of a few atoms separated by hundreds of resonant wavelengths. We also discuss how an ONF enables the excitation and detection of subradiant states, a challenging task in quantum optics.

Conclusions and outlooks are presented in Sec. 5.

Chapter 2: Polarimetric Measurement of Trapped Atoms

The evanescent field of the guided modes of an ONF provides an intensity gradient suitable for generating an optical dipole trap [80]. All current experimental realizations use two lasers in the fundamental HE_{11} guided mode [37] (see Appendix A for the mode structure). A laser red-detuned from resonance creates an attractive potential, while a blue-detuned one creates a repulsive potential preventing the atoms from sticking to the nanofiber surface. The characteristic decay length of both evanescent fields is proportional to their effective wavelengths (see Eq. (A.22) in Appendix A), producing a longer (shorter) range attractive (repulsive) potential for the red- (blue-) detuned beam. By adjusting their relative intensities it is possible to find a configuration where there is a minimum of the dipole potential away from the ONF surface, achieving trap depths of a few hundreds of microkelvins. Longitudinal confinement of the trapped atoms can be implemented by counterpropagating two red detuned beams, creating a standing wave. Stable traps can be created for different trapping beam polarizations and intensities, generating different azimuthal confinements.

The gradient of the transversal component of the guided field is always on the order of $2\pi/\lambda$, creating a non-negligible longitudinal component of the electric field

(as explained in Appendix A). Longitudinal polarizations are generally not the case for trapping beams propagating in free space, unless they are tightly focused. The phase relation between the transverse and the longitudinal component of the guided field creates elliptically polarized light, introducing significant vector light shifts in the trapped atoms [65]. Differential light shifts induced among atomic sub-levels can be suppressed with a proper choice of trapping wavelengths and polarizations [82] or they can be used as a tool for atomic state preparation [83].

These types of trapping schemes are a promising platform for integrating laser-cooled atomic ensembles with optical fibers, opening a route towards applications in the context of quantum information and quantum technologies.

2.1 Atomic dipole traps around an ONF

We now summarize how our ONF trap operates [40, 84] (see Fig. 2.1). The ONF has a waist diameter of approximately 500 nm and length of 7 mm, with tapering regions of 28 mm in length and 2 mrad half angle. A MOT loaded from a background vapor of ^{87}Rb produces a cloud of $\sim 10^8$ atoms. We overlap the cloud with the ONF waist using magnetic field shim coils and a ultra-high-vacuum mechanical manipulator. Two orthogonal imaging systems ensure the overlap between the atomic cloud and the ONF. In our experimental cycle we do 90 ms of increased MOT detuning and a 1-ms-duration optical molasses stage, cooling the atoms to $\sim 15 \mu\text{K}$. The red- and blue-detuned trap beams are on throughout the experiment. As a result of dissipation from laser cooling, some of the atoms end up in the

ONF dipole trap. For more details about the experimental setup see Ref. [43].

An ONF trap requires light that is tuned to the red of the resonant frequency (with respect to the 780 nm ^{87}Rb D2 line) to provide an attractive potential and light tuned blue of resonance to prevent atoms from striking the ONF surface (see Fig. 2.1). A 1064-nm wavelength laser beam provides the (red) attractive potential and a 750-nm wavelength beam the (blue) repulsive force. A potential minimum of a few hundred μK in depth is formed at ~ 200 nm from the fiber surface, as calculated with a simple two level atom and only scalar shifts (see Fig. 2.1 (e)).

Counter-propagating the red-detuned attractive beams, generating a standing wave, confines the atoms along the nanofiber. This configuration creates a one-dimensional lattice on each side of the ONF. The presence of a longitudinal component of the propagating electric field prevents us from having a standing wave with perfect contrast. The periodicity of the lattice is given by half the effective wavelength λ/n_{eff} . The contrast varies for different wavelengths and ONF radius, and in our case is $\sim 65\%$. However, this is not an impediment for trapping the atoms in a lattice configuration.

The azimuthal confinement of the trapped atoms is achieved by using quasi-linearly polarized trapping beams in the HE_{11} mode. A quasi-linearly polarized mode is the result of linearly polarized light propagating through the ONF, which electric field has components in all three direction due to its large spatial gradient (see appendix A). The intensity profile of a quasi-linearly polarized mode is azimuthally asymmetric, providing a tool for azimuthal confinement of the atoms (see Fig. 2.1 (c and d)).

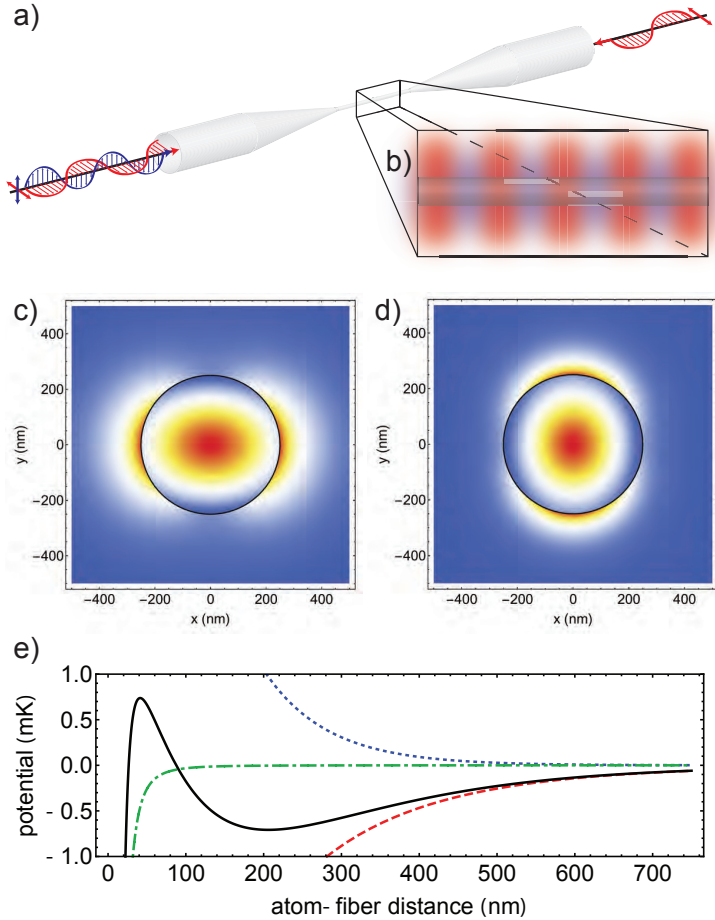


Figure 2.1: (a) Schematic of an ONF with counter-propagating 1064-nm beams and an orthogonally-polarized 750-nm beam. (b) Illustration of the intensity of the fields at the ONF waist with lattice formed by 1064-nm beams. (c) Intensity plot of quasi-horizontally-polarized 1064-nm light in an ONF with diameter 500 nm. The color scale indicates increasing intensity from blue to red. (d) Intensity profile of quasi-vertically-polarized 750-nm light through the same ONF. (e) Total trapping potential (black solid) for a 500-nm diameter ONF with contributions from 3 mW in each 1064-nm beam (red dashed), 6.5 mW of 750-nm power (blue dotted), and van der Waals (green dashed and dotted). Fig. from Ref. [43]

These operation parameters allow only zero or one atoms on each independent well because of collisional blockade [85], creating on average a filling factor of 50%. There is no particular requirement for the relative polarization of the blue and red detuned beams. A trapping minimum can be generated for polarizations varying from parallel [38] to perpendicular [37, 86], provided one uses the proper optical powers of the trapping beams. Due to intrinsic stress in the ONF from the fabrication process that produces birefringence, the light polarization at the input of the un-tapered fiber is not the same as in the nanofiber region. We overcome this issue by independently verifying the polarization of each beam at the nanofiber waist and adjusting the input polarization accordingly. We take polarization-sensitive measurements of the Rayleigh scattering of the propagating beams at the ONF waist through a high quality microscope objective positioned above the vacuum chamber where the nanofiber resides.

The number of trapped atoms in an ONF two-color dipole trap can be measured by propagating a probe beam through the nanofiber. Possible strategies are based on transmission spectroscopy and off-resonance dispersive measurements [87], as described below.

2.2 Transmission spectroscopy

Transmission spectroscopy is based on the Beer-Lambert-Bouguer law for optical absorption in a thick medium and on the knowledge of the atomic spectral lineshape. By scanning the frequency of a weak near-resonance probe beam and

measuring its transmission as a function of frequency, we can obtain the optical density of the sample [88]. If the atom-light coupling strength is known, the OD can be translated to a number of trapped atoms [37, 38, 40, 86]. When implemented for an ONF the probe power is typically of the order pW, to avoid saturation of the atoms and power broadening. The transmitted photons are counted with avalanche photodiodes and appropriate electronics. A careful bandwidth filtering is necessary to filter the background from the blue detuned laser and what appears to be fluorescence of the fiber.

This method of measuring the number of trapped atoms is a rather destructive one. The absorbed photon transfers a momentum kick to the atoms. After repeated scattering events, the atoms heat up, and eventually leave the trap.

2.3 Dispersive measurements

A less destructive atom-number measurement is to send an off-resonance probe beam through the ONF. The dispersive atom-light interaction creates an effective modification of the refractive index experienced by the propagating field, minimally altering the atomic state. The tight mode confinement provides a large atom-light nonlinear interaction and efficient readout. The main features of this technique have been explored theoretically in detail, proposing it as a tool for quantum non-demolition measurements [89]. The dispersive atom-light interaction produces a phase shift in the propagating field, proportional to the number of atoms and the atom-light coupling strength. This phase shift can be read out with polarimetric

[84, 90] and interferometric measurements [39].

The polarimetric measurement relies on the azimuthally asymmetric geometry of the trap. An ensemble of trapped atoms at each side of the ONF defines a preferential propagation axis for the evanescent field of an off-resonant quasi-linearly polarized probe beam. The atoms create an effective birefringence for the probe [90].

An interferometric measurement of the probe beam can be performed by two probe beams detuned by the same frequency above and below resonance [39]. This eliminates any possibility of modification of the potential landscape experienced by the trapped atoms. Because the sign of the phase shift depends on which side of the resonant frequency the probe is, both probe beams experience equal-magnitude but opposite-sign phase shifts. The differential phase shift between the two probes can be measured using optical homodyne interferometry, allowing the measurement of the number of trapped atoms.

2.4 State-sensitive and state-insensitive traps

When a two-level atom interacts with an oscillating electric field, *e.g.* a dipole trap, the two energy levels shift in opposite directions, an effect known as the ac-Stark shift. If the field is red-detuned from the atomic resonance, the ground state shifts down in energy and the excited state shifts up; the opposite is true for a blue-detuned optical beam. When the shift only depends on the total amplitude of the electric field it is called a scalar light shift, and when it depends on ellipticity of the field polarization it is called vector light shift. In a dipole trap, the scalar shift shifts

the atomic energy levels, causing different electronic states to experience different trapping potentials. When the dipole trap is produced by circularly polarized light the polarization of the electric field couples to the components of the angular momentum of the real (multilevel) atom, shifting also the Zeeman sub-levels, similar to what happens to the atoms in the presence of an external magnetic field. Both effects, scalar and vector light shift, create state-dependent potentials that present difficulties for coherent control of atoms, coupling the internal states to the noisier center-of-mass motion.

The scalar shift that the first excited atomic state experiences due to its coupling with the ground states can be counteracted in a multilevel-atom by an opposite shift due to its coupling with higher-excited states. The wavelength of light that creates the same shift for the ground and excited atomic states is called a magic wavelength. The idea of magic wavelengths, originally stated in the context of a possible systematic effect in precision measurements [91], shows that in a dipole trap the ground and excited electronic states of an atom can experience the same trapping potential, permitting coherent control of electronic transitions independent of the atomic center-of-mass motion [92, 93].

Vector light shifts are not present when using only linearly polarized light. However, ONF-based dipole traps use elliptically-polarized light along the nanofiber, due to the significant longitudinal component of the propagating field. Vector light shifts can still be highly suppressed by canceling the longitudinal component of the electric field, using equal intensities and polarizations for the counter-propagating trapping beams. A frequency difference between blue-detuned counter-propagating

beams creates a “walking wave” that averages to produce a uniform repulsive potential. These methods for implementing a (mostly) state-insensitive dipole trap in an ONF are proposed in Ref. [94] and first implemented in Refs. [38, 82, 95], where they trap Cs atoms 215 nm from the surface of a nanofiber, and suppress the differential scalar and vector light shifts by a factor of 250.

State-sensitive traps, which lift the degeneracy of the atomic Zeeman sublevels, can be used for state preparation and interrogation of trapped atoms. For these applications, the vector light shift in ONF-based dipole trap can be particularly useful [83, 96]. Applying additional real or fictitious magnetic fields, the state dependence of the trapping potential can be controlled, providing a mean to probe and to manipulate the motional state of the atoms in the trap by driving transitions between Zeeman sub-levels. Another possible application is to use the fictitious magnetic field induced by a nanofiber-guided light field in conjunction with an external magnetic bias field to create an effective trapping potential for atoms around the ONF [97].

Despite the difficulties that state-dependent trapping potentials impose on the coherent control of arbitrary atomic states, ground states can keep coherences for times suitable for some quantum information applications. In particular, Ref. [81] studies the ground state coherence properties of Cs atoms in a nanofiber-based two-color dipole trap. Using microwave radiation to coherently drive the clock transition ($|e\rangle = |6S_{1/2}, F = 4, m_F = 0\rangle \rightarrow |g\rangle = |6S_{1/2}, F = 3, m_F = 0\rangle$), they record Ramsey fringes as well as spin echo signals and infer a reversible dephasing time of $T_2^* = 0.6$ ms and an irreversible dephasing time of $T_2' = 3.7$ ms. Both time constants are

limited by the finite initial temperature of the atomic ensemble and the heating rate, respectively.

2.5 Possible heating mechanisms

Atoms trapped around an ONF eventually leave the trap. The heating mechanisms that lead the atoms to escape have not been fully determined. One contribution comes from elastic scattering events of the far-detuned trapping beams [80], a well-known effect in dipole traps. A less familiar contribution comes from torsional modes of the ONF [98]. Torsional modes produce stress-induced birefringence in the ONF, which couples to the polarization of all the guided fields. Since the trapping potential is sensitive to the polarization of the trapping beam, the torsional modes create a time-dependent perturbation of the potential. The frequencies of these modes are closely spaced and they are close enough to the trapping frequencies (~ 200 kHz) to consider parametric heating of the atoms as particularly strong mechanisms for losses. Torsional modes have been measured and characterized [98], and even optically excited [99, 100]. However, it is necessary to suppress them or increase their frequencies to prevent the heating of the atoms.

2.6 Characterization of the trapping potential

Experiments based on the type of dipole trap described above can benefit from a non-destructive characterization of the local potential felt by the atoms, leaving them trapped after interrogation for further experimentation. We hope that

direct and non-destructive measurements of trapping potentials grow into a standard procedure for atom traps near optical waveguides. Next, we present our work on non-destructive measurement of the ONF trapping potential, using dispersive measurement of trapped atoms.

Dynamics of trapped atoms around an optical nanofiber probed through polarimetry

PABLO SOLANO^{1,*}, FREDRIK K. FATEMI², LUIS A. OROZCO¹, AND S. L. ROLSTON¹

¹Joint Quantum Institute, Department of Physics, University of Maryland and NIST, College Park, MD 20742, USA.

²Army Research Laboratory, Adelphi, MD 20783, USA.

* Corresponding author: solano.pablo.a@gmail.com

Compiled March 16, 2017

The evanescent field outside an optical nanofiber (ONF) can create optical traps for neutral atoms. We present a non-destructive method to characterize such trapping potentials. An off-resonance linearly polarized probe beam that propagates through the ONF experiences a slow axis of polarization produced by trapped atoms on opposite sides along the ONF. The transverse atomic motion is imprinted in the probe polarization through the changing atomic index of refraction. We measure a time-dependent polarization rotation of the probe beam, allowing direct non-destructive measurement of the optical trapping frequencies. © 2017 Optical Society of America

OCIS codes: (020.7010) Laser trapping; (060.2310) Fiber optics; (060.2840) Heterodyne; (350.4238) Nanophotonics and photonic crystals

<http://dx.doi.org/10.1364/ao.XX.XXXXXX>

Nano-optical waveguides allow efficient ways to couple trapped atoms to propagating photons, a crucial element in the development of quantum technologies [1–4]. Optical nanofibers (ONF) [5] have shown to be a particularly versatile platform in this context; enabling quantum memories [6–9], switches [10, 11], diodes [12], and reflectors [13, 14]. These examples show integration of photonic and atomic systems.

An ONF consists of single-mode optical fiber heated and pulled to create a tapered profile. The tapers can adiabatically guide the propagating light in and out of a sub-wavelength diameter waist with less than 0.1% loss [15]. Because the nanofiber radius is smaller than the wavelength of the propagating mode, most of the field is outside its dielectric body as an evanescent field [16]. This field allows coupling of atoms near the ONF surface to the guided mode. The tight confinement of the propagating mode enables significant atom-light coupling.

The large spatial gradient of the evanescent field enables an optical dipole trap for atoms with two different wavelengths of light, one detuned above atomic resonance (blue-detuned) to repel the atoms from the surface, and the other detuned below resonance (red-detuned) for confinement. Such traps are an effective tool to confine atoms close to the ONF waveguide for millisecond time-scales with low optical powers, creating a robust platform for coupling propagating photons to atoms [17–21].

A typical ONF dipole trap, with retro-reflection of the red-detuned light, creates two one-dimensional arrays of atoms on each side of the ONF, sketched in Fig. 1 (a). Characterizing the atom number and trap characteristics is necessary for future ap-

plications of this platform. The number of trapped atoms can be measured on resonance [17] or off resonance [20, 22], *i.e.* destructive and dispersive measurements, respectively. The trapping potential has been characterized by parametrically heating the trapped atoms to find the resonance frequency of the trap, a destructive measurement [23–25], since it is necessary to lose trapped atoms to perform it.

In this letter we present a method to non-destructively characterize the trapping potential of an ONF dipole trap. We propagate a weak, off-resonance probe beam through the ONF that is linearly polarized and tilted 45° relative to the azimuthal axis defined by the trapping potential. The probe experiences a modified refractive index with a fast axis and a slow axis due to the presence of trapped atoms. This effective birefringence rotates the polarization of the probe as a function of the position of the atoms. Turning on the probe beam imparts a momentum kick to the trapped atoms so that they oscillate at the radial and azimuthal trapping frequencies. Detecting the time-dependent polarization change of the probe gives us a direct and non-destructive measurement of the transverse frequencies of the trapping potential.

Because the evanescent field decay constant is proportional to its wavelength, the red (blue) detuned light creates a longer (shorter) range attractive (repulsive) potential. Combining both red and blue detuned light, the atoms experience a potential energy minimum a fraction of a wavelength away from the ONF surface. This two-color dipole trap provides radial confinement for the atoms. Two counter-propagating red-detuned beams in a standing-wave configuration provide confinement along the

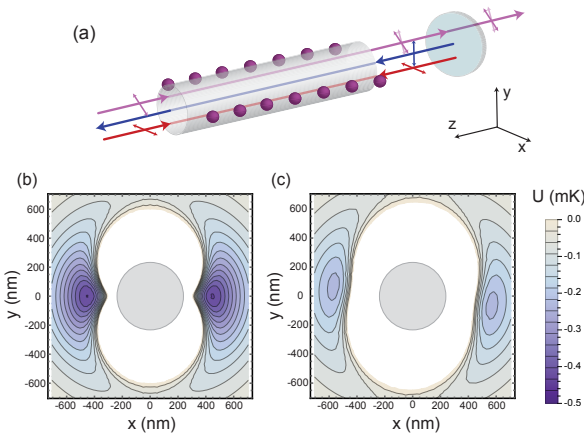


Fig. 1. (a) Schematic of the experimental setup showing the two one-dimensional array of atoms. An off-resonance probe beam propagates through the sample with linear polarization rotated by 45° . (b) Transversal view of a trapping potential, with 1 mW of power in each red-detuned beam and 3 mW of blue detuned propagating through a 235-nm radius ONF waist. (c) Modification of the trapping potential in (b) after turning on a probe beam with 70 nW of power and 200 MHz detuned to the blue of atomic resonance.

optical nanofiber, as a one-dimensional lattice. The azimuthal confinement is achieved by correctly choosing the polarization of the trapping beams. At the ONF waist linearly-polarized light becomes quasi-linearly polarized, breaking the azimuthal symmetry of the intensity profile of the propagating field. Aligning the polarization axis of the red-detuned beam orthogonal to the blue detuned one provides azimuthal confinement for the atoms (See Fig. 1(a) and (b)).

We create a dipole trap for ^{87}Rb atoms with a 235-nm radius ONF waist by coupling two counter-propagating red-detuned beams (1064 nm) in a standing wave configuration and a blue-detuned beam (750 nm). (The dominant resonances for Rb are at 780 (D2 line) and 795 nm (D1 line)). We typically use 1 mW of power for each red-detuned beam, and 3 mW for the blue-detuned beam. Fig. 1(b) shows this configuration, which produces a trapping potential with a depth of about 500 μK .

We image the light scattered from the nanofiber to characterize the polarization of the laser beams at the ONF waist. Because Rayleigh scattering preserves the polarization of the field, with the help of a linear polarizer in front of the camera we determine the polarization of the propagating field. The polarization can be controlled by wave plates at the input of the ONF. Each laser beam has to be characterized and controlled independently, since inherent stress in the ONF creates a birefringent medium that affects each wavelength differently.

A magneto-optical trap (MOT) loads cold ^{87}Rb atoms into our ONF dipole trap in a vacuum chamber kept at lower than 10^{-9} Torr. We further cool the atoms by increasing the detuning of the MOT beams for 90 ms. We then turn off the magnetic field gradient to create optical molasses for 1 ms. The atoms are typically at 15 μK when we let them fall into the dipole trap. Because of the tight confinement of the trap, the atoms are expected to be in a collisional blockade regime. This leads to a binary loading with one or zero atoms per trapping site. We typically trap a few hundred atoms for trapping lifetimes of the

order of 10 ms.

We send an off-resonant beam, detuned 200 MHz to the blue of the $F = 2 \rightarrow F' = 3$ transition of the D2 line, through the ONF to probe the trapped atoms. We align its polarization to be 45° from the trapping beams when there are no atoms present. The projection of the polarization component along the axis defined by the trapped atoms experiences a modified refractive index while the orthogonal component, which does not interact with the atoms, propagates unaltered. The motion of trapped atoms in the transverse plane of the nanofiber will change this birefringence as a function of time, producing a dynamical polarization rotation of the probe beam. Presumably there could be some oscillation in the z-component of the trap, but that may be weakly coupled to the probe and not affect the polarization rotation.

Because of the significant atom-light coupling provided by the tight mode area, more than a few tens of nW of probe power are detrimental to the trap. We use 70 nW of probe power, enough to imprint a momentum kick in the atoms to start their motion, but too weak to excite the atoms out of the trap. Fig. 1(c) shows the effect of the probe beam on the trapping potential.

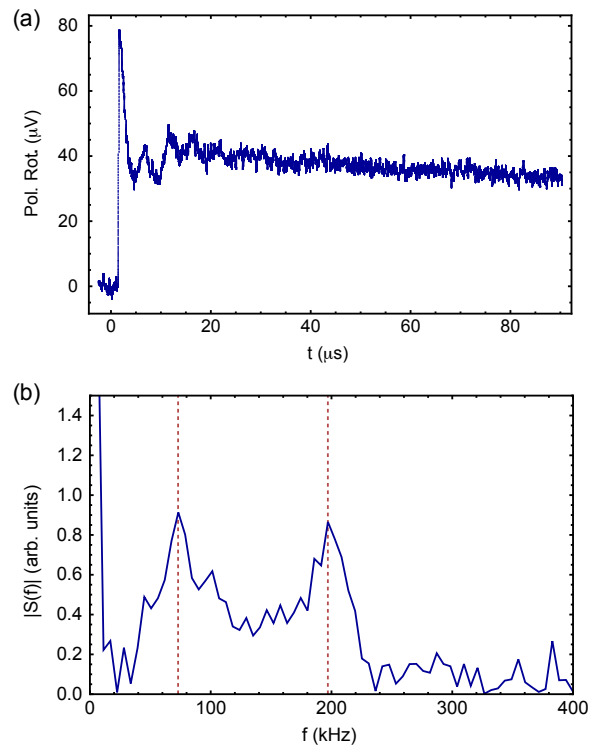


Fig. 2. (a) Polarization rotation of the probe beam (in units of measured voltage) as a function of time. The sudden spike in the signal denotes the probe turning on. (b) Power spectrum from the Fourier transform of the oscillations in (a). The two distinct peaks (at 73 ± 3 kHz and 197 ± 2 kHz), correspond to the radial and azimuthal trapping frequencies respectively, marked with red dashed lines.

The polarization rotation of such a low probe power is detected by heterodyne measurements by mixing the probe with a local oscillator (LO) with a 1 MHz relative frequency shift. We typically use 9 mW of power for the LO beam. After the probe goes through the ONF it is combined with the LO using a 50/50 beam splitter. We use one of the output paths for detection. Its

polarization components are separated by a Wollaston prism and sent to a 4 MHz bandwidth balanced photodetector. The 1 MHz beat note between the probe and the LO is mixed down to DC. This allows us to use the LO as gain for the probe, and directly detect the probe polarization rotation as a function of time with a bandwidth higher than the expected trap frequencies.

Figure 2 (a) shows a typical signal of the polarization rotation of the probe. Although the signal is visible in single-shot, the data is averaged to improve the signal to noise ratio by a factor of 10. The original data was acquired with a 2-ns bin width, and the plot is a 400-ns moving average for visualization purposes. The detector polarizations are set such that when there are no trapped atoms the measured output voltage is zero. However the zero voltage at time $t = 0$ in the plot is produced only by the LO (probe beam off). The probe field turns on at 2 μs . The signal can be decomposed in two time regimes: a short time regime where we observe oscillations due to the atoms moving back and forth in the trapping potential; and a long time regime where the oscillations vanish but the non-zero signal shows the presence of atoms in the trap. The sharp initial peak comes from atoms starting their motion closer to the ONF surface, where they interact more strongly with the probe beam, producing a larger signal. The decoherence of the oscillations comes from the large anharmonicity of the trapping potential and the thermal motion of the trapped atoms. The long timescale slope is the lifetime of the trap. In this case the characteristic decay time is $370 \pm 3 \mu\text{s}$, where the error represents the standard error of the fit. The lifetime is degraded by more than an order of magnitude when the probe beam is kept on. A small fraction of the probe beam gets absorbed by the trapped atoms and results in losses as the trapping potential becomes shallower (see Figs. 1 (b) and (c) with the depth scale).

The initial oscillations in Fig. 2 (a) encode information about transverse trapping frequencies. By taking a discrete Fourier transform of the data (after the probe turns on) we obtain the resonance frequencies of the oscillating atoms. Fig. 2 (b) shows the power spectrum of the signal. We observe two distinct peaks at $\nu_\phi = 73 \pm 3 \text{ kHz}$ and $\nu_r = 197 \pm 2 \text{ kHz}$, corresponding to the azimuthal and radial frequencies of the trap. The uncertainties in the mean are calculated from the full width at half maximum of the peak over the signal to noise ratio [26]. The width of the spectral peaks arises from the dephasing of the atoms due to the strong anharmonicity of the trap. As an approximation, we can model the problem as a damped harmonic oscillator. The fit to a Lorentzian line shape shows a linewidth of $\gamma_\phi = 64 \pm 8 \text{ kHz}$ $\gamma_r = 47 \pm 6 \text{ kHz}$ respectively, where the errors are the standard errors of the fit. This represents a decay time of the oscillations of around 20 μs , enough to measure trapping potentials of more than 50 kHz. The observation of oscillations from the azimuthal motion of the atoms depends on the alignment of the probe polarization to within few degrees. On the other hand, the detection of oscillation from radial motion of the atoms is more robust under misalignments.

We can compare the measured frequencies in Fig. 2 (b) to a numerical calculation. Taking the second derivative of the trapping potential shown in Fig. 1 (c) and knowing the atomic mass m we can calculate the expected trapping frequencies as $\nu_i = \sqrt{\frac{1}{2\pi m} \partial^2 U / \partial x_i^2}$, where the index i denotes the radial or azimuthal direction in cylindrical coordinates. For the experimental parameters listed in this paper, which produce Fig. 2 (c), we find that $\nu_\phi = 70 \pm 4 \text{ kHz}$ and $\nu_r = 195 \pm 6 \text{ kHz}$. The frequencies are extracted by fit an harmonic potential to the

bottom of the calculated potential and extracting the corresponding trapping frequency for each spatial direction. The errors represent the sensitivity of the simulation to a 5% variation of the experimental parameters, these parameters being the four lasers beams power (two red-detuned, a blue-detuned and the probe), and the four polarization angles (three relative angles). We assume that the polarizations are perfectly linearly-polarized, which is in general not true, but greatly reduces the number of free parameters in the simulation. The theoretical results are 2% above and 7% below the measured values for the azimuthal and radial frequencies respectively. The measured signal is in good agreement with the expected result within the experimental uncertainties.

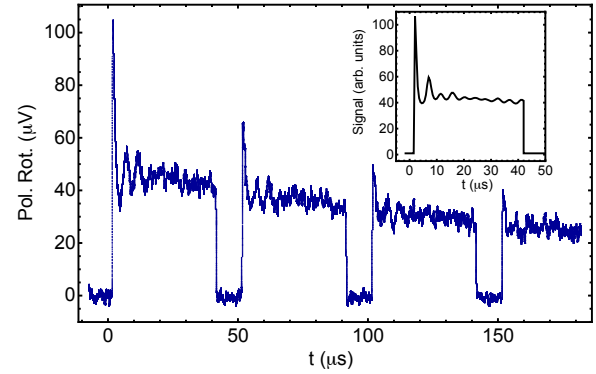


Fig. 3. Polarization rotation of the probe beam (in units of measured voltage) as a function of time, for a set of four 40 μs probe pulses. The repeatability of the process shows the non-destructive feature of the measurement technique. The inset shows a Monte Carlo simulation of the signal for radial oscillations only. The simulation considers an ensemble of atoms oscillating in the potential shown in Fig. 1 (c) from different starting positions and a decay of 265 μs .

The non-destructive feature of this method is further tested by probing the trapped atoms more than once while they still are in the trap. Fig. 3 shows the polarization rotation as a function of time for a probe beam that turns on and off four times. We see that the first pulse is enough to extract the oscillation frequency of the atoms before it decreases. Consecutively the probe turns off and on again, after 10 μs , reproducing the same oscillatory signal but with smaller amplitude. This process can be repeated as long there are enough atoms in the trap to produce a detectable signal. The signal from the four pulses shown in Fig. 3 has an over-all slope corresponding to a trapping lifetime of $265 \pm 1 \mu\text{s}$. This is almost 30% shorter lifetime compared to keeping the probe beam constantly on (as in Fig. 2 (a)), because the momentum kick of suddenly turning the probe beam on and off can induce atom loss. However, the dispersive measurement is non-destructive enough to test the characteristics of the trap while leaving a significant amount of atoms for further experimentation. The inset of Fig. 3 shows a numerical simulation of the detected signal for only radial oscillations (uncoupled motion). Using the simulated trapping potential (Fig 1 (c)) we calculate the motion of a set of 500 atoms randomly positioned with a flat distribution of $\pm 75 \text{ nm}$ centered at 80 nm towards the ONF from the potential minimum. The trajectories of the atoms, computed and averaged, give an effective trajectory. The signal is proportional to the dynamical change of the coupling into

the ONF of an atom following such an effective trajectory. The displacement of the center of the distribution of the initial atomic positions takes into account the displacement of the center of the trap when the probe beam is turned on. The parameters for the simulation are empirically found within a experimentally realistic range. This simple model captures the qualitative behavior of the detected signal.

Although the probe beam modifies the potential landscape felt by the atoms, the good agreement between the measurements and the simulations allows us to extract the trapping potential without the modification due to the probe beam. In our case we obtain $\nu_\phi = 178.3$ KHz and $\nu_\phi = 252.2$ KHz from the potential shown in Fig. 1 (b). Moreover, by optimizing the photodetection, a weaker probe beam minimally perturbs the trapping potential. In this configuration another pulsed beam can rapidly imprint a momentum kick to the atoms, so they start oscillating in phase. Colder atoms might also help to establish longer coherence time for the oscillations, since the trapping potential approximates to an harmonic trap around its minimum. The measured signal increases linearly with the number of trapped atoms. A more efficient loading of the trap may increase the number of atoms and the amplitude of the signal.

We have shown how a polarimetric measurement of an off-resonance probe beam can be used to non-destructively characterize the trapping potential of a two-color ONF-based dipole trap. This technique can be easily implemented in any ONF-based dipole trap experiment, allowing a shot-to-shot measurement of the trapping potential before performing further experiments in the same experimental sequence, an advantage over other configurations of optical dipole traps. The results are in good agreement with theoretical predictions, showing an understanding of the variables involved in the problem. This points to different strategies to improve the technique in the future. We expect that non-destructive and fast-readout characterization of local potential experienced by trapped atoms near dielectric surfaces to become standard tools in the growing field of interfacing nano-photonic platforms to cold atoms.

ACKNOWLEDGMENTS

This work has been supported by National Science Foundation of the United States (NSF) (PHY-1307416); NSF Physics Frontier Center at the Joint quantum Institute (PHY-1430094).

REFERENCES

1. J. D. Thompson, T. G. Tiecke, N. P. de Leon, J. Feist, A. V. Akimov, M. Gullans, A. S. Zibrov, V. Vuletić, and M. D. Lukin, *Science* **340**, 1202 (2013).
2. A. Goban, C.-L. Hung, S.-P. Yu, J. Hood, J. Muniz, J. Lee, M. Martin, A. McClung, K. Choi, D. Chang, O. Painter, and H. Kimble, *Nat. Commun.* **5** (2014).
3. A. Goban, C.-L. Hung, J. D. Hood, S.-P. Yu, J. A. Muniz, O. Painter, and H. J. Kimble, *Phys. Rev. Lett.* **115**, 063601 (2015).
4. J. D. Hood, A. Goban, A. Asenjo-Garcia, M. Lu, S.-P. Yu, D. E. Chang, and H. J. Kimble, *Proceedings of the National Academy of Sciences* **113**, 10507 (2016).
5. M. J. Morrissey, K. Deasy, M. Frawley, R. Kumar, E. Prel, L. Russell, V. G. Truong, and S. Nic Chormaic, *Sensors (Basel)* **13**, 10449 (2013).
6. B. Gouraud, D. Maxein, A. Nicolas, O. Morin, and J. Laurat, *Phys. Rev. Lett.* **114**, 180503 (2015).
7. C. Sayrin, C. Clausen, B. Albrecht, P. Schneeweiss, and A. Rauschenbeutel, *Optica* **2**, 353 (2015).
8. D. E. Jones, J. D. Franson, and T. B. Pittman, *Phys. Rev. A* **92**, 043806 (2015).
9. R. Kumar, V. Gokhroo, K. Deasy, A. Maimaiti, M. C. Frawley, C. Phelan, and S. Nic Chormaic, *New J. Phys.* **17**, 013026 (2015).
10. D. O'Shea, C. Junge, J. Volz, and A. Rauschenbeutel, *Phys. Rev. Lett.* **111**, 193601 (2013).
11. I. Shomroni, S. Rosenblum, Y. Lovsky, O. Bechler, G. Guendelman, and B. Dayan, *Science* **345**, 903 (2014).
12. C. Sayrin, C. Junge, R. Mitsch, B. Albrecht, D. O'Shea, P. Schneeweiss, J. Volz, and A. Rauschenbeutel, *Phys. Rev. X* **5**, 041036 (2015).
13. N. V. Corzo, B. Gouraud, A. Chandra, A. Goban, A. S. Sheremet, D. Kupriyanov, and J. Laurat, *Phys. Rev. Lett.* **117**, 133603 (2016).
14. H. L. Sørensen, J.-B. Béguin, K. W. Kluge, I. Iakourov, A. S. Sørensen, J. H. Müller, E. S. Polzik, and J. Appel, *Phys. Rev. Lett.* **117**, 133604 (2016).
15. J. E. Hoffman, S. Ravets, J. A. Grover, P. Solano, P. R. Kordell, J. D. Wong-Campos, L. A. Orozco, and S. L. Rolston, *AIP Adv.* **4**, 067124 (2014).
16. F. Le Kien, V. I. Balykin, and K. Hakuta, *Phys. Rev. A* **70**, 063403 (2004).
17. E. Vetsch, D. Reitz, G. Sagué, R. Schmidt, S. T. Dawkins, and A. Rauschenbeutel, *Phys. Rev. Lett.* **104**, 203603 (2010).
18. A. Goban, K. S. Choi, D. J. Alton, D. Ding, C. Lacroûte, M. Pototschnig, T. Thiele, N. P. Stern, and H. J. Kimble, *Phys. Rev. Lett.* **109**, 033603 (2012).
19. D. Reitz, C. Sayrin, R. Mitsch, P. Schneeweiss, and A. Rauschenbeutel, *Phys. Rev. Lett.* **110**, 243603 (2013).
20. J.-B. Béguin, E. Bookjans, S. Christensen, H. Sørensen, J. Müller, E. Polzik, and J. Appel, *Phys. Rev. Lett.* **113**, 263603 (2014).
21. S. Kato and T. Aoki, *Phys. Rev. Lett.* **115**, 093603 (2015).
22. X. Qi, B. Q. Baragiola, P. S. Jessen, and I. H. Deutsch, *Phys. Rev. A* **93**, 023817 (2016).
23. S. Friebel, C. D'Andrea, J. Walz, M. Weitz, and T. W. Hänsch, *Phys. Rev. A* **57**, R20 (1998).
24. R. Grimm, M. Weidemüller, and Y. B. Ovchinnikov, "Optical dipole traps for neutral atoms," (Academic Press, 2000), pp. 95 – 170.
25. E. Vetsch, "Optical Interface Based on a Nanofiber Atom-Trap," Ph.D. thesis, University of Mainz (2010).
26. A. Clairon, C. Salomon, S. Guellati, and W. D. Phillips, *EPL (Euro-physics Letters)* **16**, 165 (1991).

2.7 Model of the atomic motion

The trapping potential shown in the previous section can be directly calculated knowing the atomic polarizability and the electric field of the ONF mode (see Appendix A). However the nature of the detected signal is less clear.

The polarization of the probe beam rotates due to the effective index of refraction created by the atoms. The change of the index of refraction is given by the scalar atomic polarizability α_0 and the density of atoms ρ , as [101]

$$\delta n = \frac{\rho\alpha_0(\Delta)}{3\epsilon_0}. \quad (2.1)$$

The scalar atomic polarizability can be written as a function of the atomic linewidth γ_0 and the probe detuning Δ as $\alpha_0 = 3\epsilon_0\lambda^3\gamma_0/(8\pi^2\Delta)$.

The angle of polarization rotation is proportional to the optical path difference between two polarizations components of the propagating field. A polarization that interacts with the trapped atoms and an orthogonal one that (almost) does not interact with the atoms. The optical path difference between both polarizations is

$$\delta\phi = \delta n k l, \quad (2.2)$$

where k is the wavenumber and l is the length of the sample. Replacing Eq. (2.1) in Eq. (2.2) and using the expression for α_0 we obtain

$$\delta\phi = \rho\sigma_0 l \frac{\gamma_0}{\Delta} = OD \frac{\gamma_0}{\Delta}. \quad (2.3)$$

The measured signal is inversely proportional to the probe detuning and directly proportional to the optical density. The signal relates to the position of the atoms

by the OD. Comparing this result with the fact that $OD \propto \gamma_{1D}/\gamma_0$ (as shown in Eq. (1.17)), we get that the polarization rotation is related to the atomic position by the expression

$$\delta\phi(r) = n_{\text{eff}} \frac{\gamma_{1D}(r)}{\Delta}. \quad (2.4)$$

The motion of the atoms in the trap can be calculated from a Monte Carlo simulation. We randomly position a group of atoms in the trap with a flat distribution, and solve the equations of motion for each one. Adding them up, we can obtain the trajectory of an effective atom seen by the probe beam. Fig. 2.2 shows the effective atomic motion and the corresponding expected signal for two different cases. By comparing both figures, one with a bigger spread of the atomic distribution than the other, meaning higher temperature, we see how the damping of the oscillations comes from the anharmonicity of the trap. The more dispersed the atoms are in the potential well, the faster they dephase.

This simple model provides verification of our physical intuition. We can qualitatively reproduce the measured signal from a purely theoretical model that corroborates our understanding of the physically relevant parameters involved in the experiment.

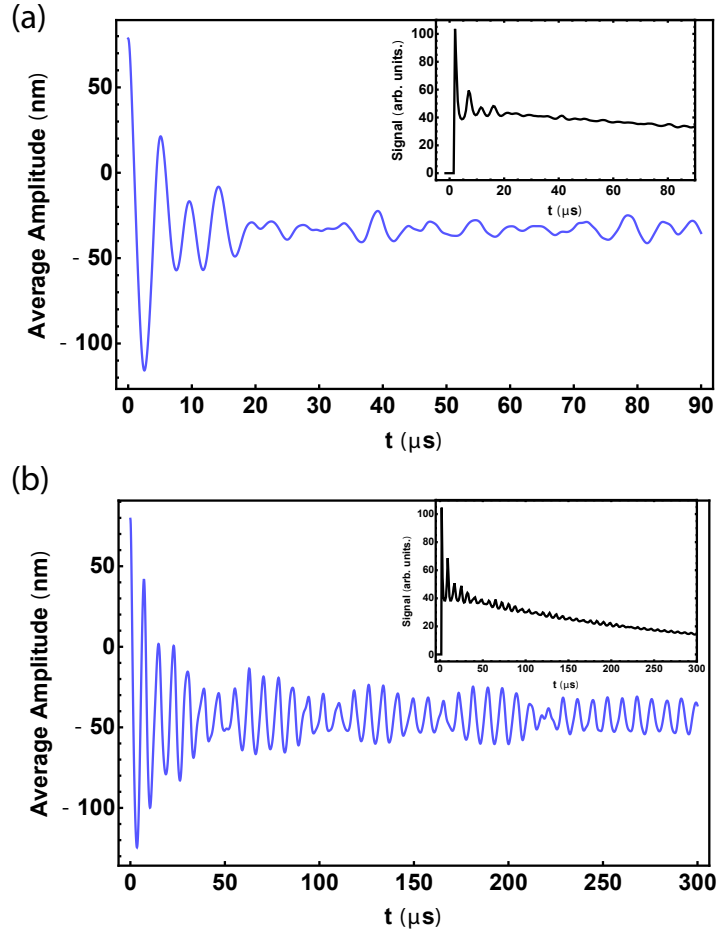


Figure 2.2: (a) Sum of the atomic trajectories under the conditions explained in Sec. 2.6. (b) Same as (a) but with a narrower distribution of atoms in the trap ($\pm 15 \text{ nm}$ instead of $\pm 75 \text{ nm}$, corresponding to approximately $5 \mu\text{K}$ and $100 \mu\text{K}$ respectively). Both figures help to contrast the cases of having atoms occupying more or less of the trapping potential. The insets represent the expected signal for each plot using Eq. (2.4), with an added exponential decay of $265 \mu\text{s}$ (not present in the main figures) that captures the measured loss of trapped atoms.

Chapter 3: Purcell effect of an ONF

Section 1 has motivated the importance of ONFs for quantum optics and quantum information. They provide a unique platform for many reasons, one being that the presence of an ONF modifies the structure of the vacuum electromagnetic field experienced by a nearby atom. This can modify atomic properties such as the spontaneous emission rate, *i.e.* the Purcell effect, [68, 102–105].

The Purcell effect is the change of the atomic spontaneous emission due to the modification of the vacuum electromagnetic field in the presence of an object [106]. As explained in Sec. 1.1, it tells us about the properties of atoms coupled to a given structure of modes, in our case radiated (reservoir) and guided modes. When only the coupling into the preferential guided mode is known, the measurement of a Purcell factor helps obtain information about the coupling of the system to the reservoir. This provides us with a tool to characterize properties of the system, such as the atom-light coupling strength for the guided or non-guided modes and the cooperativity.

We started this thesis presenting different parameters that characterize atom-light coupling (see Sec. 1.3) that are relevant for quantum optics experiments. Knowing the decay rate into the waveguide γ_{1D} and the total atomic decay rate γ_{tot} we

can calculate the four relevant parameters: emission enhancement α , coupling coefficient β , cooperativity C_1 , and Purcell factor F_p . We plot them as a function of nanofiber radius and atom-surface distance in Fig. 3.1.

Figure 3.1 shows calculations of α (see Eq. 1.10) for a single Rb atom operating on the D2 line in the HE_{11} evanescent mode of the ONF. We follow the work in Ref. [68] for the calculation of γ_{1D} (see Eq. (1.15) and Appendix A for details on the calculation on the mode structure). The total decay rate γ_{tot} (including both contribution, from photons radiated into the ONF and outside the ONF) is more challenging to calculate. However we can compute them numerically with finite-difference time-domain (FDTD) calculations [107] (as will be explained later in this chapter).

The emission enhancement can be up to 20% larger than that of free-space near to the fiber surface according to Fig. 3.1(a). As expected, it decreases to the free space value as the atom-fiber distance increases. For a typical nanofiber $\beta \ll 1$, it follows from Eq. (1.12) that $C_1 \approx \beta$, as the plots in Fig. 3.1 (b) and (c) show. Both the coupling efficiency and the cooperativity display similar spatial dependence as the emission enhancement. The modification of the total spontaneous emission due to the presence of the nanofiber is given by the Purcell factor (F_p), plotted in Fig. 3.1(d). Its non-trivial dependence on the geometrical parameters comes from the atomic dipole alignment and is discussed in more detail in Sec. 3.1. For the particular case of Fig. 3.1(d) we assume that the dipole moments point in the same direction as the electric field of the circularly polarized fundamental mode of the ONF. This means that the component along the ONF (z) is approximately the same

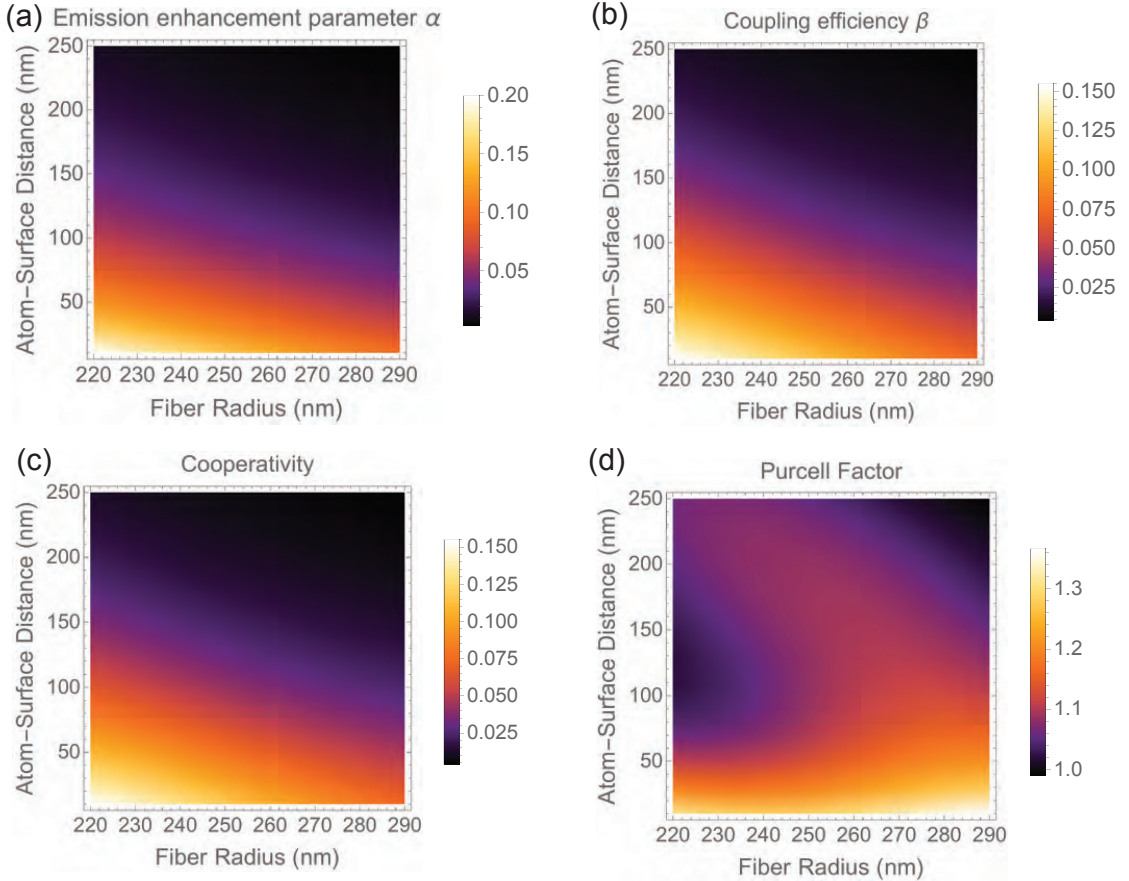


Figure 3.1: Atom-mode coupling parameters as a function of nanofiber radius and atom-surface distance for our ONF configuration. (a) Emission enhancement α , (b) coupling efficiency, β (c) single atom cooperativity C_1 , and (d) Purcell factor α/β . The Purcell factor C_1 and β depend strongly on the atomic dipole alignment relative to the ONF surface. For all the plots we consider an atomic dipole alignment along the electric field of the circularly polarized fundamental mode of the ONF, meaning a superposition of the three polarization components (z , ϕ , and r). The calculations consider a wavelength of 780 nm. Fig. from Ref. [87].

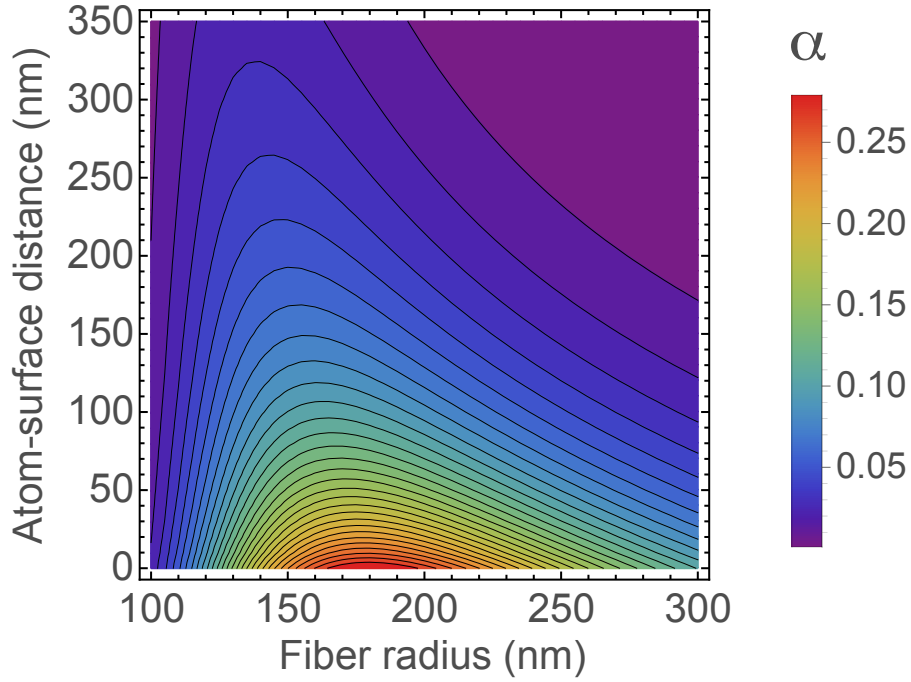


Figure 3.2: Contour plot of the spontaneous emission enhancement parameter as a function of nanofiber size and atom-surface distance. The calculation are for a wavelength of 780 nm. Fig. from Ref. [43].

as the azimuthal one (ϕ) and three times smaller than the radial (r) one.

Figure 3.2 shows that there is an optimal ONF radius that maximizes the coupling enhancement, which depends on the atom-surface distance; reducing the radius further than that decreases α . The target ONF radius during fabrication should then be decided accordingly with the wavelength that will be used and the distance from the ONF surface at which the atoms will be.

The spontaneous emission rate depends on the square of the energy matrix element of the the atom-light interaction. This is given by the dot product of the atomic dipole moment and the local vacuum electric field felt by the atom. If the surrounding media is anisotropic, the vacuum electric field can have different amplitudes for each polarization component [108]. This leads to a dependence of

the spontaneous emission on the atomic dipole alignment.

Figure 3.3 shows a calculation, using FDTD, of the modification of the spontaneous emission for a two-level atom aligned along r , ϕ , and z . We see that we can go from enhancement to inhibition of the spontaneous emission depending on the dipole alignment and the atom-surface distance.

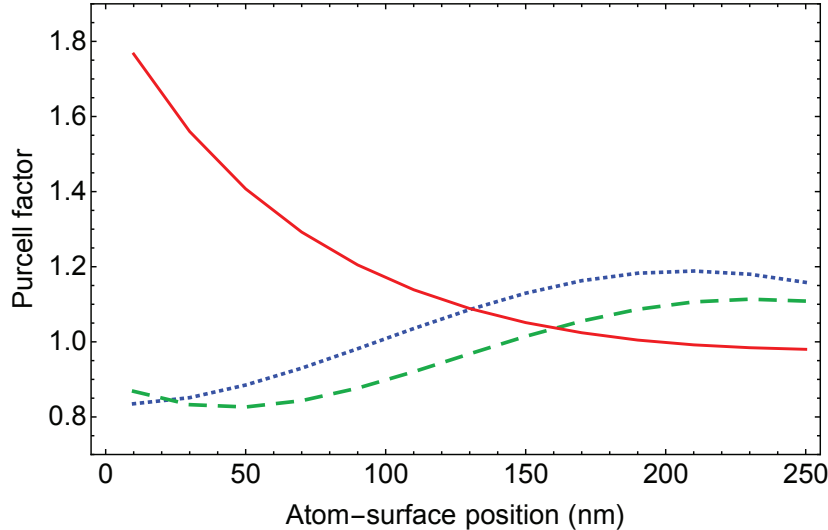


Figure 3.3: Purcell factor of an ONF of 237-nm radius as a function of the atom-to-surface distance for an atomic dipole aligned along r (solid red), along ϕ (dotted blue), and along z (dashed green). The curves come from finite-difference time-domain calculations. The calculations are for a wavelength of 780 nm. Fig. from Ref. [87].

3.1 Measuring the Purcell effect of ONFs

We present measurements of the radiative lifetime changes in the vicinity of an ONF due to the presence of a dielectric surface and to atomic dipole alignment effects. Depending upon the ONF radius and the atom-surface position (see Fig. 3.3), the alignment of the induced atomic dipoles relative to the ONF surface influences if

there is an enhancement or inhibition of the atomic decay rate. The difference can be as large as $\sim 80\%$ enhancement to $\sim 20\%$ inhibition for our current ONF parameters. Fig. 3.3 displays this dependence, showing that for a particular alignment atomic dipoles could couple differently to the environment. The alignments not only modify the total atomic decay rate, but also the coupling into different modes, modifying the branching ratios of the decays into the guided mode and radiated outside the ONF.

We use a sample of free cold atoms around the nanofiber. In this configuration, it is possible to probe closer distances than with trapped atoms and still avoid the complications of the van der Waals interaction. We measure enhancements and inhibitions of the spontaneous emission rate of $\sim 10\%$ and $\sim 5\%$ respectively, depending on the alignment of the induced dipoles and averaged over the given atomic distribution.

However the problem is far from being understood. Multi-level atoms have a radiation pattern more isotropic than the one of a dipole, contradicting the idea of imagining the atoms as classical dipoles with a well defined axis. Although numerical simulations for a two-level atom seem to agree with the measured results, we know that this model does not capture the real problem. Moreover, we know that there are discrepancies in the calculated values for the spontaneous emission rate when using different methods. This indicates that further studies on the dependence of the atomic spontaneous emission to a particular geometry are necessary to understand the system. Next, we present our study regarding these issues.

Alignment-dependent decay rate of an atomic dipole near an optical nanofiber

P. Solano,^{1,*} J. A. Grover,¹ Y. Xu,² P. Barberis-Blostein,^{1,3} J. N. Munday,² L. A. Orozco,¹ W. D. Phillips,⁴ and S. L. Rolston¹

¹Joint Quantum Institute and Department of Physics,
University of Maryland, College Park, MD 20742, USA.

²Department of Electrical and Computer Engineering and the Institute for Research in Electronics and Applied Physics,
University of Maryland, College Park, Maryland 20742-3511, USA.

³Instituto de Investigaciones en Matemáticas Aplicadas y en Sistemas,
Universidad Nacional Autónoma de México, Ciudad Universitaria, 04510, DF, México.

⁴Joint Quantum Institute, NIST and University of Maryland, Gaithersburg, Maryland 20899, USA
(Dated: April 14, 2017)

We study the modification of the atomic spontaneous emission rate, i.e. Purcell effect, of ^{87}Rb in the vicinity of an optical nanofiber (~ 500 nm diameter). We observe enhancement and inhibition of the atomic decay rate depending on the alignment of the induced atomic dipole relative to the nanofiber. Finite-difference time-domain simulations are in quantitative agreement with the measurements when considering the atoms as simple oscillating linear dipoles. This is surprising since the multi-level nature of the atoms should produce a different radiation pattern, predicting smaller modification of the lifetime than the measured ones. This work is a step towards characterizing and controlling atomic properties near optical waveguides, fundamental tools for the development of quantum photonics.

I. INTRODUCTION

Neutral atoms coupled to optical waveguides is a growing field of research [1–10]. Atom-waveguide systems enable atom-light interaction for propagating light modes. This makes them promising tools for forthcoming optical technologies in the quantum regime, such as quantum switches [11–13], diodes [14, 15], transistors [16], and electromagnetically induced transparency and quantum memories [17–20]. In order to further any of these applications it is necessary to understand and control the effects of such waveguides on nearby atoms.

Two important features result from having a waveguide with a preferential optical mode: the spatial variation of the electromagnetic field, and the change of its density of modes per unit frequency. One of the key atomic properties affected by both is the spontaneous emission rate [21]. Its modification is due to the change in the local vacuum field felt by the atom under the boundary condition imposed by the adjacent object, a phenomena known as Purcell effect [22]. When the symmetry of the free-space vacuum field is broken in the presence of an object, the alignment of the atomic dipole relative to the object also plays an important role on the atomic lifetime. For a given alignment the atom can couple more strongly (weakly) to the vacuum modes, producing an increase (decrease) of the spontaneous emission rate. The effect of waveguides on the spontaneous emission of nearby emitters has been a productive field of research [23–35].

Optical nanofiber (ONF) waveguides [36, 37] are optical fibers with a diameter smaller than the wavelength of

the guided field. Most of the electromagnetic field propagates outside the dielectric body of the ONF (in vacuum) in the form of a evanescent field, and its strong transversal confinement enables interactions with adjacent atoms. The nanofiber is adiabatically connected, through a tapered section, to a conventional single mode optical fiber, facilitating light coupling and readout. ONFs are upcoming platforms for photonic based quantum technologies due to the coupling efficiency of light, high surface quality at the nanometer scale, and simplicity and robustness of the fabrication procedure [38]. The electromagnetic mode confinement in a ONF provides a large atom-light coupling [39, 40], a feature that has been used for spectroscopy [41], atomic cloud characterizations [42, 43] and atom trapping [44–49]. It also allows the operation and control of memories [17–20], and light reflectors [50, 51] at the level of single photons. The presence of three polarization components of the propagating field gives rise to chiral effects and new possibilities for atom-light directional coupling including optical isolators [2, 3, 14, 52].

The Purcell effect experienced by an emitter near an ONF has been studied in the past [53–62]. However, there are disagreements between predicted values for the decay rates (e.g. Refs. [54] and [61] differ by approximately 30% for atoms at the ONF surface), without direct experimental evidence that allows to validate one calculation over the other. Moreover, the possibility of controlling the atomic lifetime in the vicinity of an ONF by the position and alignment of the emitter has not been emphasized or shown experimentally.

We measure the modification of the spontaneous emission decay rate of a ^{87}Rb atom placed near an ONF, in the time domain for different alignments of the induced atomic dipole, showing that the atomic lifetime can increase or decrease by properly preparing the atom.

* Corresponding author email: solano.pablo.a@gmail.com

We present a theoretical description of the system, and perform both finite-differences time-domain (FDTD) and electromagnetic modes expansion calculations of the modification of the atomic decay rate. The FDTD numerical calculations considering a simple two-level atom show quantitative agreement with our experimental result. However, given the the multi-level structure of the atoms, their radiation patterns should differs from that of a linear dipole. The more isotropic pattern of our multilevel atom raises a puzzling question about the interpretation of the measured effects. Nonetheless, this study offers insight about the possibility of controlling atomic properties near surfaces for photonics, quantum optics and quantum information applications.

This paper is organized as follows: Sec. II explains the platform under study. The details of the experimental apparatus and the measurements procedure are in Sec. III, and the results are discussed in Sec. IV. We present numerical calculations for the atomic decay rate under the experimental conditions in Sec. V and a theoretical modeling of the system in Sec. VI. We comment on the role of the multilevel structure of real atoms in our experiment in Sec. VII. Sec. VIII presents a quantitative comparison of the results to numerical simulations. Finally, we discuss the implications of this result in Sec. IX, and conclude in Sec. X.

II. DESCRIPTION OF THE EXPERIMENT

We consider an ONF that only allows the propagation of the fundamental mode HE_{11} . Excited atoms that are close to the nanofiber can spontaneously emit not only into free space, but also into the ONF mode, as sketched in Fig. 1 (a). Our goal is to measure the modified spontaneous emission rate γ of an atom placed near it, compared to the free space decay rate γ_0 . γ is the sum of the spontaneous emission rate of photons radiated into free-space (in the presence of the ONF) and into the ONF waveguide, i.e. $\gamma(\mathbf{r}) = \gamma_{fs}(\mathbf{r}) + \gamma_{wg}(\mathbf{r})$, where all the quantities are a function of the atom position \mathbf{r} . When the atom is placed far away from the ONF $\gamma_{wg} \rightarrow 0$ and $\gamma \rightarrow \gamma_0$, recovering the free space scenario.

The atomic decay rate can be calculated from Fermi's golden rule [21]. It states that the decay rate from a initial state $|i\rangle$ to a final state $|f\rangle$ is given by the strength of the interaction that mediates the transition, related to $H_{int}(\mathbf{r})$ and the density of final states per unit energy $\rho(\epsilon)$ as

$$\gamma_{i \rightarrow f}(\mathbf{r}) = \frac{2\pi}{\hbar} \rho(\epsilon) |\langle f | H_{int}(\mathbf{r}) | i \rangle|^2, \quad (1)$$

where \hbar is the reduced Plack constant. In our particular case $H_{int}(\mathbf{r}) = \mathbf{d} \cdot \mathbf{E}(\mathbf{r})$, given by the transition dipole moment \mathbf{d} and the electric field operator $\mathbf{E}(\mathbf{r})$.

The effect of the ONF dielectric body on the decay rate of a nearby atom can be thought in two analogous ways [63]: it modifies the structure of the vacuum electric

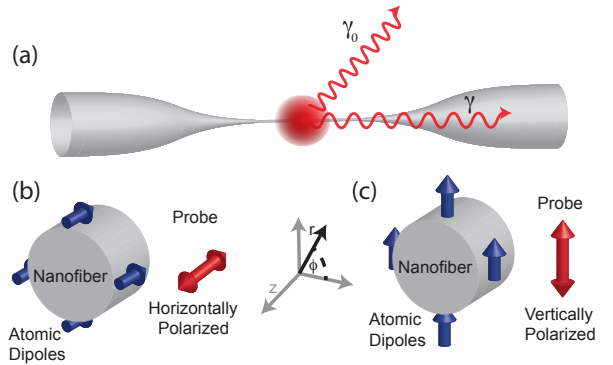


FIG. 1. (a) Sketch of the experimental configuration where an ensemble of cold atoms spontaneously emit photons at a rate γ_0 or γ when they are placed far away or close the the fiber respectively. (b) and (c) sketch of the orientation of the induced atomic dipoles relative to the nanofiber for horizontal and vertical probe beam polarization respectively. The coordinate system is used throughout the paper.

field; or it reflects the emitted field back to the atom. In both cases the electric field $\mathbf{E}(\mathbf{r})$ at the position of the atom is modified. This changes the interaction Hamiltonian $H_{int}(\mathbf{r})$ along with the decay rate. The dot product between the atomic dipole moment and the electric field in Eq. (1) depends upon their relative alignments, leading to alignment dependence of the atomic decay rate, because the ONF breaks the isotropy of the free space field.

A linearly polarized optical field will drive a two-level atom along the direction of light polarization. After a scattering event, the light will leave the atom with the polarization and radiation pattern of a classical dipole aligned in such direction. By choosing the direction of light polarization we can align the radiating dipole relative to the ONF (see Fig. 1 (b) and (c)). This allows us to observe the dependence of the atomic decay rate on the dipole orientation. Due to the tight transverse confinement of the light propagating through the ONF, the electric field has a significant vector component along the propagation axis, as well as perpendicular to it [54]. This enables an atomic dipole oscillating along the ONF to couple light into the guided mode. This is not the case for radiation in free space, where there is no radiated power along the dipole axis [64].

Modifications in the spontaneous emission rate change the atomic spectral width and can be measured in frequency space by doing precision spectroscopy [65]. However, the atomic spectrum is highly susceptible to broadening mechanisms such as Stark, Zeeman (DC and AC) and Doppler shifts, and van der Waals effects from the ONF dielectric surface. These broadenings increase systematic errors, making the measurement more challenging. Considering this, we perform a direct atomic lifetime measurement, *i.e.* in the time domain, to study the atomic decay rates.

Atoms have to be relatively close to the ONF surface (less than $\lambda/2\pi$) when we probe them to see a significant effect. Two-color dipole traps, created by the evanescent field of an ONF, are a useful tool for trapping a large number of atoms close to the nanofiber [45–51]. However, the created potential minimum is usually too far from the ONF surface (typically ~ 200 nm) to observe changes in the atomic radiative lifetime. Cold atoms that are free to move can get much closer to the ONF and spend sufficient time around it to be properly measured.

To measure γ/γ_0 we overlap a cold cloud of atoms with a single mode ONF (see Fig. 1 (a)). The atoms in the cloud are excited by a resonant probe pulse propagating perpendicularly to the nanofiber. After the pulse is suddenly turned off, spontaneously emitted light is collected and the photon-triggered signals are counted and histogrammed to get their temporal distribution, a technique known as time-correlated single photon counting (TCSPC) [66]. From the exponential decay of the temporal distribution of photons we measure the atomic lifetime $\tau = 1/\gamma$, directly related to the spontaneous emission rate. By detecting the spontaneously emitted light coupled into the ONF mode we are measuring only those atoms that are close enough to the nanofiber to couple light in. This allows us to obtain the modified spontaneous emission rate of atoms near the ONF surface. Note that the measured decay is the total decay rate γ , regardless of the mode used for the detection. The decay rates into different channels, in our case γ_{fs} and γ_{wg} , only determine the branching ratio of the total decay.

We are interested in the effect of the atomic dipole alignment relative to the ONF. For this we externally drive the atomic dipole in a particular direction set by the polarization of the probe pulse. That polarization can be set to be linear in the direction along the ONF (horizontally polarized) or perpendicular to it (vertically polarized). When probing with horizontally polarized light the atomic dipoles for two-level atoms are oriented along z , (see Fig. 1 (b)). For the case of a vertically polarized probe, the atomic dipoles are oriented along r on top and bottom, but along ϕ on each side, relative to the direction of propagation of the probe. In the vertical polarization case, we have a continuous distribution of dipole alignments, from dipoles along r to dipoles along ϕ (see Fig. 1 (c)).

III. APPARATUS AND MEASUREMENTS PROCEDURE

Figure 2 (a) shows a schematic of the experimental apparatus. The ONF waist is 7 mm in length with an approximately 240 ± 20 nm radius, where the uncertainty represents the variation in any given fabrication of an ONF, as destructively measured by an scanning electron microscope and independently confirmed with non-destructive techniques [67]. Any given ONF is uniform to within 1% through its full length. We

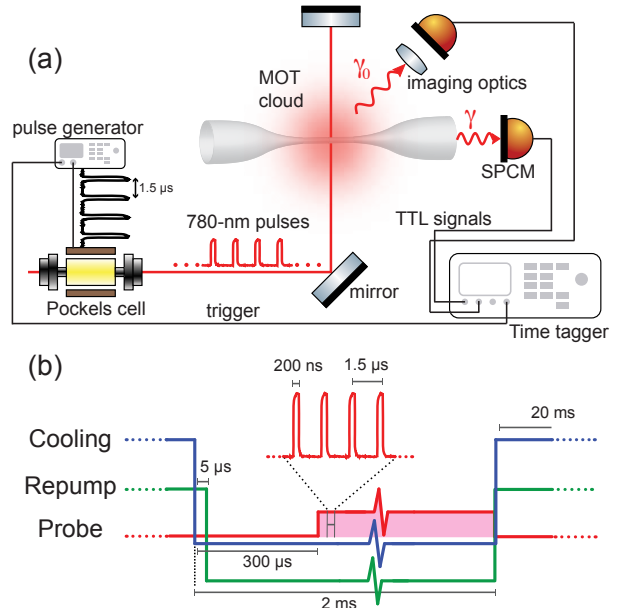


FIG. 2. (a) Schematic of the experimental setup. A train of pulses generated from a Pockels cell is directed to an ensemble of cold ^{87}Rb atoms placed near an optical nanofiber. The spontaneously emitted photons into the nanofiber are collected and time tagged to obtain the atomic radiative lifetime. Photons emitted into free space are also measured to verify possible systematic errors. (b) Experimental sequence of light pulses to cool, repump and probe the atoms.

placed the ONF inside an ultrahigh vacuum (UHV) chamber. Inside the chamber, the ONF is overlapped with a cloud of cold ^{87}Rb atoms created from a magneto optical trap (MOT), loaded from a background gas of atoms released from a dispenser. The atoms are excited by pulses of a probe beam incident perpendicularly to the nanofiber and retroreflected to reduce photon-to-atom momentum transfer. These pulses are resonant with the $F = 2 \rightarrow F' = 3$ transition of the D2 line and created with a Pockels cell (Conoptics 250-160) for a fast turn off, with a pulse extinction ratio of 1:170 in 20 ns. The on-off stage of the pulses is controlled with an electronic pulse generator (Stanford Research Systems DG645). The probe beam is a 7 mm $1/e^2$ full-width collimated beam and kept at a saturation parameter $s < 0.05$ to reduce atomic excitations during the off period (where $s = I/I_{\text{sat}} = 2(\Omega/\gamma_0)^2$, with $I_{\text{sat}} = 3.58 \text{ mW cm}^{-2}$ the average saturation intensity for a uniform sub-level population distribution over all m_F in $F = 2$, and Ω is the on-resonance excitation Rabi frequency). A linear polarizer with extinction ratio of $10^5 : 1$ sets the probe polarization for driving the atomic dipoles along a particular direction. Any atoms in the cloud, close or far from the ONF, can be excited. The photons emitted into the nanofiber and those emitted into free space are independently collected with avalanche photodiodes (APDs, Laser Components COUNT-250C-FC, with less than 250 dark counts per second). The TTL pulses created from photons de-

tected by the APDs are processed with a PC time-stamp card (Becker and Hickl DPC-230) and time stamped relative to a trigger signal coming from the pulse generator. We detect of the order of 10^{-3} photons per probe pulse, consistent with considering atomic excitation probability, coupling into the ONF, power losses through band-pass filters and other optical elements, and detection efficiencies.

The experimental cycle is described in Fig. 2 (b). Acousto-optic modulators (AOMs) control the amplitude and frequencies of the MOT and repump beams. After the atomic cloud reaches steady state, the MOT cooling and repump beams are turned off with a fall time of less than $0.5 \mu\text{s}$. The repump turns off $5 \mu\text{s}$ after the cooling beams to end with the maximum number of atoms in the $F = 2$ ground state. We wait $300 \mu\text{s}$ until the AOMs reach maximum extinction. The atomic cloud constitutes a cold thermal gas around the ONF. The atom that interacts significantly with the nanofiber mode does so for approximately $1.5 \mu\text{s}$ (see atomic transit measurements in [42]). Because the atomic cloud expansion reduces the density of atoms, we limit the probing time to 1.7 ms. During this time we send a train of 200-ns probe pulses every $1.5 \mu\text{s}$ (approx. 1100 pulses). The probe beam is turned off and the MOT beams on. We reload the MOT for 20 ms and repeat the cycle. The average acquisition time for an experimental realization is around 5 hours, for a total of about 1×10^9 probe pulses.

When atoms are around the nanofiber, they tend to adhere to it due to van der Waals attraction. After a few seconds of exposing the ONF to rubidium atoms, it becomes coated with rubidium and light cannot propagate through. In order to prevent this, we use approximately 500 μW of 750 nm laser (Coherent Ti:Saph 899) during the MOT-on stage of the experimental cycle to create a repulsive potential that keeps the atoms away from the nanofiber surface. When the MOT beams turn off so does the blue beam, allowing the probed atoms to get closer to the ONF. We have also seen that $500 \mu\text{W}$ of blue detuned beam is intense enough to heat the nanofiber and accelerate atomic desorption from the surface.

Regarding the reduction of systematic errors, all the components of the magnetic field at the position of the MOT are carefully minimized. Using three sets of Helmholtz coils we reduce all residual field components to the level of 10 mG . This reduces low frequency quantum beats among different Zeeman sub-levels (with different m_F) that will shorten the apparent lifetime, and effects of atomic precession during the decay *i.e.* the Hanle effect. The intensity of the probe pulse is kept much lower than the saturation intensity, in order to reduce the atomic excitation when the pulse is nominally off. Another systematic error is the lengthening of the measured lifetime due to radiation trapping, which is the multiple scattering of a photon between different atoms [68]. Light trapped in the sample can re-excite atoms near the ONF, creating the appearance of a longer atomic lifetime. We confirm that the atomic density is low enough by mea-

suring the lifetime of atoms emitting into free space as a control measurement, similar to the approach followed in [69]. The photons collected from emission into free space come mainly from atoms far away from the ONF surface, so their time distribution should give us the well known atomic lifetime $\tau_0 = 26.24(4) \text{ ns}$ [70] in the absence of significant systematic error. We also consider the modification of the probe polarization after being scattered by the nanofiber. However, given the symmetry of the problem, a horizontally polarized incoming beam does not change polarization after interacting with the ONF. On the other hand, vertically polarized light changes polarization in the transversal plane of the nanofiber. This leads to a different arrangement of dipoles aligned along r and ϕ compare to a probe beam propagating unaltered, but does not change the overall distribution of dipoles aligned along both directions.

What about the superradiant effect?

IV. LIFETIME MEASUREMENTS

We show the normalized time distribution of photons collected through the ONF mode in Fig. 3. The red circles correspond to the data obtained for vertically polarized probe light, and the blue squares, for the horizontal one. The curves are horizontally shifted apart for clarity. The bin size is 1 ns and we typically have a thousand counts per bin at the peak. The error bars come from the statistical error of the data collection. The solid black lines are the fits to an exponential decay, and the plot underneath shows the corresponding normalized residuals. The fitting function is $Ae^{-\gamma t} + O$, where the amplitude A and the decay rate γ are the only fitting parameters, and the offset parameter O comes from the average value of the background at long times.

We vary the starting and ending point of the fitting curves and verify that as long as we are in a region within one to three natural lifetimes after the pulse turns off, there is no significant dependence on the chosen data points. Varying the end points did not change the obtained decay rate by more than 0.1%. We consider only the fits with reduced χ^2 between 0.9 and 1.5. The averaged decay rates extracted from these fits are $\langle \gamma \rangle_v / \gamma_0 = 1.088 \pm 0.015$ and $\langle \gamma \rangle_h / \gamma_0 = 0.943 \pm 0.014$ for the atoms driven by vertical and horizontal polarized probe light respectively. For these two data sets, the average of the measured free-space decay rates is $\langle \gamma_0 \rangle / \gamma_0 = 0.989 \pm 0.012$, corresponding to atoms far away fro the ONF. The uncertainties represent the amount that the fitting parameter γ has to be varied to changes the χ^2 by plus or minus one.

To study the systematic errors, we vary the magnetic field around 60 mG without observing a significant change on the decay rate. We also change the atomic density, and effects of radiation trapping bigger than the statistical errors appear when the density increases by a factor of three. The polarization of the probe pulse might also contribute with an error from a possible tilt of

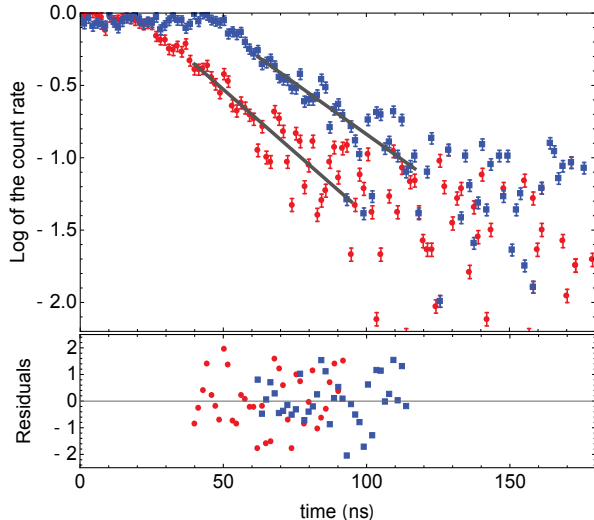


FIG. 3. Normalized time distribution of the collected photon count rate in logarithmic scale with a time bin of 1 ns. The red circles (blue squares) correspond to the data for vertically (horizontally) polarized probe light. The black solid lines are fits to exponential decays, and their residuals normalized to the standard deviation are displayed below the plot. The curves have been displaced 30 ns apart for clarity.

the ONF. We estimate this uncertainty to smaller than 10 mrad, and its effect into the total decay rate to be smaller than 0.1%.

Even though our signal to background should be in principle limited by the extinction ratio of the probe pulse (better than 1:170 after 20 ns), the signal is small enough that dark counts from the APDs become important and are our ultimate limiting factor. In our case the dark counts are around 500 counts per second, a factor of two higher than the specifications. However, the obtained signal is enough to measure a difference in the modified spontaneous emission decay rate for the two probe polarizations of almost 10 standard deviations.

V. NUMERICAL SIMULATIONS FOR A TWO-LEVEL ATOM

Most of the literature about modified spontaneous emission rates considers two-level atoms, *i.e.* classical dipoles, and we will follow that in this section. We will discuss the ramifications of our multi-level atoms in a later section.

The radiative decay rate of an atom can be modified by the boundary conditions of the electromagnetic vacuum. We consider calculating this modification by two different approaches. Each is presumably equally valid and provides a different perspective and intuition of the problem [63]. In the first one, when the mode expansion of the electromagnetic field of the full space is known, the contribution of each mode to the spontaneous emission rate

can be calculated using Fermi's golden rule (see Eq.(1)). In particular, the mode expansion of the vacuum electromagnetic field for an ONF has an analytical expression [54]. A second strategy, useful when the modes are unknown or too complicated to compute analytically, is to solve the problem from classical electrodynamics. We calculate the modification of the radiated power of a classical dipole under equivalent boundary conditions, and take that to be the modification of the radiative decay rate of the atom [71]

$$\frac{\gamma}{\gamma_0} = \frac{P}{P_0}, \quad (2)$$

where γ and γ_0 are the modified and unmodified atomic decay rates respectively, and P and P_0 are the classically calculated modified and unmodified radiative power. The modification of the radiative spontaneous emission is explained by the effect of the electric field reflected from the boundaries to the dipole position.

The latter approach allows us to develop an intuitive picture based on the idea that a two-level atom radiates as a linear dipole oscillating along the direction of the excitation field: When the atomic dipole is aligned along z and ϕ , parallel to the ONF surface, the radiated light can be reflected from the front and back interfaces created by the dielectric. These multiple reflections add at the position of the dipole affecting its emission. Because there is interference between reflections, the dipole radiation is sensitive to changes in the ONF radius. For these cases, the effect of the nanofiber can lead to enhancement or inhibition of the radiative spontaneous decay rate. On the other hand, for a dipole aligned along r we can expect little radiation reflected from the back surface of the ONF to the dipole, given the radiation pattern. For this case, the decay rate depends mainly on the distance between the atom and the ONF surface and only slightly on the nanofiber radius. An alternative viewpoint is to consider image charges. The atomic dipole induces an image dipole inside the ONF aligned in the same axis and in phase. They radiate more power than the normal atomic dipole, producing an enhancement of the decay rate for the distances we consider.

Using the second strategy, based on a classical dipole, we calculate the modification of the atomic decay rate near an optical nanofiber as a function of the ONF radius and the distance from the atom to the nanofiber surface for different atomic dipole orientations. The calculation is performed numerically with a finite-difference time-domain (FDTD) algorithm [72]. It considers the wavelength of the emitted light, and the nanofiber index of refraction to be $\lambda = 780.241$ nm and $n = 1.45367$, respectively. The result of these calculations are shown in Fig. 4 (a)-(c). It shows the modification of the atomic decay rate as a function of distance to the nanofiber and radius of the nanofiber for dipoles aligned (in cylindrical coordinates) in the (a) z -direction, (b) ϕ -direction, and (c) r -direction relative to the ONF (as sketched in Fig. (1) (b) and (c)). We identify these rates as γ_z , γ_ϕ and γ_r

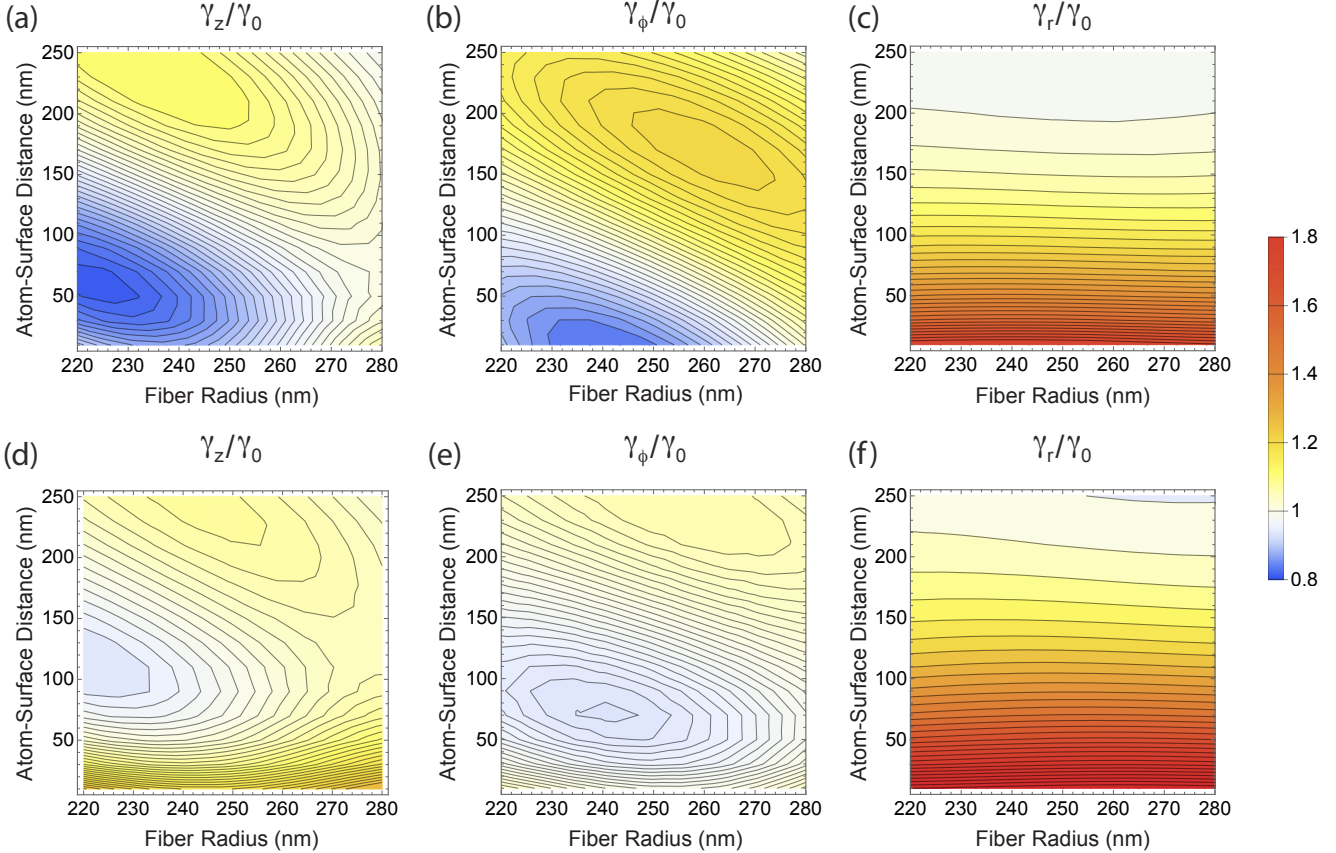


FIG. 4. Modification of the atomic spontaneous emission rate due to the presence of the ONF normalized by the free space decay rate. The results are displayed as function of the distance between the atom and the fiber surface, and the ONF radius. The three possible atomic dipole orientations can be along z , ϕ , and r . (a)-(c) show the result of FDTD calculation. (d)-(e) Show the result of a mode expansion calculation

respectively. The values of γ/γ_0 for these three cases are normalized so they are equal to one at large atom-surface distance.

The atomic decay rate of an atomic dipole aligned along z , Fig. 4 (a), is mostly inhibited close to the ONF surface compared to the free space decay rate, and it is highly dependent on the nanofiber radius. This is also true for dipoles aligned along ϕ , Fig. 4 (b). For a dipole aligned along r , Fig. 4 (c), the decay rate is enhanced and depends mostly on the distance between the atom and the ONF surface and not on the nanofiber radius.

These results are compared with the calculations of the radiative lifetime using the electromagnetic field mode expansion (taken from Ref. [54]) in Fig. 4 (d)-(f). We are interested in the limit where only the fundamental mode of the ONF can propagate, which is valid when the ONF radius is smaller than 284 nm for a wavelength of 780 nm. We observe that both calculations are qualitatively similar, but quantitatively different. The main discrepancy occurs at the fiber surface, where the mode expansion calculation seems to give a larger enhancement of the decay rate. The reason for the disagreement be-

tween both results is not understood. We have verified that other calculations based on finding the electric field at the position of the atom are in agreement with the mode expansion approach (compare Ref. [54] and [53]). On the other hand, our FDTD calculations are in agreement with previous results using the same method [61].

VI. THEORETICAL MODEL

The modification of the atomic spontaneous emission is a function of the position of the atom. Because the atoms are not trapped at a particular position, the measured decay time is a spatial average of the atomic distribution around the ONF. The main factor that determines such distribution is the van der Waals interaction between the atoms and the ONF. Moreover, atoms emit into the ONF mode with different probabilities, depending on their relative orientation and proximity to the nanofiber, altering the average of the decay time. We describe the necessary physical considerations to model the spatial average of the atomic distribution and the dipole orientation aver-

age corresponding to a multilevel atom.

A. Van der Waals potential

At short distances from the ONF the atoms feel an attractive force due to the van der Waals and Casimir-Polder (vdW-CP) potentials. These two potentials can be smoothly connected in a simple equation written as [73, 74]

$$U_{g,e}(r) = -\frac{C_4^{(g,e)}}{r^3 \left(r + C_4^{(g,e)} / C_3^{(g,e)}\right)}, \quad (3)$$

valid for the atomic ground (g) and excited (e) states, where C_3 and C_4 are the van der Waals and Casimir-Polder coefficients of the atom interacting with the nanofiber. Using the procedure described in Ref. [75] we can obtain the value of these coefficients. For a ^{87}Rb atom in the $5S_{1/2}$ ground level in front of an infinite half space fused silica medium, with index of refraction $n = 1.45$, the van der Waals and Casimir-Polder coefficients are $C_3^{(g)} = 4.94 \times 10^{-49} \text{ J}\cdot\text{m}^3$ and $C_4^{(g)} = 4.47 \times 10^{-56} \text{ J}\cdot\text{m}^4$ respectively. For the $5P_{3/2}$ excited state $C_3^{(e)} = 7.05 \times 10^{-49} \text{ J}\cdot\text{m}^3$ and $C_4^{(e)} = 12.2 \times 10^{-56} \text{ J}\cdot\text{m}^4$. The vdW-CP potential affects the experimental measurement in two different ways, by reducing the local density of atoms and by shifting the atomic levels.

By sending probe pulses to the entire atomic cloud, we actually measure a spatial average over an ensemble of atoms with a density distribution $\rho(r)$ at a radius r from the ONF surface. The vdW-CP attraction accelerates the atoms reducing the local density around the nanofiber, all of them initially in the ground state. Assuming only the radial degree of freedom and thermal equilibrium, a simple steady state density distribution can be obtained from the ideal gas law and energy conservation [75], as

$$\rho(r) \approx \rho_0 \frac{1}{1 - U_g(r)/E}, \quad (4)$$

where ρ_0 and $E = \frac{3}{2}k_B T$ are the atomic density and the average (kinetic) energy of the atoms far away from the fiber, with atoms typically at $T \approx 150 \mu\text{K}$ for our atomic cloud. By only considering U_g , we neglect the small fraction of atoms in the excited state. Fig. 5 shows an example of this distribution (blue dotted line). This approximation agrees with previous analytical results [76], and differs at most by 30% with Monte Carlo simulations of atomic trajectories [73].

The vdW-CP potentials also shift the atomic energy levels, affecting the probability to absorb the otherwise resonant probe beam as [77]

$$p_{\text{abs}}(r) = \frac{N}{1 + s + 4(\frac{\delta(r)}{\gamma_0})^2}, \quad (5)$$

where N is just a probability normalization factor and $\delta(r) = (U_e(r) - U_g(r))/2\pi\hbar$ is the detuning induced by

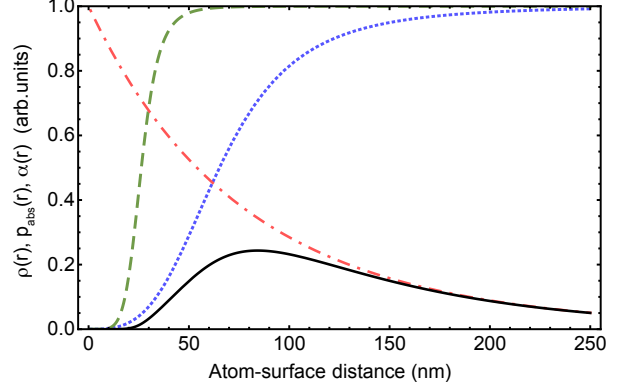


FIG. 5. Plot of the spatial dependence of $\rho(r)$ (dotted blue), $p_{\text{abs}}(r)$ (dashed green), and $\alpha(r)$ (dotted dashed red) in arbitrary units as a function of the atom-surface distance. The black solid line is the direct multiplication of these functions and it represents the distribution over which the spatial average is taken in a realistic experiment, as stated in Eq. (10).

the ONF, which for us is always red shifted. This distribution is plotted with a green dashed line in Fig. 5, neglecting s since we work in the low saturation limit.

B. Coupling into the waveguide

Another factor to consider when measuring the spontaneously emitted light into the ONF, is the fact that atoms that are closer to the nanofiber surface contribute more to the measured signal than those further away. This effect is characterized by the emission enhancement parameter

$$\alpha(r) = \frac{\gamma_{\text{wg}}(r)}{\gamma_0}. \quad (6)$$

This factor is different from the more commonly used coupling efficiency $\beta(r) = \gamma_{\text{wg}}(r)/\gamma(r)$ [78]. $\alpha(r)$ is proportional to the total number of photons emitted into the guided mode, and $\beta(r)$ is the percentage of photons emitted into the mode relative to the total number of emitted photons. The difference between α and β becomes clear with the following example: When the coupling efficiency $\beta(r)$ is very large, close to one, most of the emitted photons couple to the waveguide. However, the total number of photons emitted into the waveguide can still be close to zero if the total spontaneous emission where to be greatly inhibited, $\gamma \ll \gamma_0$ (which is not our particular case). The amplitude of the signal measured through the guided mode is then represented by the emission enhancement parameter $\alpha(r)$.

An analytical expression for $\gamma_{\text{wg}}(r)$ can be found in the literature [54, 55], and it is proportional to the norm squared of the evanescent electric field, as expressed in Eq. (1). For a single mode ONF, the spatial dependence of each component of the evanescent electric field is given

by the sum of one or two modified Bessel function of the second kind $K_i(qr')$ of order $i = 0, 1, 2$; where $r' = r_0 + r$, and r_0 and r are the ONF radius and the radial position from the ONF surface; $q = \sqrt{\beta^2 - k^2}$ is the transverse component of the wave vector, β is the field propagation constant in the ONF, and $k = 2\pi/\lambda$ is the free space wavenumber. For our particular case of an ONF with radius $r_0 = 230$ nm propagating a field of wavelength $\lambda = 780$ nm, $q = 0.56k$. Provided that $qr' > 1$ away from the ONF surface, we can simplify the calculation with the asymptotic expansion of $K_i(qr') \approx \sqrt{\pi/2}qr'e^{-qr'}$, and approximate the spatial dependence of $\gamma_{\text{wg}}(r)$ as [42]

$$\alpha(r) = \frac{\gamma_{\text{wg}}(r)}{\gamma_0} \propto \frac{1}{r_0 + r} e^{-2(0.56kr)}, \quad (7)$$

approximation that has been tested against exact numerical results with excellent agreement. Any other constant pre-factor will not contribute to the final average after the appropriate normalization. Its spatial distribution is plotted as the red dotted and dashed line in Fig. 5. For our experimental parameters $\alpha \approx 0.2$ at the ONF surface.

Atomic dipoles aligned along different direction will couple to the guided mode with different strengths. We denote the emission enhancement parameter with a subindex to specify the alignment of the emitting dipole as $\alpha_i(r)$ with $i \in \{z, \phi, r\}$. It can be shown, from the calculation in Ref. [54], that to a good approximation $\alpha_z \approx \alpha_\phi \approx \alpha_r/3$ for our ONF, independent on the radial position of the atom. The different coupling strength for atomic dipoles aligned along r comes from the fact that the radial component of the guided field is discontinuous and larger than the others due to the dielectric boundary conditions.

Figure 5 shows the spatial dependence of each one of the described distributions that affect the measured average decay rate. The black solid line in the plot represents the direct multiplication of them. This effectively describes the probability of observing a photon emitted from an atom at a position r into the ONF guided mode. Noticed that for a given ONF the only experimentally tunable parameter for the final distribution is the temperature of the atomic cloud. The atomic distribution is weakly dependent on the temperature in Eq.(4).

C. Averaged signal

The measured signal is an average of atoms decaying at different rates. If these decay rates are close enough to each other the measured decay rate is approximately equal to the spatially averaged decay rate $\langle \gamma \rangle$. As a proof let us consider that the decay rates differ by an small quantity ϵ with a distribution $g(\epsilon)$, then the measured signal is given by

$$\int d\epsilon g(\epsilon) e^{-\gamma(1+\epsilon)t} = e^{-\gamma t} \int d\epsilon g(\epsilon) e^{-\gamma \epsilon t}. \quad (8)$$

For small ϵ (and short times) the exponential of order ϵ can be expanded in series, averaged, and exponentiate again, to obtain

$$e^{-\gamma(1+\langle \epsilon \rangle)t} = e^{-\langle \gamma \rangle t} \quad (9)$$

The measured decay rate $\langle \gamma \rangle$ is a spatial average of the actual decay rate weighted by the atomic density distribution $\rho(r)$, the excitation probability $p_{\text{abs}}(r)$ and the emission enhancement parameter $\alpha(r)$.

$$\langle \gamma \rangle = \frac{\int \gamma(r) \alpha(r) \rho(r) p_{\text{abs}}(r) r dr}{\int \alpha(r) \rho(r) p_{\text{abs}}(r) r dr}. \quad (10)$$

In the particular case of driving the atoms with light polarized vertically, there are atomic dipoles oriented along r and ϕ (see Fig. 1 (c)). In this case the proper α_i has to be taken into account to obtain the averaged signal.

VII. CONSIDERATION OF THE MULTI-LEVEL ATOMIC STRUCTURE

The radiation pattern of a real atom differs from that of an ideal linear dipole. A multi-level atom (with more than one Zeeman sub-level m_F in the ground state) can decay to a ground state through a π - or σ -transition, when $\Delta m_F = 0$ or $\Delta m_F = \pm 1$ respectively. In our case, we consider the quantization axis to be along the direction of the linear polarization of the probe, and π and σ are with respect to this quantization axis.

We model the decay rate of a multi-level atom by an incoherent superposition of linear dipoles [79] that describes the real radiation pattern. An atom decaying through a π -transition is described by a linear dipole aligned along the probe polarization axis. An atom decaying through a σ -transition, is considered as a linear dipole rotating in the plane perpendicular to the probe polarization axis. The atomic decay rate depends on the norm squared of the dot product of the electric field and the dipole polarization (see Eq. (1)). This implies that the decay rate of a rotating dipole (σ -transition) is the incoherent sum of the decay rate of two orthogonal linear dipoles oscillating in the rotation plane.

All the information necessary to calculate the decay rate of different transitions of a real atom are then calculated from the decay rates of classical linear dipoles, in the spirit of Fig. 4. To calculate the total decay rate we need to know the branching ratios of the transitions. We denote the probability of decay through a π - or σ -transition as P_π and P_σ respectively. This depends on the state preparation of the atoms.

The measured signal will be a spatial average over the contribution of such classical dipoles, weighted according to the coupling efficiency of each dipole into the waveguide. Considering this, the spatially averaged decay rate

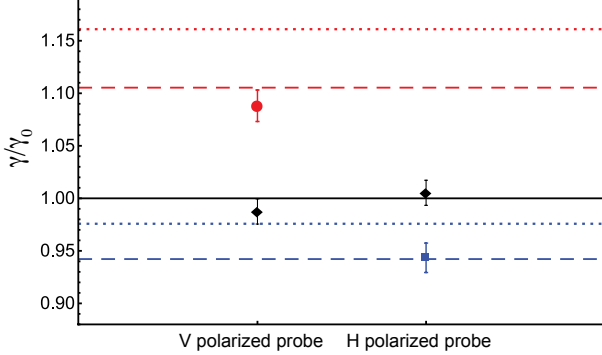


FIG. 6. Normalized decay rates for different polarizations of the probe with respect to the nanofiber. The red circle (blue square) corresponds to the measured modified lifetime of atoms driven by vertically (horizontally) polarized probe light. The black diamonds are the simultaneously measured free space decay time for each configuration. The solid black line is the expected decay rate in free space. The dashed blue and red lines are the calculated values from the two-level atom FDTD calculation for a horizontal polarized probe and a vertically polarized probe respectively. The dotted lines are the calculated values from the two-level atom mode expansion calculation. Both calculation are done considering the spatial average in Eq. (10).

can be obtained using Eqs. (4), (5) and (6), as

$$\langle\gamma\rangle_\pi = \frac{\int (\gamma_\pi(r)P_\pi\alpha_\pi(r) + \gamma_\sigma(r)P_\sigma\alpha_\sigma(r))\rho(r)p_{\text{abs}}(r)rdr}{\int (P_\pi\alpha_\pi(r) + P_\sigma\alpha_\sigma(r))\rho(r)p_{\text{abs}}(r)rdr}. \quad (11)$$

where $\gamma_i(r)$ with $i \in \{\pi, \sigma\}$ are obtained from the numerical simulation displayed in Fig. 4. The subscript π in the spatial average denotes the polarization of the probe beam that drives the atomic transition.

VIII. COMPARISON BETWEEN THEORY AND EXPERIMENT

We can compare the measurements with the theoretical simulations calculating the average $\langle\gamma\rangle/\gamma_0$ by introducing the numerical values of $\gamma(r)/\gamma_0$, displayed in Fig 4, into Eq. (10) for a particular ONF radius. It is important to notice that when we realize the experiment probing the atoms with horizontally polarized light we are measuring the spatially averaged decay rate for an atomic dipole aligned along z . For atoms driven by a vertically polarized probe pulse we measure a decay rate that is averaged over the different dipole alignments in addition to the spatial average (along ϕ and r as is shown in Fig. 1 (c)). This means that we can not separately measure the decay rate for dipoles aligned along r and ϕ .

Figure 6 shows a comparison between the measurements and the numerical simulations for a two-level atom. It shows the extracted atomic decay rates for both experimental configurations normalized by the free space one.

The blue lines are the calculated value of the modified decay rate $\langle\gamma\rangle_h/\gamma_0$, corresponding to the probe beam horizontally polarized, to be compared with the experimental value (blue square). The blue dashed line corresponds to the FDTD calculation and the dotted one the mode expansion calculation. The red lines are the calculated values of the modified decay rate $\langle\gamma\rangle_v/\gamma_0$, corresponding to the probe beam vertically polarized, to be compared with the experimental value (red circle). The red dashed line corresponds to the FDTD calculation and the dotted one the mode expansion calculation. For each experimental realization we simultaneously measure the modified atomic decay rate of atoms close to the ONF and the free space decay rate from atoms in the MOT, where the great majority of them are away from the nanofiber. The black diamonds in Fig. 6 are the measurements of the decay time into free space for the two different polarizations. When the measured decay rate is off by more than few percent of the expected value, because for example an unexpected fluctuation of the atom density, the data collected through the ONF mode was discarded.

For a multilevel atom we have to consider its initial state. During the period the probe beam is on, the atoms get pumped into a particular ground state. The steady state solution for optical pumping the $F = 2 \rightarrow F' = 3$ transition of ^{87}Rb with linearly polarized light is biased towards the $m_F = 0$ state (the fractional populations are approx. 0.04, 0.24, and 0.43 for $|m_F|$ equal 2, 1, and 0 respectively). A π excitation (linearly polarized) of such initial state, will lead to probability $P_\pi = 0.55$ of emitting π radiation and $P_\sigma = 0.45$ of emitting as a σ radiation (circularly polarized). This effect has to be taken into account when calculating the averaged decay rate using Eq. (11). Considering this, neither of our calculations, the FDTD nor the mode expansion, predict the measured values. They tend to be approximately equal to the natural decay rate for both polarizations. Even if the population distribution is different from the calculated optical pumping values, almost all population distributions tend towards producing more isotropic distributions than a linear dipole, as any amount of sigma polarization reduces the angular contrast.

The fact that the radiation pattern of a real atom is more isotropic than the one of a linear dipole questions the idea of having any significant alignment dependent effect. The spontaneous decay of an atom to a particular ground states does not depend on the atomic dipole coherence induced by the excitation, but it depends only on the branching ratio of the decay of the excited state (proportional to the square of the Clebsch–Gordan coefficients). This is an outstanding puzzle: our measurements are in good agreement with a radiating linear dipole and in disagreement with the radiation expected for the actual multi-level atom. We note that the problem of the radiation of multi-level atoms with degenerate ground states near systems with a modified environment has not been thoroughly addressed or experimentally studied.

IX. DISCUSSION

The numerical calculations have only the ONF radius and the atomic cloud temperature as adjustable parameters to match the experimental results, the former one showing a stronger effect in the expected decay rate. The fact that the decay time of an atomic dipole oriented along the fiber is strongly dependent on the nanofiber radius, gives us a possible method to measure this radius. From the error bars in the collected data, and considering the dependence on the nanofiber radius of the simulations, we determine the radius to be 235 ± 5 nm, based on the two-level atom FDTD calculation. This value is close the estimated ONF radius from the fabrication (240 nm ± 20). Having fixed the nanofiber radius, there are no free parameters in the calculation of $\langle \gamma \rangle_v / \gamma_0$ (red dotted line in Fig. 6) other than the MOT temperature, set to be $150 \mu\text{K}$.

When we calculate the spatial average, as is explained in Sec. VI, we make a series of approximations. These include the van der Waals and Casimir-Polder coefficients calculated for a dielectric plane instead of a cylinder in Eq.(3), an equilibrium distribution of the atomic density in Eq.(4), and the asymptotic expansion of the guided mode for determining the shape of $\alpha(r)$ in Eq.(6). However, when we vary all these quantities (C_3 , C_4 , ρ , and α) for 20% of their values, the final averaged decay rate does not change by more than the estimated error bars of the measurements.

We can use the physical model presented in this paper to design other experiments. From Fig. 4 (a)-(c) we can see that by positioning the atoms, for example at 50 nm from a 230 nm radius ONF, we can create atomic states can go from an approximately 40% enhancement of the spontaneous emission to 20% inhibition. This is possible by using only the atomic dipole alignment as a tuning knob for its coupling to the mode of the nanofiber and the environment. We can also use ONFs that support higher order modes to allow us to have a better control of the probe polarization, using the evanescent field of guided light, which can be used to drive different atomic dipole orientations, such as purely radial or azimuthal.

The discrepancy between different calculations has yet to be understood. It is also necessary to develop better physical picture that explains the measured behavior for a real multi-level atom near an ONF. This problem bring fundamental questions that need to be revised and systematically study in the future, crucial for any future application of multi-level atoms coupled to optical wave-

guides.

X. CONCLUSION

We have experimentally observed the modification of the rate of spontaneous emission of atoms near an optical nanofiber and its dependence on the atomic dipole alignment. The experiment is implemented by placing an ONF at the center of a cold atomic cloud. A linearly polarized resonant probe pulse drives the atomic dipoles in a particular alignment. We measured the time distribution of spontaneously emitted photons into the ONF to obtain the atomic lifetime. The modification of the atomic lifetime is measured for different probe polarizations in order to show the dependence on the atomic dipole alignment of the spontaneous emission rate.

A physical model of the experiment is also presented and used to perform a numerical calculation of the modification of the spontaneous emission rate. This shows a good quantitative agreement with the experimental measurements considering two-level atoms. Some basic physical aspect remain elusive, regarding the multi-level structure of a real atom. This work clearly demonstrates that there are open problems that need further investigation - a perhaps surprising conclusion given the fundamental nature of the simple problem of an atom radiating near a dielectric. A better understanding of the problem will allow us to extend this knowledge to more general cases. With this knowledge of how atomic properties change under different conditions, we can start implementing a new toolbox for precisely manipulating and controlling atoms coupled to optical waveguides.

DISCLAIMER

Any mention of commercial products in a publication having NIST authors is for information only; it does not imply recommendation or endorsement by NIST.

ACKNOWLEDGMENTS

We would like to thank H. J. Charmichael and A. Asenjo-Garcia for their valuable contributions to the discussion. This research was supported by the National Science Foundation of the United States (NSF) (PHY-1307416); NSF (CBET-1335857); NSF (PHY-1430094); and the USDOC, NIST, Joint Quantum Institute (70NANB16H168).

[1] J. D. Thompson, T. G. Tiecke, N. P. de Leon, J. Feist, A. V. Akimov, M. Gullans, A. S. Zibrov, V. Vuletić, and

M. D. Lukin, *Science* **340**, 1202 (2013).

- [2] J. Petersen, J. Volz, and A. Rauschenbeutel, *Science* **346**, 67 (2014).
- [3] R. Mitsch, C. Sayrin, B. Albrecht, P. Schneeweiss, and A. Rauschenbeutel, *Nature Communications* **5**, 5713 (2014).
- [4] A. Goban, C.-L. Hung, J. . Hood, S.-P. Yu, J. A. Muniz, O. Painter, and H. . Kimble, *Physical Review Letters* **115**, 063601 (2015).
- [5] A. Goban, C.-L. Hung, S.-P. Yu, J. D. Hood, J. A. Muniz, J. H. Lee, M. J. Martin, A. C. McClung, K. S. Choi, D. E. Chang, O. Painter, and H. J. Kimble, *Nature Communications* **5**, 3808 (2014).
- [6] R. Yalla, F. Le Kien, M. Morinaga, and K. Hakuta, *Physical Review Letters* **109**, 063602 (2012).
- [7] C. Junge, D. O'Shea, J. Volz, and A. Rauschenbeutel, *Physical Review Letters* **110**, 213604 (2013).
- [8] J. Volz, M. Scheucher, C. Junge, and A. Rauschenbeutel, *Nature Photonics* **8**, 965 (2014).
- [9] R. N. Patel, T. Schröder, N. Wan, L. Li, S. L. Mouradian, E. H. Chen, and D. R. Englund, *Light: Science & Applications* **5**, e16032 (2016).
- [10] S. Rosenblum, O. Bechler, I. Shomroni, Y. Lovsky, G. Guendelman, and B. Dayan, *Nature Photonics* **10**, 19 (2016).
- [11] D. O'Shea, C. Junge, J. Volz, and A. Rauschenbeutel, *Physical Review Letters* **111**, 193601 (2013).
- [12] I. Shomroni, S. Rosenblum, Y. Lovsky, O. Bechler, G. Guendelman, and B. Dayan, *Science* **345**, 903 (2014).
- [13] T. G. Tiecke, J. D. Thompson, N. P. de Leon, L. R. Liu, V. Vuletić, and M. D. Lukin, *Nature* **508**, 241 (2014).
- [14] C. Sayrin, C. Junge, R. Mitsch, B. Albrecht, D. O'Shea, P. Schneeweiss, J. Volz, and A. Rauschenbeutel, *Physical Review X* **5**, 041036 (2015).
- [15] Y. Shen, M. Bradford, and J.-T. Shen, *Physical Review Letters* **107**, 173902 (2011).
- [16] D. E. Chang, A. S. Sørensen, E. A. Demler, and M. D. Lukin, *Nature Physics* **3**, 807 (2007).
- [17] B. Gouraud, D. Maxein, A. Nicolas, O. Morin, and J. Laurat, *Physical Review Letters* **114**, 180503 (2015).
- [18] C. Sayrin, C. Clausen, B. Albrecht, P. Schneeweiss, and A. Rauschenbeutel, *Optica* **2**, 353 (2015).
- [19] D. E. Jones, J. D. Franson, and T. B. Pittman, *Physical Review A* **92**, 043806 (2015).
- [20] R. Kumar, V. Gokhroo, and S. Nic Chormaic, *New Journal of Physics* **17**, 123012 (2015).
- [21] E. Fermi, *Nuclear Physics* (The University of Chicago Press, 1949).
- [22] E. M. Purcell, *Physical Review* **69**, 674 (1946).
- [23] F. Le Kien and A. Rauschenbeutel, *Physical Review A* **93**, 043828 (2016).
- [24] V. Bordo, *Journal of the Optical Society of America B* **29**, 1799 (2012).
- [25] J. Barthes, G. Colas des Francs, A. Bouhelier, J.-C. Weeber, and A. Dereux, *Physical Review B* **84**, 073403 (2011).
- [26] P. Lodahl, A. Floris van Driel, I. S. Nikolaev, A. Irman, K. Overgaag, D. Vanmaekelbergh, and W. L. Vos, *Nature* **430**, 654 (2004).
- [27] D. Englund, D. Fattal, E. Waks, G. Solomon, B. Zhang, T. Nakaoaka, Y. Arakawa, Y. Yamamoto, and J. Vučković, *Physical Review Letters* **95**, 013904 (2005).
- [28] P. Lodahl, S. Mahmoodian, and S. Stobbe, *Rev. Mod. Phys.* **87**, 347 (2015).
- [29] B. le Feber, N. Rotenberg, and L. Kuipers, *Nature Communications* **6**, 6695 (2015).
- [30] A. T. Nguyen and T. H. Dung, *The European Physical Journal D* **46**, 173 (2008).
- [31] H. Nha and W. Jhe, *Journal of the Korean Physical Society* **32**, 342 (1998).
- [32] C. Creatore, L. C. Andreani, M. Miritello, R. Lo Savio, and F. Priolo, *Applied Physics Letters* **94**, 103112 (2009).
- [33] M. S. Eggleston, K. Messer, L. Zhang, E. Yablonovitch, and M. C. Wu, *Proceedings of the National Academy of Sciences* **112**, 1704 (2015).
- [34] E. Yablonovitch, *Physical Review Letters* **58**, 2059 (1987).
- [35] C. Ropp, Z. Cummins, S. Nah, J. T. Fourkas, B. Shapiro, and E. Waks, *Nature Communications* **6**, 6558 (2015).
- [36] M. J. Morrissey, K. Deasy, M. Frawley, R. Kumar, E. Prel, L. Russell, V. G. Truong, and S. Nic Chormaic, *Sensors* **13**, 10449 (2013).
- [37] G. Y. Chen, *The Open Optics Journal* **7**, 32 (2013).
- [38] J. E. Hoffman, S. Ravets, J. A. Grover, P. Solano, P. R. Kordell, J. D. Wong-Campos, L. A. Orozco, and S. L. Rolston, *AIP Advances* **4**, 067124 (2014).
- [39] F. L. Kien, J. Liang, K. Hakuta, and V. Balykin, *Optics Communications* **242**, 445 (2004).
- [40] X. Qi, B. Q. Baragiola, P. S. Jessen, and I. H. Deutsch, *Physical Review A* **93**, 023817 (2016).
- [41] K. Nayak, M. Das, F. L. Kien, and K. Hakuta, *Optics Communications* **285**, 4698 (2012), special Issue: Optical micro/nanofibers: Challenges and Opportunities.
- [42] J. A. Grover, P. Solano, L. A. Orozco, and S. L. Rolston, *Physical Review A* **92**, 013850 (2015).
- [43] M. J. Morrissey, K. Deasy, Y. Wu, S. Chakrabarti, and S. Nic Chormaic, *Review of Scientific Instruments* **80**, 053102 (2009).
- [44] E. Vetsch, D. Reitz, G. Sagué, R. Schmidt, S. T. Dawkins, and A. Rauschenbeutel, *Physical Review Letters* **104**, 203603 (2010).
- [45] D. Reitz, C. Sayrin, R. Mitsch, P. Schneeweiss, and A. Rauschenbeutel, *Physical Review Letters* **110**, 243603 (2013).
- [46] S. Kato and T. Aoki, *Physical Review Letters* **115**, 093603 (2015).
- [47] A. Goban, K. S. Choi, D. J. Alton, D. Ding, C. Lacroûte, M. Pototschnig, T. Thiele, N. P. Stern, and H. J. Kimble, *Physical Review Letters* **109**, 033603 (2012).
- [48] J.-B. Béguin, E. M. Bookjans, S. L. Christensen, H. L. Sørensen, J. H. Müller, E. S. Polzik, and J. Appel, *Physical Review Letters* **113**, 263603 (2014).
- [49] P. Solano, F. K. Fatemi, L. A. Orozco, and S. L. Rolston, *arXiv:1703.09122* (2017).
- [50] N. V. Corzo, B. Gouraud, A. Chandra, A. Goban, A. S. Sheremet, D. V. Kupriyanov, and J. Laurat, *Physical Review Letters* **117**, 133603 (2016).
- [51] H. L. Sørensen, J.-B. Béguin, K. W. Kluge, I. Iakourov, A. S. Sørensen, J. H. Müller, E. S. Polzik, and J. Appel, *Physical Review Letters* **117**, 133604 (2016).
- [52] P. Lodahl, S. Mahmoodian, S. Stobbe, P. Schneeweiss, J. Volz, A. Rauschenbeutel, H. Pichler, and P. Zoller, *Nature* **541**, 473 (2017).
- [53] V. V. Klimov and M. Ducloy, *Physical Review A* **69**, 013812 (2004).
- [54] F. Le Kien, S. Dutta Gupta, V. I. Balykin, and K. Hakuta, *Physical Review A* **72**, 032509 (2005).

- [55] F. Le Kien and A. Rauschenbeutel, *Physical Review A* **90**, 023805 (2014).
- [56] F. Le Kien, V. I. Balykin, and K. Hakuta, *Physical Review A* **73**, 013819 (2006).
- [57] F. L. Kien and K. Hakuta, *Physical Review A* **77**, 013801 (2008).
- [58] F. Le Kien and K. Hakuta, *Physical Review A* **78**, 063803 (2008).
- [59] K. Hakuta and K. P. Nayak, *Advances in Natural Sciences: Nanoscience and Nanotechnology* **3**, 015005 (2012).
- [60] M. Almokhtar, M. Fujiwara, H. Takashima, and S. Takeuchi, *Optics Express* **22**, 20045 (2014).
- [61] N. R. Verhart, G. Lepert, A. L. Billing, J. Hwang, and E. A. Hinds, *Optics Express* **22**, 19633 (2014).
- [62] M. Gaio, M. Moffa, M. Castro-Lopez, D. Pisignano, A. Camposeo, and R. Sapienza, *ACS Nano* **10**, 6125 (2016).
- [63] E. A. Hinds, in *Advances In Atomic, Molecular, and Optical Physics*, Vol. 28, edited by D. B. a. B. Bederson (Academic Press, 1990) pp. 237–289.
- [64] A. Corney, *Atomic and Laser Spectroscopy* (Oxford University Press, 1979).
- [65] C. W. Oates, K. R. Vogel, and J. L. Hall, *Physical Review Letters* **76**, 2866 (1996).
- [66] D. O'Connor and D. Phillips, *Time-correlated single photon counting* (Academic Press, 1984).
- [67] F. K. Fatemi, J. E. Hoffman, P. Solano, E. F. Fenton, G. Beadie, S. L. Rolston, and L. A. Orozco, *Optica* **4**, 157 (2017).
- [68] A. F. Molisch and B. P. Oehry, *Radiation Trapping in Atomic Vapours* (Oxford University Press, 1998).
- [69] J. E. Simsarian, L. A. Orozco, G. D. Sprouse, and W. Z. Zhao, *Physical Review A* **57**, 2448 (1998).
- [70] U. Volz and H. Schmoranzer, *Physica Scripta* **1996**, 48 (1996).
- [71] L. Novotny and B. Hecht, *Principles of Nano-Optics* (Cambridge University Press, 2012).
- [72] A. Taflove and S. C. Hagness, *Computational Electrodynamics: The Finite-Difference Time-Domain Method, Third Edition*, 3rd ed. (Artech House, 2005).
- [73] F. Le Kien and K. Hakuta, *Physical Review A* **77**, 042903 (2008).
- [74] L. Russell, D. A. Gleeson, V. G. Minogin, and S. Nic Chormaic, *Journal of Physics B: Atomic, Molecular and Optical Physics* **42**, 185006 (2009).
- [75] J. A. Grover, *Atom-trapping and photon-counting experiments with optical nanofibers*, Ph.D. thesis, University of Maryland (2015).
- [76] G. Sagué, E. Vetsch, W. Alt, D. Meschede, and A. Rauschenbeutel, *Physical Review Letters* **99**, 163602 (2007).
- [77] C. J. Foot, *Atomic Physics* (Oxford University Press, 2005).
- [78] Q. Quan, I. Bulu, and M. Lončar, *Physical Review A* **80**, 011810 (2009).
- [79] D. Polder and M. F. H. Schuurmans, *Physical Review A* **14**, 1468 (1976).

Chapter 4: Atom-atom interaction mediated by an ONF

ONF guided modes create a preferential channel for the atomic radiation field. This is a virtually lossless channel that mediates the interaction between distant atoms along the nanofiber, even when they are not trapped. This presents a novel realization of many-body states in one-dimension with, so called, infinite-range interaction.

Infinite-range interactions are a newly experimentally accessible physical phenomena allowed by interfacing atoms with the guided mode of an optical waveguide. Photons emitted from one atom into the waveguide can propagate unaltered and interact with the same coupling strength with all the other atoms along the line. The only way that the photon can leave the waveguide is if it were scattered out by an atom. The relevant parameter for infinite-range interactions is the ratio between the rate of emission into the waveguide and out of the waveguide. This is the definition of cooperativity, as defined in Chap.1. High cooperativity means that the system is effectively one dimensional, where every excitation in the system has to interact with all the atoms, because it does not have anywhere else to go. Sec. 4.1 presents an introduction to this effect.

Systems interacting at infinite-range lead to interesting features that are elu-

sive, or even not accessible, for more than one dimension. One particular example is self-organization. When an ensemble of atoms interact strongly enough with each other through the common guided mode they tend to self-organize, as in a crystal. Provided with excitations, atoms go through multiple scattering event of photons in both directions of the waveguide. The spontaneous emission provides a dissipation mechanisms that leads the system to an equilibrium where it stays at its energy minimum. This is briefly discussed in Sec. 4.2.

Another fascinating consequence of infinite-range interaction is that they allow macroscopically separated collective atomic states. Collective states are the states of a composite system that evolve as a whole with dynamics that differs from that of the individual subsystems, as it is discussed in Sec. 4.3. These states, while entangled, differ from just entangled states in their dynamics. Interaction between the subsystems are necessary to create a collective state. Since separated subsystems can interact with each other through the waveguide along distances of many wavelengths, we can in principle create a system that is macroscopically delocalized. We will present a way to observe this kind of system in Sec. 4.4, by using an ONF and through the observation of superradiance, the main result of this chapter. Finally, in Sec. 4.5 we discuss how ONFs can help us to study subradiance, an effect that is otherwise challenging to observe.

4.1 Infinite-range interactions

When two atoms are in free-space, they interact with each other through a dipolar interaction mediated by the propagating electromagnetic field. This is like two cross-talking antennae. Because the radiated field decays inversely with distance, when the atoms are more than a wavelength apart their interaction quickly becomes negligible. Free-space atom-atom interactions are long range compared to the size of the atoms, but remain short range compared to size of a usual atomic ensemble. This implies that in a cold atomic gas, or in a lattice of atoms, the atom-atom interaction usually occurs among nearest neighbors.

The electromagnetic field that propagates in a waveguide does not present this problem, because being confined, it does not decay with distance. When two atoms can radiate into the guided mode of an ideal waveguide, the mediating field does not decrease its amplitude with distance, with a sinusoidal spatial modulated. This allows coupling of atoms at infinite range. When there are more than two atoms coupled to the same waveguide, they can all interact with each other with the same coupling strength. The constraint of nearest neighbor interaction mentioned above are removed. This could in principle create novel many-body systems where all the subsystems can identically couple to each other.

Although some current experiments, such as those using ONF and photonic waveguides, have the capability to observe infinite-range interaction between distant subsystems, it has not been experimentally studied. The observation of this effect is the main goal of Sec. 4.4. There have been a few theoretical works considering

the implication of infinite-range interaction [56, 109, 110].

4.2 Self-Organization of atoms around an ONF

An interesting system to study is the collective off-resonant scattering of coherent light by a cold gas in a one dimensional configuration [111]. The scattering into a one dimensional waveguide induces infinite-range interactions. Via interference of light, scattered by different atoms, that can propagate through the ONF, it is possible to observe phase transitions of the atomic spatial order as a function of the external pump intensity. This is evidence of self-organization: a crystallization of the atomic ensemble in a periodic array, similar to Ref. [112].

Similar studies have been carried for slightly different nanophotonic structures and under different conditions[109, 113, 114]. In particular, ONFs could in principle provide the platform necessary to have coupling among all the atoms in the system, leading to spontaneous organization. For a detailed discussion about the role of long-range interaction in self-organized systems see Ref.[115].

4.3 Single excitation collective states

Before going into the details of the observation of collective states (super and subradiance) in an ONF, we introduce the theoretical framework.

The master equation that describes the dynamics of an ensemble of atomic dipoles coupled to a single common mode is given by [116]

$$\dot{\rho} = -i [H_{dd}, \rho] + \mathcal{L}_{dd}[\rho]. \quad (4.1)$$

where ρ is the density matrix of the atomic ensemble, and the Hamiltonian and Lindblad super operator are

$$H_{dd} = \frac{1}{2} \sum_{i,j} \hbar \Omega_{ij} \sigma_i^\dagger \sigma_j, \quad (4.2)$$

$$\mathcal{L}_{dd}[\rho] = \frac{1}{2} \sum_{i,j} \hbar \gamma_{ij} \left(2\sigma_j \rho \sigma_i^\dagger - \sigma_i^\dagger \sigma_j \rho - \rho \sigma_i^\dagger \sigma_j \right), \quad (4.3)$$

with σ_i (σ_i^\dagger) being the atomic lowering (raising) operator for an excitation of the i -th atom.

The non-dissipative or dispersive evolution of the system is given by the frequencies Ω_{ij} , often call dipole-dipole coupling. Ω_{ij} is the contribution of the i -th atom to the energy shift of the j -th atom, and vice versa. The dissipative evolution of the system is given by the decay rates γ_{ij} . γ_{ij} is the contribution of the i -th atom to the decay rate of the j -th atom, and vice versa. The effect of Ω_{ij} and γ_{ij} on the dynamic of the system is ultimately determined by the atomic dipoles, as expressed in Eqs. (4.2) and (4.3) respectively.

For atoms interacting in free-space, Ω_{ij} and γ_{ij} are proportional to the real and imaginary part – respectively – of the complex electric field radiated by a linear dipole [116]

$$\Omega_{ij} = \gamma_0 \frac{3}{4} \left\{ -[1 - (\hat{d} \cdot \hat{r}_{ij})^2] \frac{\cos \xi_{ij}}{\xi_{ij}} + [1 - 3(\hat{d} \cdot \hat{r}_{ij})^2] \left(\frac{\sin \xi_{ij}}{\xi_{ij}^2} + \frac{\cos \xi_{ij}}{\xi_{ij}^3} \right) \right\} \quad (4.4)$$

$$\gamma_{ij} = \gamma_0 \frac{3}{2} \left\{ -[1 - (\hat{d} \cdot \hat{r}_{ij})^2] \frac{\sin \xi_{ij}}{\xi_{ij}} + [1 - 3(\hat{d} \cdot \hat{r}_{ij})^2] \left(\frac{\cos \xi_{ij}}{\xi_{ij}^2} - \frac{\sin \xi_{ij}}{\xi_{ij}^3} \right) \right\} \quad (4.5)$$

where $\xi_{ij} = kr_{ij}$ is proportional to the distance r_{ij} between the i -th and j -th atom and k is the norm of the wavevector.

Notice that the coupling strength between two atoms decays inversely with

their separation, imposing a limit on how far the interacting atoms have to be. In addition, the dispersive term Ω_{ij} diverges as the atoms get closer, producing a large frequency shift [117]. This does not present an issue for only two interacting atoms. However, when more than two atoms are close together, this term creates dephasing between the interacting dipoles, destroying the collective state. These two effects combined impose a fundamental limit in the number of atoms that can be in a collective state interacting through free-space, since they would all have to be closer than a wavelength, but not too close.

This scenario changes when using waveguides to confine the electromagnetic field in one dimension. If the coupling rate of a single atom into the waveguide is γ_{1D} and into modes radiated out of the waveguide is γ_{rad} , the dispersive and dissipative term of the master equation, ignoring direct (non-guided) coupling, are given by [56]

$$\Omega_{ij} = \gamma_{1D} \sin(k |z_i - z_j|); \quad (4.6)$$

$$\gamma_{ij} = \gamma_{\text{rad}} \delta_{ij} + \gamma_{1D} \cos(k |z_i - z_j|) \quad (4.7)$$

where z_i is the position of the i -th atom along the waveguide, and δ_{ij} is a Kronecker delta. $\gamma_{ii} = \gamma_{\text{rad}} + \gamma_{1D}$ is the total decay rate of a single atom, γ_{tot} .

Atomic dipoles interacting through a waveguide do not have the constraint present in the free-space case. The dispersive term Ω_{ij} does not diverge, and atoms interact at virtually infinite distances.

We are interested in collective states in the weak excitation limit, for which we follow the mathematical treatment in Ref. [118]. Let us consider only one excitation

in a system composed of N atoms, represented by the state

$$|\Psi\rangle = \sum_{\mathbf{k}} a_{\mathbf{k}}(t) |g_1 g_2 \cdots g_N\rangle |1_{\mathbf{k}}\rangle + \sum_{j=1}^N b_j(t) |g_1 g_2 \cdots e_j \cdots g_N\rangle |0\rangle \quad (4.8)$$

where the sum over \mathbf{k} is done over modes of the electromagnetic field where the excitation decays. g_i and e_i are the ground and excited state of the i -th atom. The normalization of the states imposes that $\sum_{\mathbf{k}} |a_{\mathbf{k}}(t)|^2 + \sum_{j=1}^N |b_j(t)|^2 = 1$ at all time t .

Assuming that we start the evolution of the system with one excitation in the atoms and none in the field, *i.e.* $a_{\mathbf{k}}(0) = 0$, we can write the Schrödinger equation in the Markov approximation for the coefficients $b_i(t)$ as

$$\dot{b}_i(t) = - \sum_{j=1}^N \Lambda_{ij} b_j(t) \quad (4.9)$$

where $\Lambda_{ij} = \gamma_{ij} - i\Omega_{ij}$ captures the full dynamics of the system.

We can solve the set of equations (4.9) in matrix form as

$$\dot{B} = -\Lambda B, \quad (4.10)$$

where B is a vector with the $b_j(t)$ coefficients as entries and Λ is a symmetric matrix with the values of Λ_{ij} as entries. Considering the system to be in an eigenstate of Λ with eigenvalue λ_i , we obtain

$$B_i(t) = e^{-\lambda_i t} B_i(0). \quad (4.11)$$

where $B_i(t)$ is an eigenvector that gives the eigenstate of the system.

The eigenvectors of Eq. (4.10) represent the collective states of the system, with evolution governed by λ_i . The imaginary part of λ_i is proportional to the

energy shift of the state i -th eigenstate. The system decays with a rate given by the real part of λ_i . If the real part of a particular λ_i is larger or smaller than γ_{tot} we call it a superradiant or a subradiant state respectively.

4.4 Super- and sub-radiance mediated by an ONF

We observe infinite-range interaction by creating and measuring a collective atomic state of atoms along an ONF. These type of states are enabled by interacting subsystems. If they interact constructively, they decay faster. If they interact destructively, they decay slower. We call these two behaviors super- and sub-radiance respectively. The observation of a super or a subradiant behavior is a signature of the interaction among at least two atoms out of the ensemble. If we observe this effect from atoms separated further than a wavelength, coupled to each other through the ONF, there is evidence of infinite-range interactions.

Collective effects become readily visible for a large enough coupling efficiency, with the figure of merit being the cooperativity (see Eqs. (1.12) and (1.3)). To achieve high cooperativity we need to place the atoms as close as possible to the ONF. We do so using the following pumping scheme on ^{87}Rb atoms: All the atoms in the MOT are prepared in the $F = 1$ hyperfine state. We send a pump beam thorough the ONF resonant with the $F = 1 \rightarrow F = 2$ transition, to pump into the $F = 2$ state only the atoms that interact with the ONF guided mode. The position of the pumped atoms can be selected by detuning the pump laser to the red, such that atoms at a particular distance from the ONF experience a van der Waals shift (see

Sec. 3.1 for details) that makes them resonant with the pump beam. In particular, we shift the pump frequency by 15 MHz, pumping those atoms that are in average 30 nm away from the ONF surface. At this position we reach an efficiency $\beta \sim 0.13$. This allows atom-atom interactions mediated by the nanofiber. With this scheme, we see evidence for infinite-range interactions through superradiance.

Superradiance mediated by infinite-range interaction presents another advantage over free space superradiance. This is related to the dispersive part of the interaction, as explained in the previous section. When atoms interact, there are two collective effects that take place, dissipation and dispersion [117]. The dissipative part of interaction is the one related to the decay rate of the system (super or subradiance). The dispersive part is related to the spectrum of the system. For atoms interacting in free space, the dispersive part diverges as they get closer. This imposes a limit for the observation of collective states of many atoms in free space. Infinite-range interactions solve this. The dispersive part of the interaction does not diverge, making possible, as a future field of study, the observation of a collective state of thousands of atoms along an ONF. In this scenario, a possible ultimate limit is the number of atoms that can be placed within the coherence length of a spontaneously emitted photon.

Here we present our work on the observation of infinite-range interaction in an ONF.

Super- and sub-radiance reveal infinite-range interactions through a nanofiber

P. Solano¹, P. Barberis-Blostein^{1,2}, F. K. Fatemi³, L. A. Orozco¹, and S. L. Rolston¹

¹Joint Quantum Institute. Department of Physics and NIST, University of Maryland, College Park, MD 20742, USA. ²Instituto de Investigaciones en Matemáticas Aplicadas y en Sistemas, Universidad Nacional Autónoma de México, Ciudad Universitaria, 04510, DF, México. ³Army Research Laboratory, Adelphi, MD 20783, USA.

Atoms interact with each other through the electromagnetic field, creating collective states that can radiate faster or slower than a single atom, i.e. super- and sub-radiance^{1,2}. The generation and control of such states by engineering the dipolar interactions between atoms can enable new tools for atomic-based technologies³. Atom-atom interactions in free space are limited in range, since the amplitude of the radiated field decreases inversely with distance. When the field is confined to one dimension it propagates unaltered, allowing infinite-range interactions⁴. Here we present the first report of infinite-range interactions between atomic dipoles mediated by an optical waveguide. This is evidenced by the collective radiative decay of a single-photon distributed between distant atoms. We use cold ⁸⁷Rb atoms in the vicinity of a single-mode optical nanofiber (ONF)⁵ that coherently exchange evanescently coupled photons through the ONF mode. In particular, we observe super-radiance of a few atoms separated by hundreds of resonant wavelengths. This effect is not possible for atoms separated by more than a wavelength interacting through free space. The same platform allows us to measure sub-radiance, a rarely observed effect⁶, presenting a novel tool for quantum optics. This result constitutes a proof-of-principle for collective behavior of macroscopically delocalized atomic states, a crucial element for new proposals in quantum information^{7,8} and many-body physics^{9,10}. Given the application of one-dimensional waveguides in photonic-based quantum technologies^{11–21}, we envision infinite-range interactions as the natural next step towards interconnecting quantum systems on scales suitable for practical applications.

A new class of quantum technologies exploits the interfaces between propagating photons and cold atoms. Recent realizations using nanophotonic platforms include optical isolators¹², switches^{13–15}, memories^{20,21}, and reflectors^{22,23}. These devices guide the electromagnetic field, a feature that could allow us to engineer and control a collective time evolution of macroscopically separated subsystems. States that evolve as a whole with dynamics different to that of the independent subsystems, are called collective state. These states emerge from atoms interacting via a common mode of the electromagnetic field.

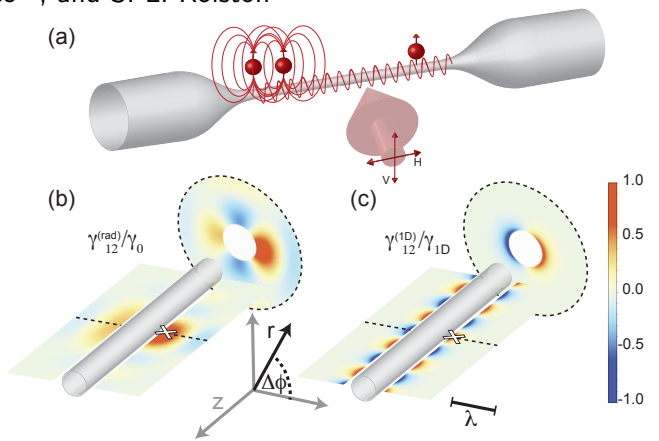


Figure 1 | (a) Schematic of an ONF as a platform for generating single-photon collective atomic states, excited from the side by a weak probe of polarization V or H. When two atoms are close together the dipolar interaction is mostly mediated by the modes of the electromagnetic field radiating outside the nanofiber. This is a limited-range interaction that decays inversely with distance. When the atoms are widely separated, the guided mode of an ideal ONF mediates the interaction for arbitrary distances. (b) and (c) show the atom-atom interaction rate γ_{12} (see Eq (4)) experienced by an atom around the fiber given another atom at the position denoted by the white cross (see Methods for the details of the calculation). Its amplitude is shown for a longitudinal and a transversal cut (specified by dashed black lines). Both plots share the color scale, but in (b) the interaction rate is normalized by the single atom total decay rate γ_0 and in (c) by the decay rate into the guided mode γ_{1D} . Along the z-axis the interaction among atoms through free space radiation modes decreases as $\gamma_{12}^{(\text{rad})} \propto \sin(k|\Delta z|)/k\Delta z$ (with k being the wavenumber and Δz the separation between two atoms). The infinite interaction through the ONF guided mode changes as $\gamma_{12}^{(1D)} \propto \cos(k\Delta z)\cos(\Delta\phi)$ (with $\Delta\phi$ the angle difference in cylindrical coordinates). The wavelength λ sets the scale of the graphic.

For an ensemble of N two level atoms, in the single excitation limit,

$$|\Psi_j(t)\rangle \propto e^{-\frac{1}{2}(\gamma_j+i\Omega_j)t} \sum_{k=1}^N c_{jk}|g_1g_2 \cdots e_k \cdots g_N\rangle \quad (1)$$

represents the j -th collective state of the system, where γ_j and Ω_j are its collective decay and frequency shift respectively, and $\sum_{k=1}^N |c_{jk}|^2 e^{-\gamma_j t}$ is the probability of having an excitation in the atoms. When γ_j is larger (shorter) than the natural radiative decay time γ_0 , the system is super- (sub-) radiant¹. In the simplest case, collective states emerge when all the atoms lie within

a wavelength²⁴. By externally exciting the atoms, super-radiant states are readily observed (see *e.g.* Goban *et al.*¹⁹), but because sub-radiant states are decoupled from the electromagnetic vacuum field, they are challenging to produce⁶.

The master equation that describes the dynamic of an ensemble of atomic dipoles, of density matrix ρ , coupled through a single common electromagnetic mode is given by²⁵

$$\dot{\rho} = -i [H_{\text{eff}}, \rho] + \mathcal{L}[\rho]. \quad (2)$$

The effective Hamiltonian H_{eff} of the dipolar interaction between atoms and the Lindblad super operator \mathcal{L} in Eq. (2) modify two atomic properties: the resonance frequency and the spontaneous decay rate respectively. They are given by

$$H_{\text{eff}} = \frac{1}{2} \sum_{i,j} \hbar \Omega_{ij} \sigma_i^\dagger \sigma_j, \quad (3)$$

$$\mathcal{L}[\rho] = \frac{1}{2} \sum_{i,j} \hbar \gamma_{ij} (2\sigma_j \rho \sigma_i^\dagger - \sigma_i^\dagger \sigma_j \rho - \rho \sigma_i^\dagger \sigma_j), \quad (4)$$

with σ_i (σ_i^\dagger) being the atomic lowering (raising) operator for an excitation of the i -th atom. Ω_{ij} is the rate of photons exchanged between atoms and γ_{ij} is the coupling term responsible for collective radiative decays, where $\gamma_{ii} = \gamma_0$. The decay of an excitation in such a system, that leads to a collective state as in Eq. (1), depends on the coupling amplitudes and relative phase between the atoms given by γ_{ij} .

When atoms are far apart in free space their interaction is mediated by a propagating field with an expanding wavefront, and a separation of few wavelengths is enough to make the interaction negligible. As atoms get closer together, Ω_{ij} in Eq. (3) diverges, reducing the coherence of a system with more than two atoms. These constraints can be circumvented by using longer wavelengths with larger atomic-dipole moments, such as Rydberg atoms²⁶, or long-range phonon modes, implemented with trapped ions^{27,28}. However, these techniques are limited to subwavelength distances.

Waveguides offer an alternative by confining the mediating field. The guided field propagates unaltered, facilitating the coupling of atoms separated by many wavelengths (see Fig. 1). Dipole-dipole interactions, given by Ω_{ij} , are finite for atoms along the waveguide, removing a practical limit for creating superradiant states of a large number of atoms. Such a system has been implemented with superconducting waveguides and two artificial atoms one wavelength apart²⁹, but has not been realized for many atoms at multi-wavelength distances in the optical regime.

We present the implementation of collective atomic states through infinite-range interactions via a one-dimensional nanophotonic waveguide. We use a few atoms evanescently coupled to a single-mode optical nanofiber (ONF)⁵. We observe super- and sub-radiant radiative decays of a single excitation in the system, evidencing collective behavior.

Atoms around the ONF interact at short and long distances (see Fig 1 (a)), the latter mediated by the ONF guided mode. The dipolar interaction that leads to a collective decay, is separated into two contributions of the electromagnetic field: from modes radiating outside the ONF, $\gamma_{12}^{(\text{rad})}$, and from the guided mode, $\gamma_{12}^{(1D)}$ ²⁵ (see Fig. 1 (b) and (c)).

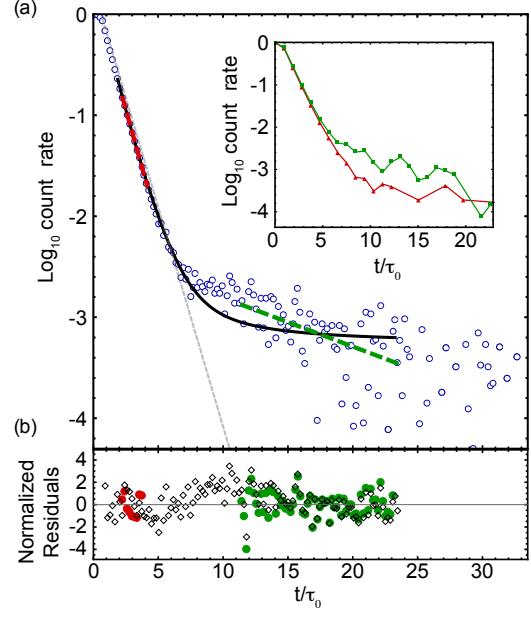


Figure 2 | (a) Normalized rate of photons detected through the ONF mode (blue circles in a logarithmic scale) as a function of time in units of natural lifetime ($\tau_0 = 1/\gamma_0 = 26.24$ ns) with 5 ns bins. The signal is taken after a probe beam polarized along the nanofiber turns off. In this realization $OD = 0.66 \pm 0.05$. The individual statistical error bars are not plotted but they are taken into account for the normalized residuals in (b). We see two distinct slopes (red and green), at short and long times. The initial slope (red) deviates towards decay rates faster than γ_0 , a signature of super-radiance. The gray dotted line is the natural decay rate, for comparison. The second slope (green) comes from the natural post-selection of purely sub-radiant states. The red dashed (green dashed) line is the best fit to a pure exponential decay of the initial (final) decay. The decay rate of the fit at short times is $1.10 \pm 0.02 \gamma_0$, and $0.13 \pm 0.01 \gamma_0$ for the fit at longer times, with one-sigma error. The one-sigma fractional systematic errors are ± 0.01 . The full description of the measured temporal evolution of the system involves averaging over many different decay rates through Monte Carlo methods (explained in Methods). The solid black line is a simulation of 7 atoms along the ONF, with reduced χ^2 of 1.60. The inset shows two different decay signals from an excitation driving the atoms with light polarized along (green rectangles) and perpendicular (red triangles) to the ONF for 25 ns bins. When the driving field is polarized along the ONF we observe super and sub-radiance, and when it is polarized perpendicular to the ONF the super-radiance increases and the sub-radiance decreases. This feature is qualitatively captured by the theoretical model. **(b)** The red circles, green circles, and black diamonds are the normalized residuals of the exponential fits to the initial decay, final decay, and the theoretical model.

We overlap a cold atomic cloud of ^{87}Rb atoms from a magneto-optical trap (MOT) with a 240 nm radius ONF. This ONF is single mode at the D2 resonant wavelength of 780 nm. After the MOT is turned off, the atoms form a cold thermal gas around the ONF. They are prepared in the $F = 1$ ground level by an external free propagating beam. A repumper beam driving the $F = 1 \rightarrow F = 2$ transition propagates through the nanofiber, leaving in the $F = 2$ ground state only atoms that interact with the ONF guided mode. By detuning the repumper below resonance we address atoms near the nanofiber (whose levels have been shifted by van der Waals

interactions) such that the atomic density distribution peaks at ~ 30 nm away from the surface. A weak free space probe pulse, propagating perpendicular to the fiber, excites atoms for 50 ns using the $F = 2 \rightarrow F' = 3$ transition. After the probe turns off (extinction ratio better than 8×10^3 in 20 ns), we collect photons spontaneously emitted into the ONF mode to measure the decay time using time-correlated single-photon counting.

Collective states can be tailored by positioning the atoms in a particular arrangement. This kind of control has been challenging to implement for atoms trapped close enough to the ONF (tens of nanometers) to ensure significant mode coupling. However, collective states are still observed when atoms from a MOT are free to go near the ONF. Their random positioning leads to probabilistic super- or sub-radiant states on each experimental realization. Sub-radiant states have lifetimes much longer than most other processes, favoring their observation. Super-radiance can be measured as an enhanced decay rate at short times. Both effects can provide quantitative experimental evidence of collective states.

Figure 2 shows a typical signal of the atomic decay as measured through the ONF. Its time dependence can be described by two distinct exponential decays. The slow decay (green dashed line in Fig. 2 (a)) corresponds to an average of sub-radiant decays due to pairs of atoms located within a wavelength, i.e. free space interaction (Fig. 1 (b)). Infinite-range interactions also produce sub-radiant decay rates. However, these events are obscured by the dominant signal of slower decays produced from free space interactions. In our case $\gamma_{1D} \approx 0.13\gamma_0$, so sub-radiance from infinite-range interactions is limited to $\gamma_0 - \gamma_{1D} \approx 0.87\gamma_0$. This is a factor of six faster than the observed sub-radiant rates. Sub-radiance of atoms interacting in free space has been observed in a very optically dense cloud of atoms⁶, but here we observe it for optical densities (*OD*) as small as 0.3. The fast decay rate (red dashed line in Fig. 2 (a)) is larger than the natural decay rate, showing the presence of super-radiant initial states.

A full description of the temporal evolution of the entire data sample requires numerical (Monte Carlo) methods, as the solid black line in Fig. 2 shows. We use two free parameters for this simulation: the average number of atoms (*N*) and the initial atomic dipole induced by the probe pulse. Once the amplitude of the induced dipoles is found, the same value is used to predict the behavior for different data sets with different *N* with equally good agreement, allowing for variations of the background up to one-sigma. The discrepancy between simulation and data (see Fig. 2 (b) between 7 and 15 τ_0) could come from otherwise longer living subradiant state that get prematurely destroyed because an atoms fall onto the ONF, emitting the excitation into guided mode. The initial state preparation –the polarization of the incoming pulse that produces the collective one-photon state– can favor super- or sub-radiant states, as the inset of Fig. 2 shows.

An important difference between sub- and super-radiant decay rates in ONF is that the latter increases as a function of *N*. We can vary *N* from one to six by changing the MOT density, and quantify it through the *OD* of the ONF mode. $n_{\text{eff}}OD = N\gamma_{1D}/\gamma_0$, where n_{eff} is the mode effective refractive index, and in our case $n_{\text{eff}} \approx 1.15$. We measure the transmission spectrum through the ONF to extract the *OD*. The decay rate increases with *N*, as shown by the blue circles in Fig. 3, indicating super-radiance. The gray region represents the confidence bands of a linear fit to the data showing a linear dependence of the super-radiant decay rate for increasing *N*. The theoretical model implemented for the fit shown in Fig. 2 (solid black line) also predicts a linear dependence

on *N* of the decay rate γ at short times. The red dashed line in Fig. 3 shows this prediction, corroborating the experiment.

The average spacing between atoms is larger than a wavelength for most of the realizations, meaning that infinite-range interactions are always present. However, to provide an unambiguous proof of infinite-range interactions, we split the atomic cloud in two (see inset of Fig. 3). We see that two atomic clouds separated by 400 wavelengths present the same super-radiant collective behavior as a function of the *OD* as a single atomic cloud. This shows that the relevant parameter is the total *OD* (or *N*) along the ONF mode, regardless the separation between atoms.

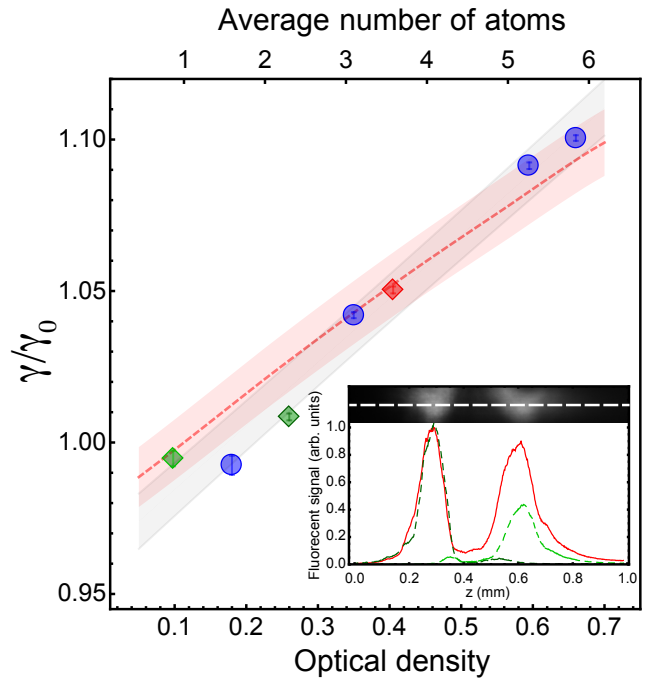


Figure 3 | Fast decay rates as a function of the *OD* (lower abscissa) and *N* (upper abscissa) measured through the ONF guided mode. The blue circles correspond to the signals from a single cloud of atoms. We split the atomic cloud in two, as the inset shows. The light and dark green diamonds, and the red square correspond to the right, left, and the combination of both atomic clouds respectively. The systematic errors (not shown) are estimated to be 1% for the decay rates and smaller than 20% for the atom number. The gray region represent the one-sigma confidence band of a linear fit to the data. The red dashed line is the theoretical prediction, with a confidence interval set by a fractional error of 1%. The curve goes below $\gamma/\gamma_0 = 1$ because the natural decay rate is modified given the geometry of the ONF and the alignment of the atomic dipoles (Purcell effect)³⁰. The top of the inset shows in black and white a fluorescence image of a split MOT. The white dotted line represents the ONF location. The fluorescence signal of the split MOT along the nanofiber is plotted as a function of position. The light (dark) green dashed lines is the intensity distribution of the right (left) atomic cloud when the other one is blocked. The solid red line is the intensity distribution when both clouds are present. The separation between the center of both clouds is $318 \pm 1 \mu\text{m}$, given by standard error of the mean of a Gaussian fit. This distance is equivalent to 408 wavelengths.

Optically guided modes can be used to mediate atom-atom in-

teractions, creating macroscopically delocalized collective atomic states. We use the super-radiant behavior of distant atoms as evidence of infinite-range interaction, but other interesting collective quantum properties remain to be tested. The practical limits of infinite-range interactions are an open question, since in principle optical fibers can be easily connected and rerouted along several meters. An intriguing next step is the study of quantum systems beyond the Markov approximation, coupling atoms at distance greater than what light travels in an atomic lifetime. Moreover, by achieving fine control on the positioning of the interacting particles, and/or using the directional coupling produced by chiral atom-light interaction¹⁶, one can engineer desired states tailored to address specific applications. The implementation of infinite-range interactions opens new possibilities for quantum technologies and many-body physics.

Acknowledgments We are grateful to A. Asenjo-Garcia, H. J. Carmichael, D. E. Chang, J. P. Clemens, M. Foss-Feig, B. D. Patterson, W. D. Phillips, and P. R. Rice for the useful discussions. We specially thank P. Zoller for helping us to improve the manuscript. This research is supported by the National Science Foundation of the United States (NSF) (PHY-1307416); NSF Physics Frontier Center at the Joint Quantum Institute (PHY-1430094); and the USDOC, NIST, Joint Quantum Institute (70NANB16H168).

Author Contributions P.S., F.K.F., L.A.O., and S.L.R. conceived the project. P.S. realized the measurements. P.B-B. and P.S. developed the theoretical model. All authors discussed the results, contributed to the data analysis and worked together on the manuscript.

Author Information P. Solano. solano.pablo.a@gmail.com

Methods

Experimental methods A tapered single mode ONF, with waist of 240 ± 20 nm radius and 7 mm length, is inside an ultrahigh vacuum (UHV) chamber, where it overlaps with a cloud of cold ^{87}Rb atoms (less than half a millimeter width) created from a magneto optical trap (MOT). The MOT is loaded from a background gas produced by a ^{87}Rb dispenser. Acousto optic modulators (AOMs) control the amplitude and frequencies of the MOT beams. After the atomic cloud loading reaches steady state, the MOT beams are extinguished. A free space propagating depump beam, resonant with the $F = 2 \rightarrow F' = 2$ transition (150 μs duration) prepares all atoms in the cloud in the $F = 1$ ground state. A 0.4 nW fiber-repump beam, detuned below resonance by 15 MHz to the $F = 1 \rightarrow F' = 2$ transition, propagates through the ONF during the entire cycle. It pumps back to the $F = 2$ ground state only those atoms close enough to the ONF to interact with the guided mode. This detuning repumps only those atoms close enough to the ONF surface to experience an energy shift due to the van der Waals interaction with the dielectric body. This produces a narrow density distribution of atoms of 5 nm width centered around 30 nm away from the surface. We wait 300 μs until the AOMs reach maximum extinction. The atomic cloud free falls and expands around the ONF for 2.5 ms creating a cold thermal gas (approx. 150 μK), where each atom interacts with the nanofiber mode for approximately 1.5 μs ³¹. The atomic density reduction due to the cloud expansion limits the probing time of the cycle. The atoms are excited by pulses of a weak probe beam incident perpendicularly to

the nanofiber (see Fig. 1 (a)) and linearly polarized along the ONF for the data set shown in Fig. 3. The pulses are resonant with the $F = 2 \rightarrow F' = 3$ transition of the $D2$ line and created with a double-passed Pockels cell (Conoptics 350-160), with a pulse extinction ratio of 1:8000 in 20 ns. The on-off stage of the light pulses is controlled with an electronic pulse generator (Stanford Research Systems DG645). The probe power is kept low, i.e. saturation parameter $s < 0.1$, to ensure a single photon excitation while staying in the limit of low-excitation and reduce photon pileup effects. Only those atoms that interact with the ONF guided mode are in the $F = 2$ ground state and will be excited by the probe beam. During the probing time we send a train of 50 ns probe pulses every 1 μs . The probe is a 7 mm $1/e^2$ diameter collimated beam. After 2 ms of probing (approx. 2000 pulses) the probe beam is turned off and the MOT beams are turned back on. During the probing time the atomic density remains constant. We wait 20 ms after the MOT reloads and repeat the cycle. The average acquisition time for an experimental realization is around 5 hours, giving a total of about 1×10^9 probe pulses. The photons emitted into the nanofiber and those emitted into free space are independently collected with avalanche photodiodes (APDs, Laser Components COUNT-250C-FC, with less than 250 dark counts per second). The TTL pulses created from photons detected by APD are processed with a PC time-stamp card (Becker and Hickl DPC-230) and time stamped relative to a trigger signal coming from the pulse generator. We use time-correlated single-photon counting³² to extract the decay rate of a single excitation in the system, eliminating after-pulsing events from the record.

When atoms are around the nanofiber, they tend to adhere due to van der Waals forces. After a few seconds of having the ONF exposed to rubidium atoms it gets coated, suppressing light propagation. To prevent this, we use 500 μW of 750 nm blue-detuned light (Coherent Ti:Saph 899) during the MOT-on stage to create a repulsive potential that keeps the atoms away from the ONF surface. This is intense enough to heat the ONF and accelerate the atomic desorption from the surface. The blue-detuned beam is turned off at the same time as the MOT beams, so the probed atoms are free to get close to the nanofiber.

Photons from the probe beam can be scattered multiple times by the atoms producing a signal that looks like a long decay, an effect known as radiation trapping. This effect can obscure subradiant signals. However, the small ODs involved in the experiment allow us to neglect contributions from radiation trapping. We confirm this assumption by observing the same temporal evolution of the signal at constant OD for several detunings of the probe beam.⁶

The atomic lifetime can also be altered by modification of the electromagnetic environment of the atoms in the presence of a ONF, i.e. the Purcell effect. However this effect is characterized separately³⁰ and well understood. More importantly, it does not depend on the number of atoms, in contrast with the super-radiant behavior.

Further evidence of collective states can be found in the resonance spectrum of the system (see Eqs. (2) and (3)). The dispersive part of the interaction modifies the resonance frequencies of the system, due to avoiding crossing of otherwise degenerate levels. This effect is in principle visible in the transmission spectrum. In our particular case the frequency splitting is a small percentage of the linewidth. Broadening mechanisms and other systematic errors prevent us from clearly observing such signal. However, a line-shape dependence on N can be inferred from the statistical

analysis of the fit of the spectrum to a Lorentzian. This effect might enable the exploration of features of collective states in the spectral domain.

ONFs can provide chiral atom-light coupling¹⁶. Even though this is a promising feature of the platform, it requires a particular positioning of the atoms and a preparation of their internal-state. This first exploration of infinite-rage interactions involves detecting only on one end of the ONF and azimuthally averaging the atomic position, preventing studies of chiral effects that we do not consider crucial to our measurements.

Theoretical model We follow the work of Svidzinsky and Chang³³ to implement the theoretical simulations of the experiment. Consider the Hamiltonian of N atoms interacting with an electromagnetic field in the rotating-wave approximation

$$\hat{H}_{int} = - \sum_k \sum_{j=1}^N \hbar G_{kj} [\hat{\sigma}_j \hat{a}_k^\dagger e^{i(\omega-\omega_0)t} + h.c.] \quad (5)$$

where $\hat{\sigma}_j$ is the lowering operator for atom j ; \hat{a}_k^\dagger is the photon creation operator in the mode k -th; ω_0 and ω are the frequencies of atomic resonance and k -th mode of the field respectively. This is a general expression for the Hamiltonian, which leads to the master equation in Eq. (2) after some approximations. The sum on j is done over the atoms and the sum on k goes over the electromagnetic field modes, guided into the nanofiber and radiated outside. These modes can be found in the work of Le Kien *et al.*²⁵ The sum over the guided modes is $\sum_\mu = \sum_{f,p} \int_0^\infty d\omega$, where f and p are the propagation direction and polarization in the circular basis (plus or minus) of the guided mode respectively, and μ stands for modes with different parameters (ω, f, p). The sum over the radiated modes is $\sum_\nu = \sum_{m,p} \int_0^\infty d\omega \int_{-k}^k d\beta$; where m is the mode order, k is the wavenumber, β is the projection of the wave vector along the fiber or propagation constant, and ν stands for modes with different parameters (ω, β, m, p). Then the total sum is $\sum_k = \sum_\mu + \sum_\nu$. The electromagnetic field modes and their relative coupling strength have been previously studied²⁵. The coupling frequencies G_{kj} for the guided and radiated modes can be written as

$$G_{\mu j} = \sqrt{\frac{\omega \beta'}{4\pi\epsilon_0\hbar}} [\mathbf{d}_j \cdot \mathbf{e}^{(\mu)}(r_j, \phi_j)] e^{i(f\beta z_j + p\phi_j)} \quad (6)$$

$$G_{\nu j} = \sqrt{\frac{\omega}{4\pi\epsilon_0\hbar}} [\mathbf{d}_j \cdot \mathbf{e}^{(\nu)}(r_j, \phi_j)] e^{i(\beta z_j + m\phi_i)} \quad (7)$$

where $\beta' = d\beta/d\omega$, \mathbf{d}_j is the dipole moment of the j -th atom, and $\mathbf{e}^{(\mu,\nu)}$ are the electric field profile function (or spatial dependence of the amplitude) of the guided and radiated modes (μ and ν).

Atoms interact with each other mediated by the electromagnetic field. The interaction between the atomic dipoles is proportional to the product of the atom-light coupling frequencies of the form $G_{ki}G_{kj}$, were k labels the mediating field mode (the repetition of the letter implies summation if there is more than one mode) and i and j label the i -th and j -th atom. It is possible to identify two contributions from the coupling of atoms to the dynamics of the system, a dispersive and a dissipative one, as shown in Eq. (2). The dispersive part contributes to the unitary evolution of the system (see Eq. (3)), and it can be decomposed as $\Omega_{ij} = \Omega_{ij}^{(rad)} + \Omega_{ij}^{(1D)}$, were $\Omega_{ij}^{(rad)}$ and $\Omega_{ij}^{(1D)}$ come from the interaction of the i -th and j -th atoms mediated by the radiated and guided modes respectively. Ω_{ij} is usually called the dipole-dipole coupling

frequency. The dissipative part contributes to the decay of the system (see Eq. (4)), and it can be decomposed as $\gamma_{ij} = \gamma_{ij}^{(rad)} + \gamma_{ij}^{(1D)}$, were $\gamma_{ij}^{(rad)}$ and $\gamma_{ij}^{(1D)}$ come from the interaction of the i -th and j -th atoms mediated by the radiated and guided modes respectively. For simplicity, here we consider the case of atomic dipoles oriented along the ONF (z -axis) placed in the position $\mathbf{r}_i = (r_i, \phi_i, z_i)$ with reduced dipole moment d_i , obtaining

$$\gamma_{ij}^{(1D)} = \frac{2\omega_0\beta'_0}{\epsilon_0\hbar} d_i d_j e_z^{(\mu_0)}(r_i) e_z^{*(\mu_0)}(r_j) \cos(\phi_i - \phi_j) \cos \beta_0(z_i - z_j) \quad (8)$$

$$\gamma_{ij}^{(rad)} = \frac{2\omega_0}{\epsilon_0\hbar} d_i d_j \sum_m \int_0^{k_0} d\beta e_z^{(\nu)}(r_i) e_z^{*(\nu)}(r_j) \times \cos m(\phi_i - \phi_j) \cos \beta_0(z_i - z_j) \quad (9)$$

$$\Omega_{ij}^{(1D)} \approx \frac{\omega_0\beta'_0}{\epsilon_0\hbar} d_i d_j e_z^{(\mu_0)}(r_i) e_z^{*(\mu_0)}(r_j) \cos(\phi_i - \phi_j) \sin \beta_0(z_i - z_j) \quad (10)$$

where μ_0 parametrizes the guided modes on resonance. The dispersive component of the interaction given by the radiated modes as $\Omega_{ij}^{(rad)}$ is a complicated expression and hard to solve even numerically. We follow the work of Le Kien *et al.*³⁴ and use the free space value of $\Omega_{ij}^{(rad)}$ throughout the calculation as a reasonable approximation. $\gamma_{ii} = \gamma_0$ with γ_0 the single atom natural decay rate. $\gamma_{12}^{(rad)}$ and $\gamma_{12}^{(1D)}$ are plotted in Fig. 1 (b) and (c) respectively for an atom fixed at $\mathbf{r}_1 = (30 \text{ nm} + 240 \text{ nm}, 0, 0)$ (240 nm being the ONF radius and 30 nm the distance of the atom to the surface). When atoms are too close to each other, the radiated terms $\Omega_{ij}^{(rad)}$ and $\gamma_{ij}^{(rad)}$ dominate over the guided ones ($\Omega_{ij}^{(1D)}$ and $\gamma_{ij}^{(1D)}$), with $\Omega_{ij}^{(rad)}$ diverging and $\gamma_{ij}^{(rad)}$ approaching the total decay rate. With a low number of atoms randomly distributed along the ONF the effects of short-range interaction are small but still observable.

We are interested in the decay of only one excitation in the system, represented by the state

$$|\Psi\rangle = \sum_{\mathbf{k}_\mu, \mathbf{k}_\nu} \alpha_{\mathbf{k}}(t) |g_1 g_2 \cdots g_N\rangle |1_{\mathbf{k}}\rangle + \sum_{j=1}^N \beta_j(t) |g_1 g_2 \cdots e_j \cdots g_N\rangle |0\rangle + \alpha_g(t) |g_1 g_2 \cdots g_j \cdots g_N\rangle |0\rangle \quad (11)$$

where $\mathbf{k}_{\mu(\nu)}$ represents the sum over the guided (radiated) modes. Assuming that we start the cycle with the excitation in the atoms, i.e. $\alpha_{\mathbf{k}}(0) = 0$, we can write the Schrödinger equation in the Markov approximation for the coefficients $\beta_i(t)$ in a matrix form as³³

$$\dot{\mathbf{B}}(t) = -\Gamma \mathbf{B}(t) \quad (12)$$

where $\mathbf{B}(t)$ is a vector with entries given by the $\beta_i(t)$, and Γ is a non-hermitian symmetric matrix with entries $2\Gamma_{ij} = \gamma_{ij} + i\Omega_{ij}$, representing the couplings between the i -th and j -th atoms calculated from the optical nanofiber modes, radiated and guided. The eigenvalues η_i of Eq. (12) give the possible decay rates of the system. This are the collective states mentioned in Eq. (1). The eigenvectors form a basis $\{|B_i\rangle\}$ that allows us to write the state of the system as

$$|\Psi\rangle = \sum_{\mathbf{k}_\mu, \mathbf{k}_\nu} \alpha_{\mathbf{k}}(t) |g_1 g_2 \cdots g_N\rangle |1_{\mathbf{k}}\rangle + \sum_{j=1}^N c_j e^{-\eta_j t} |B_j\rangle |0\rangle + \alpha_g(t) |g_1 g_2 \cdots g_j \cdots g_N\rangle |0\rangle \quad (13)$$

where the coefficients c_j are given by the initial state. In contrast with Eq. (1), here we have also included the states with one excitation in the field.

Following this approach the many-body problem, of calculating the decay of one excitation distributed among N interacting atoms, becomes an eigenvalue problem in a Hilbert space of dimension N^2 instead of 2^{2N} . This speeds the calculations, allowing us to compute the decay rate of the system with Monte Carlos simulations for a large N in random positions.

The electromagnetic field operator for the guided modes is²⁵

$$\hat{\mathbf{E}}_{\text{guided}}^{(+)} = i \sum_{fp} \int_0^\infty d\omega \sqrt{\frac{\hbar\omega\beta'}{4\pi\epsilon_0}} \hat{a}_\mu e^{(\mu)} e^{-i(\omega t - f\beta z - p\phi)}. \quad (14)$$

The formal solution of the Heisenberg equation for $\hat{a}_\mu(t)$ in the Markov and rotating wave approximation is

$$\hat{a}_\mu(t) = \hat{a}_\mu(t_0) + 2\pi \sum_j G_{\mu j}^* \delta(\omega - \omega_0) \hat{\sigma}_j(t), \quad (15)$$

The substitution of this expression into Eq. (14) gives the guided field operator as a function of the dipole operators.

Assuming that the guided modes are initially empty and that all the dipoles are oriented in the z direction and at the same distance from the ONF, the intensity of the guided field as a function of the atomic dipole operators is

$$\langle \hat{\mathbf{E}}_{\text{guided}}^{(-)} \hat{\mathbf{E}}_{\text{guided}}^{(+)} \rangle = |\mathcal{E}(r)|^2 \left(\sum_j \langle \hat{\sigma}_j^{ee}(t) \rangle - \sum_j |\langle \hat{\sigma}_j(t) \rangle|^2 + |d(t)|^2 \right), \quad (16)$$

where $\hat{\sigma}_j^{ee} = \hat{\sigma}_j^\dagger \hat{\sigma}_j$,

$$d(t) = \sum_j e^{i(\beta z_j + \phi_j)} \langle \hat{\sigma}_j(t) \rangle, \quad (17)$$

$$|\mathcal{E}(r)|^2 = \frac{2\hbar\omega_0}{n_{\text{eff}} c \epsilon_0} \frac{\gamma_{1D}(r)}{A_{\text{eff}}(r)}, \quad (18)$$

considering $\gamma_{1D}(r) = \gamma_{ii}^{(1D)}(r)$ from Eq. (8) and $A_{\text{eff}(z)}(r) = |n_{\text{eff}} e_z^{(\mu_0)}(r)|^{-2}$ to be the effective mode area of the z component of the electric field²⁵. Eq. (18) relates the total radiated power into the waveguide with the energy radiated per unit time, *i.e.* $I(r) A_{\text{eff}(z)}(r) = \hbar\omega_0 \gamma_{1D}(r)$, where $I(r)$ is the intensity of the radiated field.

The first term in the right-hand side of Eq. (16) is the usual term relating the intensity of the emitted electric field with the amplitude of the atomic excitation. The other two terms can be interpreted together as the correlations between pairs of atomic dipoles. In particular, the last term can be interpreted on its own as the interference of classical dipole antennae, leaving the first two terms to be thought as the variance of each atomic dipole.

Theoretical methods We use Monte Carlo simulations, randomly positioning N atoms around the ONF. The position of each atom is given in cylindrical coordinates by $\mathbf{r}_i = (r_0, \phi_i, z_i)$, where $r_0 = 240 \text{ nm} + 30 \text{ nm}$, $\phi_i \in [0, 2\pi]$, and z_i is obtained from a Gaussian distribution with a FWHM of $200 \mu\text{m}$, determined by the atomic cloud size. The radial position of the atoms is fixed, determined by the experimental procedure of repumping the atoms close to the nanofiber surface. In our case all the atoms are at a constant radial position of 30 nm away from the surface of an ONF

of 240 nm radius, with $\gamma_{1D}/\gamma_0 \approx 0.13$. This is a good approximation given the narrow radial distribution of the atoms ($\sim 5 \text{ nm}$), as explained in the experimental methods.

The initial state will depend on the amplitude and phase of the excitation beam. We assume that the initial state corresponds to a superposition of all the atoms in the ground state except one with an induced atomic dipole. From the data, we find the induced dipole to be 20% excited. For each random realization we solve Eq. (12) and calculate the decay of the excitation and the dipoles. We take the mean of all the obtained decays, for every random realization, as a function of time. Using these results in Eq. (16) we calculate the guided field intensity as a function of time. Typically, 100,000 realizations are required to converge to a level of precision higher than what it is visible in Figs. 2 and 3.

If the initial state does not have a dipole, $|d(t)|^2 = 0$, no super-radiant decay is predicted by the theory. This is because the super- and sub-radiant components of the initial state cancel when averaging. Nevertheless, when there is an initial dipole, the theory predicts super-radiant decay measurable at short times of the field decay. The origin for this is the term proportional to the atomic dipoles, $|d(t)|^2$ in Eq. (16). There is a correlation between super-radiance (sub-radiance) configurations and constructive (destructive) interference of the field emitted by the dipoles into the ONF (see Eq. (17)); the effect of these correlations when we take the mean over all the realizations is that super-radiance configurations contributes more than sub-radiance configurations to $|d(t)|^2$, for an electric field detected through the ONF.

The theoretical model prediction for different dipole moment orientations relative to the ONF²⁵ qualitatively agrees with the observed experimental behavior: The long term sub-radiance disappears on our signal-to-background-ratio window when exciting with vertically polarized light (see inset of Fig. 2).

A sensitivity analysis to the ONF radius shows no significant changes in the predictions up to a $\pm 10 \text{ nm}$ variation. The deviations of the theory from the experiment are mainly attributed to the lack of knowledge of the actual initial states that are being prepared. Although a more careful study of the state preparation and its control is needed for future applications, the quantitative behavior of the observations is captured by the model.

1. R. H. Dicke. Coherence in Spontaneous Radiation Processes. *Physical Review*, 93(1):99, 1954.
2. Marlan O. Scully and Anatoly A. Svidzinsky. The Super of Superradiance. *Science*, 325(5947):1510, 2009.
3. Marlan O. Scully. Single Photon Subradiance: Quantum Control of Spontaneous Emission and Ultrafast Readout. *Physical Review Letters*, 115(24):243602, 2015.
4. D E Chang, L Jiang, A V Gorshkov, and H J Kimble. Cavity qed with atomic mirrors. *New Journal of Physics*, 14(6):063003, 2012.
5. Michael J. Morrissey, Kieran Deasy, Mary Frawley, Ravi Kumar, Eugen Prel, Laura Russell, Viet Giang Truong, and Sile Nic Chormaic. Spectroscopy, Manipulation and Trapping of Neutral Atoms, Molecules, and Other Particles Using Optical Nanofibers: A Review. *Sensors*, 13(8):10449, 2013.
6. William Guerin, Michelle O. Araújo, and Robin Kaiser. Subradiance in a Large Cloud of Cold Atoms. *Physical Review Letters*, 116(8):083601, 2016.
7. H. J. Kimble. The quantum internet. *Nature*, 453(7198):1023–1030, 2008.
8. A. Asenjo-Garcia, M. Moreno-Cardoner, A. Albrecht, H. J. Kimble, and D. E. Chang. Exponential improvement in photon storage fidelities using subradiance and "selective radiance" in atomic arrays. *arXiv:1703.03382*, 2017.
9. C.-L. Hung, Alejandro González-Tudela, J. Ignacio Cirac, and H. J. Kimble. Quantum spin dynamics with pairwise-tunable, long-range interactions. *Proceedings of the National Academy of Sciences*, 113(34):E4946, 2016.

10. J. S. Douglas, H. Habibian, C.-L. Hung, A. V. Gorshkov, H. J. Kimble, and D. E. Chang. Quantum many-body models with cold atoms coupled to photonic crystals. *Nature Photonics*, 9(5):326, 2015.
11. J. D. Thompson, T. G. Tiecke, N. P. de Leon, J. Feist, A. V. Akimov, M. Gullans, A. S. Zibrov, V. Vuletić, and M. D. Lukin. Coupling a Single Trapped Atom to a Nanoscale Optical Cavity. *Science*, 340(6137):1202, 2013.
12. Clément Sayrin, Christian Junge, Rudolf Mitsch, Bernhard Albrecht, Danny O'Shea, Philipp Schneeweiss, Jürgen Volz, and Arno Rauschenbeutel. Nanophotonic Optical Isolator Controlled by the Internal State of Cold Atoms. *Physical Review X*, 5(4):041036, 2015.
13. Danny O'Shea, Christian Junge, Jürgen Volz, and Arno Rauschenbeutel. Fiber-Optical Switch Controlled by a Single Atom. *Physical Review Letters*, 111(19):193601, 2013.
14. T. G. Tiecke, J. D. Thompson, N. P. de Leon, L. R. Liu, V. Vuletić, and M. D. Lukin. Nanophotonic quantum phase switch with a single atom. *Nature*, 508(7495):241, 2014.
15. Itay Shomroni, Serge Rosenblum, Yulia Lovsky, Orel Bechler, Gabriel Guendelman, and Barak Dayan. All-optical routing of single photons by a one-atom switch controlled by a single photon. *Science*, 345(6199):903, 2014.
16. Jan Petersen, Jürgen Volz, and Arno Rauschenbeutel. Chiral nanophotonic waveguide interface based on spin-orbit interaction of light. *Science*, 346(6205):67, 2014.
17. Jürgen Volz, Michael Scheucher, Christian Junge, and Arno Rauschenbeutel. Nonlinear π phase shift for single fibre-guided photons interacting with a single resonator-enhanced atom. *Nature Photonics*, 8(12):965, 2014.
18. Jonathan D. Hood, Akihisa Goban, Ana Asenjo-Garcia, Mingwu Lu, Su-Peng Yu, Darrick E. Chang, and H. J. Kimble. Atom-atom interactions around the band edge of a photonic crystal waveguide. *Proceedings of the National Academy of Sciences*, 113(38):10507, 2016.
19. A. Goban, C. L. Hung, J. D. Hood, S. P. Yu, J. A. Muniz, O. Painter, and H. J. Kimble. Superradiance for Atoms Trapped along a Photonic Crystal Waveguide. *Physical Review Letters*, 115(6):063601, 2015.
20. B. Gouraud, D. Maxein, A. Nicolas, O. Morin, and J. Laurat. Demonstration of a Memory for Tightly Guided Light in an Optical Nanofiber. *Physical Review Letters*, 114(18):180503, 2015.
21. C. Sayrin, C. Clausen, B. Albrecht, P. Schneeweiss, and A. Rauschenbeutel. Storage of fiber-guided light in a nanofiber-trapped ensemble of cold atoms. *Optica*, 2(4):353, 2015.
22. Neil V. Corzo, Baptiste Gouraud, Aveek Chandra, Akihisa Goban, Alexandra S. Sheremet, Dmitriy V. Kupriyanov, and Julien Laurat. Large bragg reflection from one-dimensional chains of trapped atoms near a nanoscale waveguide. *Phys. Rev. Lett.*, 117:133603, 2016.
23. H. L. Sørensen, J.-B. Béguin, K. W. Kluge, I. Iakoupov, A. S. Sørensen, J. H. Müller, E. S. Polzik, and J. Appel. Coherent backscattering of light off one-dimensional atomic strings. *Phys. Rev. Lett.*, 117:133604, 2016.
24. R. G. DeVoe and R. G. Brewer. Observation of Superradiant and Subradiant Spontaneous Emission of Two Trapped Ions. *Physical Review Letters*, 76(12):2049, 1996.
25. Fam Le Kien, S. Dutta Gupta, K. P. Nayak, and K. Hakuta. Nanofiber-mediated radiative transfer between two distant atoms. *Phys. Rev. A*, 72:063815, 2005.
26. Vera Bendkowsky, Bjorn Butscher, Johannes Nipper, James P. Shaffer, Robert Low, and Tilman Pfau. Observation of ultralong-range Rydberg molecules. *Nature*, 458(7241):1005, 2009.
27. P. Richerme, Z. Gong, A. Lee, C. Senko, J. Smith, M. Foss-Feig, S. Michalakis, A. V. Gorshkov, and C. Monroe. Non-local propagation of correlations in quantum systems with long-range interactions. *Nature*, 511(198):198, 2014.
28. Justin G. Bohnet, Brian C. Sawyer, Joseph W. Britton, Michael L. Wall, Ana Maria Rey, Michael Foss-Feig, and John J. Bollinger. Quantum spin dynamics and entanglement generation with hundreds of trapped ions. *Science*, 352(6291):1297, 2016.
29. Arjan F. van Loo, Arkady Fedorov, Kevin Lalumi  re, Barry C. Sanders, Alexandre Blais, and Andreas Wallraff. Photon-mediated interactions between distant artificial atoms. *Science*, 342(6165):1494, 2013.
30. P. Solano, J. A. Grover, Y. Xu, P. Barberis-Blostein, J. N. Munday, L. A. Orozco, W. D. Phillips, and S. L. Rolston. Alignment-dependent decay rate of an atomic dipole near an optical nanofiber. *To be Published*, 2017.
31. J. A. Grover, P. Solano, L. A. Orozco, and S. L. Rolston. Photon-correlation measurements of atomic-cloud temperature using an optical nanofiber. *Phys. Rev. A*, 92:013850, 2015.
32. Desmond O'Connor and David Phillips. *Time-correlated single photon counting*. Academic Press, London, 1984.
33. Anatoly Svidzinsky and Jun-Tao Chang. Cooperative spontaneous emission as a many-body eigenvalue problem. *Phys. Rev. A*, 77:043833, 2008.
34. Fam Le Kien and A. Rauschenbeutel. Nanofiber-mediated chiral radiative coupling between two atoms. *Phys. Rev. A*, 95:023838, 2017.

4.5 Comments on subradiance mediated by an ONF

The observation of subradiance has always been a challenge, and therefore a fascinating topic in quantum optics. This is why it is worth using ONFs as a platform for creating and studying subradiance.

A perfectly subradiant system is one that does not decay, being completely decoupled from its environment. Likewise, a system that is decoupled from the outside world is then difficult to access. It is, ideally, an isolated system, impossible to excite and impossible to observe. However, a non-perfectly subradiant state can be accessed from the outside, and observed through the ONF, under the right conditions.

Subradiance has been observed in the past for two trapped ions [119], in a very specific configuration with a rather small effect. More recently it has been observed in a large cloud of atoms [120] in the limit of one excitation, *i.e.* one photon. But there has not been a platform that allows the observation of long subradiant decay times of a few atoms.

We showed in the previous section the experimental observation of subradiance in our ONF system. This can come from two different scenarios: infinite-range interactions and free space interaction.

Subradiant states created by infinite-range interaction in the single-excitation regime have a hard limit on how subradiant they can be. Once two atoms along the ONF destructively interfere with each other, they can no longer emit into that decay channel (the guided mode). However, nothing stops them from emitting outside the

ONF (into a radiated mode). Then the smallest subradiant decay rate allowed by infinite-range interactions is $\gamma_{\text{Tot}} - \gamma_{1D} = \gamma_{\text{rad}}$ (equal to $0.87\gamma_0$ in the case of our experiment).

The subradiant decay times we observe through the ONF are a factor of six smaller than the previously stated limit. This means that they come from atoms interacting through free space. The presence of the nanofiber dielectric body alters the radiated field that couple the atoms, allowing atoms from even opposite sides of the ONF to interact. The large coupling of nearby atoms into the guided mode facilitates the detection of such subradiant states.

Monte Carlo simulations of the system show this behavior. Fig. 4.1 shows the probability of creating a given decay rate, in units of the natural decay rate, by exciting a finite sample of atoms coupled to the ONF. If the fiber is infinitely long, it means that the sample is diluted enough that all the atom-atom interactions are through infinite range. Reducing the nanofiber length, it becomes more likely to have two atoms interacting with each other through free space (but still in the presence of the ONF). We can see how for purely infinite-range interaction, the most subradiant state is limited by $1 - \alpha = 0.87$ in our experimental realization. As atoms can get closer, there are more subradiant states due to free space interaction. On the other hand, the superradiant behavior is not greatly affected by increasing the chance of having atoms closer together. This means that the superradiant signal is dominated by infinite-range interaction, since all the atoms interacting with the guided mode can contribute without an upper limit (in contrast to the case of a lower limit for subradiance).

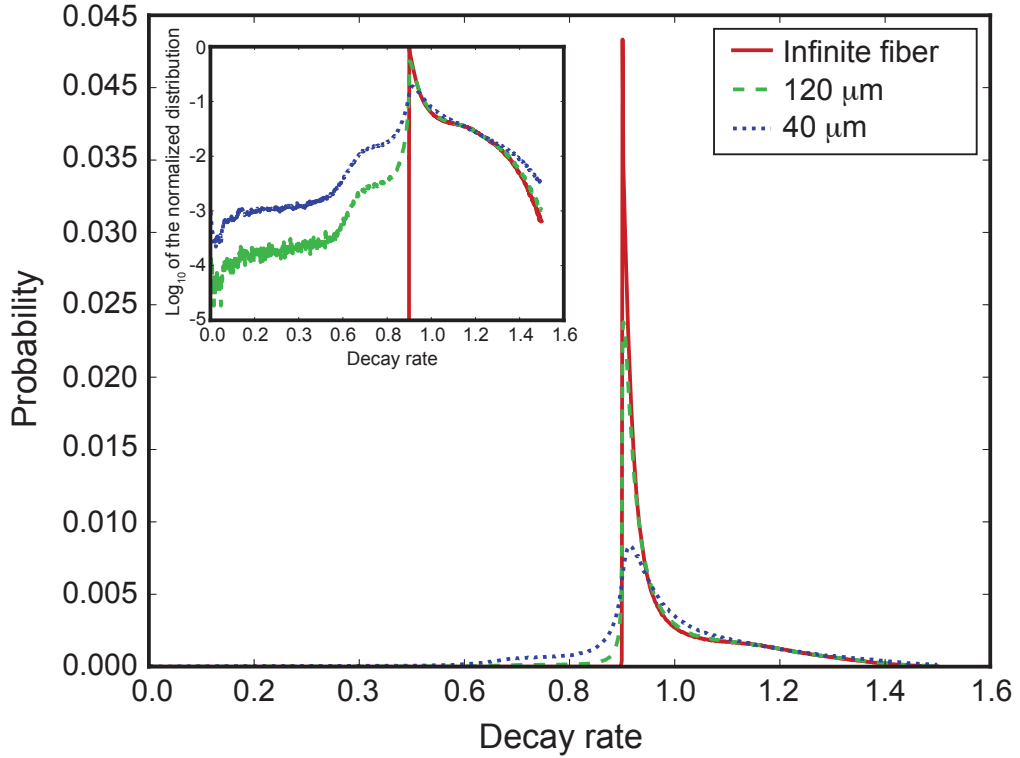


Figure 4.1: Probability of observing a given decay rate for 10 atoms randomly distributed around a 230 nm radius ONF at a distance of 30 nm from the surface. The plot shows the allowed collective states for a ONF of infinite length (solid red), as well as for 120 μm (dashed green) and 40 μm (dotted blue). The inset shows the same results as in the main figure, but in a \log_{10} scale and normalized to the peak of the red curve to show the probability of having a given decay rate represented in order of magnitudes.

Chapter 5: Conclusions and outlook

Optical nanofibers are a promising platform for fundamental research in quantum optics and applications in quantum information. In this work, we have shown some aspects in which they provide advantages and novel features compared with other systems. We focused on three particular experiments based on ONFs: atom trapping and non-destructive characterization, modification of the atomic lifetime, and collective atomic effects at infinite-range. All of them present an starting point for future investigations in the field.

Dipoles traps created by the evanescent field of an ONF have been implemented in a few experimental groups in the past 10 years, and their applications are on the rise. These experiments can certainly benefit from the development of a method to characterize the traps in a short time and without losing atoms, as presented here. Polarimetric measurements of the trapping frequencies can become a standard procedure, as part of a toolbox for working with this type of system. We think that there is room for improvements of the proposed technique. Improving the sensitivity of the detection would allow the use of less probe power and reduce its effect on trapped atoms. If some other experiment is being performed with trapped atoms, a real time characterization of the trapping potential, at the beginning of a

experimental cycle, can also be used to correct for long time drifts of the experiment. Using feedback, drifts can be corrected without stopping the experiment and data acquisition. Given the anharmonicity of the trap, a proper characterization of the frequency of atomic motion can be related to the temperature of the atoms. A proper understanding of the trapping can help to further cool the atoms in the trap to their motional ground state. We consider that these are some of the promising paths to explore with this new technique.

We have also studied the effect of an ONF on the spontaneous emission of nearby atoms. We measure different atomic decay rates when exciting the atoms with different light polarizations. The dependence of the atomic properties on the atomic dipole alignment can be used as a control knob for future applications involving atoms coupled to optical waveguides. This could be a useful effect in other waveguide systems with larger Purcell effect (or ONF with smaller radius), where the lifetime of an excitation in the system can be tuned based on the polarization of the field or the internal atomic state. During the search for a theoretical modeling of this problem we found in the literature discrepancies in the predictions. We find some agreement between the measurement and a numerical calculation using FDTD, however the calculations assume a two-level atom that behaves as a classical dipole. We could not find a theoretical description that explains the measurements considering the multi-level structure of the atom. The full description of this basic, but still complicated, aspect of the experiment remains to be found. This presents a challenge for all the future implementations of this kind of platform. Since the case of a single real (multilevel) atom interacting with a waveguide is the fundamental

unit of a bigger system, it needs to be understood, indicating the necessity of further theoretical and experimental studies.

Using ONFs we were able to interact atoms at macroscopic distances. We presentd evidence of the infinite-range interaction among atoms, allowed by the ONF guided mode, by observing a collective evolution of the atomic system. In particular, we measured subradiance between atoms hundreds of resonant wavelengths apart. During our search for evidence of infinite-range interactions, we also found that ONFs allow us to excite and observe subradiant states. Subradiant states are in general difficult to measure, and their observation presents ONFs as a exciting platform for quantum optics. On the other hand, superradiant states due to infinite-range interaction opens the field to a several new possibilities. Superradiance of many atoms is limited in free space because atoms need to be closer than a wavelength but not too close, otherwise decoherence mechanisms alters the process. This sets a technical upper bound on how many atoms can be prepared in a superradiant state. Atoms interacting through a guided mode lack this difficulty, since they do not need to be closer than a wavelength. For the particular case of collective decays of atoms the limiting spatial scale is the distance at which two atoms can emit indistinguishable photons, *i.e.* the coherence length of an spontaneously emitted photon, which is of the order of meters. This is the scale limit for sub- and super-radiance, but does not mean that atoms cannot coherently interact at longer distances. Even though the coupling of single atoms into the waveguide can be small compared to its decay into free space, superradiace modifies this proportional to the number of atoms. This implies that tens of superradiant atoms are

enough to exceed the decay rate out of the ONF. The effect of having several atoms, all interacting with each other, also opens the possibility to implement and study spatial configuration of many-body systems. Moreover, all the technological development in the fiber optics industry can be applied to ONFs, allowing distribution of signals with minimum losses, routing them, and connecting several distant systems in non-trivial arrangements. We envision this to be a step towards implementation of quantum information protocols at scales of practical uses.

Appendix A: Nanofiber electromagnetic modes

A standard step-index optical fiber is a cylindrical waveguide having a light-guiding core of typical radius of $2 - 3 \mu\text{m}$ and refractive index n_1 , surrounded by a cylindrical cladding with index n_2 . In commercial, single-mode fibers, the refractive index difference is small, with $0.001 \lesssim (n_1 - n_2) \lesssim 0.02$, and the waveguide is considered to have “weakly guiding” core-cladding guidance. Fig 1.1 shows schematically that as the fiber is tapered down this geometry adiabatically transforms to a step-index waveguide in which the light is entirely guided with air (or vacuum) as the cladding (“cladding-air” guidance), having an index difference close to 0.5. Detailed vector-mode solutions are required for such “strongly guiding” waveguides, and are described in a number of treatments [121–126], while in the weakly guiding limit, a scalar treatment is sufficient. Here we present a summary of the vector-mode solutions from [127], and discuss some of the relevant aspects of optical nanofibers.

The electric and magnetic fields, \mathbf{E} and \mathbf{H} , are shown below in cylindrical coordinates for a single-step index geometry with core radius, a , of index n_1 , and an infinite cladding of index n_2 . The solution of the Maxwell Equations in cylindrical coordinates leads to the following expressions for the field components along the radial (r), azimuthal (ϕ), and longitudinal (z , propagation) directions inside ($r < a$)

and outside ($r > a$) the core.

For $r < a$:

$$E_{r,\pm} = \frac{-i\beta}{h^2} \left[\pm \frac{i\mu_0\omega l}{\beta r} BJ_l(hr) + AhJ'_l(hr) \right] e^{i(\omega t - \beta z \pm l\varphi)} \quad (\text{A.1})$$

$$E_{\phi,\pm} = \frac{-i\beta}{h^2} \left[\pm \frac{il}{r} AJ_l(hr) - \frac{\mu_0\omega h}{\beta} BJ'_l(hr) \right] e^{i(\omega t - \beta z \pm l\varphi)} \quad (\text{A.2})$$

$$E_{z,\pm} = AJ_l(hr)e^{i(\omega t - \beta z \pm l\varphi)} \quad (\text{A.3})$$

$$H_{r,\pm} = \frac{-i\beta}{h^2} \left[\mp \frac{i\varepsilon_1\omega l}{\beta r} AJ_l(hr) + BhJ'_l(hr) \right] e^{i(\omega t - \beta z \pm l\varphi)} \quad (\text{A.4})$$

$$H_{\phi,\pm} = \frac{-i\beta}{h^2} \left[\frac{\varepsilon_1\omega}{\beta} AhJ'_l(hr) \pm \frac{il}{r} BJ_l(hr) \right] e^{i(\omega t - \beta z \pm l\varphi)} \quad (\text{A.5})$$

$$H_{z,\pm} = BJ_l(hr)e^{i(\omega t - \beta z \pm l\varphi)}, \quad (\text{A.6})$$

and $r > a$,

$$E_{r,\pm} = \frac{i\beta}{q^2} \left[\pm \frac{i\mu_0\omega l}{\beta r} DK_l(qr) + ChK'_l(qr) \right] e^{i(\omega t - \beta z \pm l\varphi)} \quad (\text{A.7})$$

$$E_{\phi,\pm} = \frac{i\beta}{q^2} \left[\pm \frac{il}{r} CK_l(qr) - \frac{\mu_0\omega h}{\beta} DK'_l(qr) \right] e^{i(\omega t - \beta z \pm l\varphi)} \quad (\text{A.8})$$

$$E_{z,\pm} = CK_l(qr)e^{i(\omega t - \beta z \pm l\varphi)} \quad (\text{A.9})$$

$$H_{r,\pm} = \frac{i\beta}{q^2} \left[\mp \frac{i\varepsilon_2\omega l}{\beta r} CK_l(qr) + DqK'_l(qr) \right] e^{i(\omega t - \beta z \pm l\varphi)} \quad (\text{A.10})$$

$$H_{\phi,\pm} = \frac{i\beta}{q^2} \left[\frac{\varepsilon_2\omega}{\beta} CqJ'_l(qr) \pm \frac{il}{r} DK_l(qr) \right] e^{i(\omega t - \beta z \pm l\varphi)} \quad (\text{A.11})$$

$$H_{z,\pm} = DK_l(qr)e^{i(\omega t - \beta z \pm l\varphi)}, \quad (\text{A.12})$$

where β is the mode propagation constant, $h = \sqrt{k^2 - \beta^2}$, $q = \sqrt{\beta^2 - k^2}$, $k = 2\pi/\lambda$

is the wavenumber, and ε_i gives the dielectric constant in regions $i = 1, 2$. The parameter l is a non-negative integer that gives the order of the guided mode and its angular momentum. We also use the notation $J'_l(hr) = \partial J_l(hr)/\partial(hr)$, $K'_l(qr) =$

$\partial K_l(qr)/\partial(qr)$ for derivatives of Bessel functions J_l and modified Bessel functions of the second kind K_l of order l .

Boundary conditions impose the following relations for the interior constants A and B , and for the exterior constants C and D :

$$\frac{B}{A} = \pm \left[\left(\frac{1}{ha} \right)^2 + \left(\frac{1}{qa} \right)^2 \right] \left[\frac{J'_l(ha)}{haJ_l(ha)} + \frac{K'_l(qa)}{qaK_l(qa)} \right]^{-1} \quad (\text{A.13})$$

$$\frac{C}{A} = \frac{J_l(ha)}{K_l(qa)} \quad (\text{A.14})$$

$$\frac{D}{A} = \frac{B}{A} \frac{J_l(ha)}{K_l(qa)} - \frac{l^2 \beta^2}{k_0^2} \left[\left(\frac{1}{ha} \right)^2 + \left(\frac{1}{qa} \right)^2 \right]^2, \quad (\text{A.15})$$

so that the knowledge of the propagation constant β and amplitude normalization constant A completely define the system.

An eigenvalue equation determines the propagation constant β :

$$\frac{J_{l-1}(ha)}{haJ_l(ha)} = \frac{(n_1^2 + n_2^2)}{4n_1^2} \left[\frac{K_{l-1}(qa) + K_{l+1}(qa)}{qaK_l(qa)} \right] + \frac{l}{(ha)^2} \pm R, \quad (\text{A.16})$$

where

$$R = \sqrt{\frac{(n_1^2 - n_2^2)^2}{(4n_1^2)^2} \left[\frac{K_{l-1}(qa) + K_{l+1}(qa)}{qaK_l(qa)} \right]^2 + \frac{l^2 \beta^2}{n_1^2 k_0^2} \left[\left(\frac{1}{ha} \right)^2 + \left(\frac{1}{qa} \right)^2 \right]^2}, \quad (\text{A.17})$$

and the $\pm R$ solutions correspond to *EH* and *HE* modes, respectively. A normalized frequency called the *V*-number is defined by the relation

$$V = \frac{2\pi}{\lambda} a \sqrt{n_1^2 - n_2^2}, \quad (\text{A.18})$$

which scales the optical frequency by the fiber radius and its numerical aperture ($\sqrt{n_1^2 - n_2^2}$). We can numerically solve Eq. (A.16) for a particular *V*-number (see Eq. (A.18)) and l by finding the points of intersection of its left hand side and right

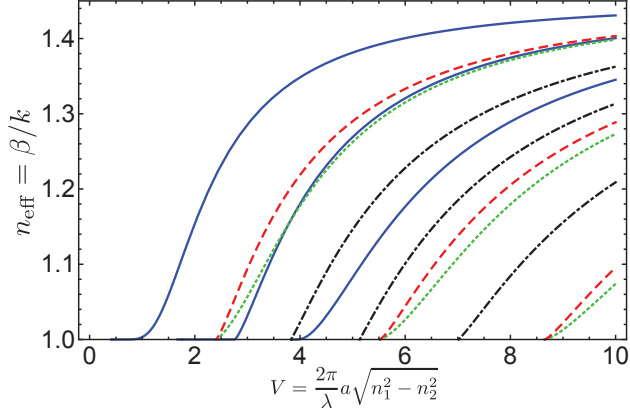


Figure A.1: Effective index of refraction as a function of V-number. The families of modes and their colors are HE (solid blue), EH (dashed-dotted black), TE (dashed red), TM (dotted green). Fig. from Ref. [87].

hand side. Modes are labeled with subscripts lm , e.g. HE_{lm} , where for a given l , the successive points of intersection signify increasing m . Fig. A.1 plots the result of this calculation (where $n_{\text{eff}} = \beta/k$) as a function of V for various families of modes. Note that the cutoff occurs at $V = 2.405$ and that the fundamental HE_{11} mode propagates for any $V > 0$. In the weak guiding limit, these vector mode solutions, HE_{lm} , become degenerate in the linearly-polarized (LP) basis, meaning that they have the same propagation constant.

The last parameter to determine is A , which is calculated using energy conservation. We normalize the time-averaged Poynting vector in the z-direction relative to the input power,

$$P = \langle S_z \rangle_t = A^2 \pi (D_{\text{in}} + D_{\text{out}}) , \quad (\text{A.19})$$

where D_{in} and D_{out} will be found analytically. For the HE_{lm} and EH_{lm} modes,

these parameters are

$$D_{\text{in}} = \frac{\pi a \beta^2}{4\mu_0 \omega} \frac{\beta}{h^2} [(1+sl)(N_1^2 + sl)[J_{l+1}^2(ha) - J_l(ha)J_{l+2}(ha)] \\ + (1-sl)(N_1^2 - sl)[J_{l-1}^2(ha) - J_l(ha)J_{l-2}(ha)]] \quad (\text{A.20})$$

$$D_{\text{out}} = \frac{-\pi a \beta^2}{4\mu_0 \omega} \frac{\beta}{q^2} \left(\frac{J_l(ha)}{K_l(qa)} \right)^2 [(1+sl)(N_2^2 + sl)[K_{l+1}^2(qa) - K_l(qa)K_{l+2}(ha)] \\ + (1-sl)(N_2^2 - sl)[K_{l-1}^2(qa) - K_l(qa)K_{l-2}(qa)]] , \quad (\text{A.21})$$

where $N_i = n_i k / \beta$ and $s = B \mu_0 \omega / (il\beta)$ (with B given by Eq. (A.13)).

Figure A.2 offers a summary by plotting the mode structure of the HE_{11} mode, showing the intensity (Fig. A.2 a)) as well as the norm of each electric field component normalized to their value at the fiber surface (Fig. A.2 b), c) and d)). These values correspond to a 360-nm-diameter fiber with index of refraction $n_1 = 1.45367$ and propagating wavelength of 780 nm. Note that the intensity has a sharp discontinuity at the fiber surface. The two largest components, E_x and E_z , are comparable. The presence of a sizable longitudinal component E_z plays a critical role in nanophotonic atom-photon interactions [65].

The radial decay of the evanescent field amplitude is not a simple exponential, but a complicated sum of modified Bessel functions of the second kind $K_l(qr)$ (see Eqs. (A.7), (A.8) and (A.9)). Since r is the distance from the center of the ONF and we are interested in the field outside the dielectric media, the asymptotic expansion for large argument $K_l(qr) \approx \sqrt{\pi/2qr} e^{-qr}$ is a good approximation, for any order l . Considering this, the radial dependence of the evanescent electric field is

$$E_i(qr) \approx c_i r^{-\frac{1}{2}} e^{-qr} , \quad (\text{A.22})$$

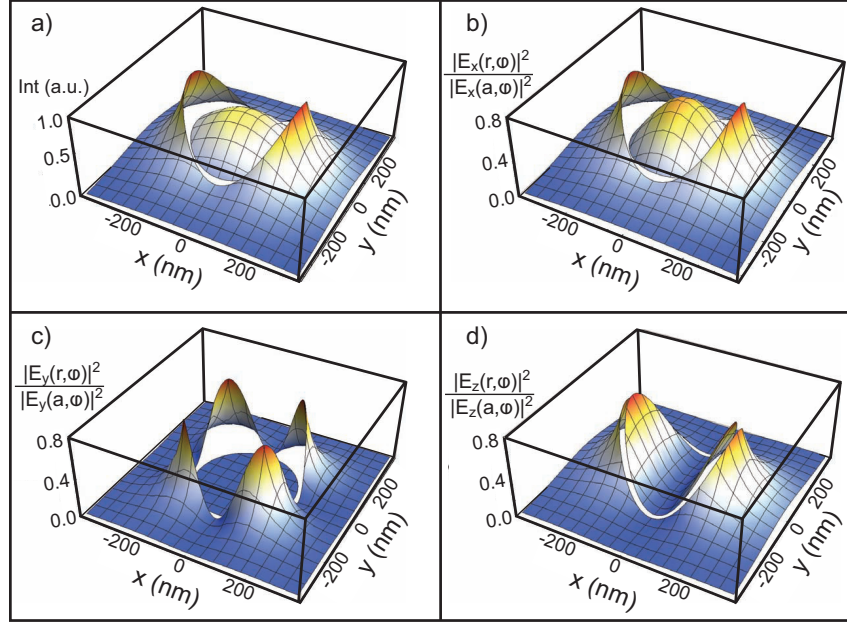


Figure A.2: Fundamental (HE_{11}) mode structure of 360-nm diameter nanofiber.

Fig. from Ref. [87].

where E_i is the i -th component of the electric field with amplitude proportional to c_i . This shows that the evanescent field decays faster than an exponential decay. We have tested this approximation against exact numerical calculation showing excellent agreement, providing a simpler and more intuitive mathematical expression for the evanescent field.

When we launch linearly polarized light into a fiber it will excite both the $\pm l\phi$ solutions. We can represent the mode in the quasilinear basis, as represented below.

$$\mathbf{E}_{\text{lin}} = \frac{1}{\sqrt{2}} [\mathbf{E}_+ \pm \mathbf{E}_-] \quad (\text{A.23})$$

$$\mathbf{H}_{\text{lin}} = \frac{1}{\sqrt{2}} [\mathbf{H}_+ \pm \mathbf{H}_-]. \quad (\text{A.24})$$

It is useful to think of this as analogous to representing linearly polarized light as a superposition of left and right circularly polarized.

The polarization of the propagating field can be characterized at the ONF waist with polarimetric measurement of the scattered light. Because Rayleigh scattering is dipolar, the scattered field preserves the polarization of the incoming one. This allows us to measure the polarization of the guided field at each point along the nanofiber. We can control the polarization at the ONF waist by modifying the input polarization. For more details see [86].

The calculations show that E_z can be significant in an optical nanofiber [63]. This is generally true for tightly-focused laser beams and waveguides in the strong-guiding regime. The existence of longitudinal polarizations is intimately related to the first of Maxwell's equations (Gauss' law). While in everyday paraxial optics rays and transverse polarizations suffice to characterize optical phenomena, when there are significant gradients on the transverse field they have to be accompanied by a corresponding longitudinal component of the electric field. [128] carries out a systematic (perturbational) approach starting with Gauss' law as a function of a small parameter λ/w where λ is the wavelength of the light and w the characteristic transverse width of the field: the transverse size of the beam. As w decreases the ray optics approximation with transverse fields fails and longitudinal components appear. This is a serious issue when focusing laser beams to small sizes and their polarization properties have been studied and measured in [129].

Gauss' law ($\nabla \cdot \mathbf{E} = 0$) establishes that a focused light beam of wavelength λ and angular frequency ω that propagates along $\pm z$ with a slowly-varying amplitude

has a longitudinal component

$$E_z = \pm \frac{i}{k} \nabla \cdot \mathbf{E}_\perp. \quad (\text{A.25})$$

where the \pm corresponds to the two possible directions of propagation and \mathbf{E}_\perp is the transverse field. The presence of i in the expression for E_z means that E_z is $\pm\pi/2$ out of phase with the transverse components, depending on the propagation direction. The existence of this longitudinal field and resulting transverse component of elliptical polarization is at the source of the chirality observed in nanophotonic systems as stated in [52].

Appendix B: Other ONF Papers

This appendix includes references and comments for other papers related to ONF published during my PhD.

When I first joined the group I had the pleasure to work with Jonathan Hoffman on the ONF pulling experient and learn from him all the details about fabrication and characterization of nanofibers. To me, this experiment needs a good balance of knowledge and skills, the closest to art I have seen in the lab. I had the great opportunity of contribute to build and perfect the current fiber puller apparatus that we use at UMD. This work lead to the fabrication of the ONFs with highest transmission in the world (for now), as shown in an AIP Advances paper published in 2014 [127].

After learning about ONF fabrication I started working with cold atoms, and coupling them to our nanofibers. This is when I started working with Jeffrey Grover. I shadowed him, and learned from him, while he implemented the ONF atomic dipole trap. Soon after, we got interested on doing quantum optics with this platform, the moment in which all the curiosity and ideas that led to this thesis started. We worked on photon-correlation measurements of atoms evanescently coupled to the ONF. This allowed me to learn about photon counting and other standard tools and tricks

of quantum optics experiments. We observed photon antibunching and bunching, when transitioning from one to several atoms interacting with the nanofiber mode. We realized that the second-order correlation function of spontaneously emitted photons can also be used to characterize the dynamics and the temperature of atoms around the ONF. These results are published in the 2015 Phys. Rev. A paper [130].

At the end of 2015 our theory collaborators Zachary Eldredge and Alexey Gorshkov, invited us to participate in the discussion of one of their ideas. They were working on self-organizing chiral systems and the possibility to implement it with ONF. The collaboration started, I think, because they wanted our opinion as experimentalists about the feasibility of their proposal. I doubt that my input changed even a little their motivations, calculations, and fascinating ideas. However, I feel glad that they approached us, because it helped me to see the same system I had been working on for the past two years with a different perspective, a theorist perspective. As a result of that work we published a Phys. Rev. A paper on 2016 [114].

During 2016 we finished the measurements from an old idea that Jonathan Hoffman left behind when he graduated. Fortunately the ghost of the idea was haunting us, impersonated by our long term close collaborator Fredrik Fatemi. Running the fiber pulling experiment after a couple of years of not being in use could be a challenge. Thankfully I had the help of Eliot Fenton (a skilled second year undergraduate student!) to make everything run in perfect conditions. This project represents to me a good summary of all the things we learned about ONF fabrication, characterization, and understanding of its mode structure. We use the beat

note between propagating higher order modes to extract the ONF radius. The difference between the propagation constant of the modes is proportional to the radius of the nanofiber. This produces a spatial beating frequency between different modes propagating along the ONF, providing a way to characterize the ONF radius. We collect the signal of the interference pattern, by evanescently coupling a probe optical fiber and scanning its position along the nanofiber. We are able to measure the nanofiber radius with sub-Angstrom sensitivity. Our results are published in the 2017 Optica paper [131].

More recently, we were invited by the editors of Advances in Atomic and Molecular Optics to contribute with a review paper (to be published soon) about ONF as a platform for quantum optics [87], which contains information complementary to this thesis.

Ultrahigh transmission optical nanofibers

J. E. Hoffman,¹ S. Ravets,^{1,2} J. A. Grover,¹ P. Solano,¹ P. R. Kordell,¹ J. D. Wong-Campos,¹ L. A. Orozco,¹ and S. L. Rolston^{1,a}

¹*Joint Quantum Institute, Department of Physics, University of Maryland, and National Institute of Standards and Technology, College Park, MD 20742, U.S.A.*

²*Laboratoire Charles Fabry, Institut d'Optique, CNRS Univ Paris-Sud, Campus Polytechnique, RD 128, 91127 Palaiseau cedex, France*

(Received 26 March 2014; accepted 13 May 2014; published online 17 June 2014)

We present a procedure for reproducibly fabricating ultrahigh transmission optical nanofibers (530 nm diameter and 84 mm stretch) with single-mode transmissions of $99.95 \pm 0.02\%$, which represents a loss from tapering of 2.6×10^{-5} dB/mm when normalized to the entire stretch. When controllably launching the next family of higher-order modes on a fiber with 195 mm stretch, we achieve a transmission of $97.8 \pm 2.8\%$, which has a loss from tapering of 5.0×10^{-4} dB/mm when normalized to the entire stretch. Our pulling and transfer procedures allow us to fabricate optical nanofibers that transmit more than 400 mW in high vacuum conditions. These results, published as parameters in our previous work, present an improvement of two orders of magnitude less loss for the fundamental mode and an increase in transmission of more than 300% for higher-order modes, when following the protocols detailed in this paper. We extract from the transmission during the pull, the only reported spectrogram of a fundamental mode launch that does not include excitation to asymmetric modes; in stark contrast to a pull in which our cleaning protocol is not followed. These results depend critically on the pre-pull cleanliness and when properly following our pulling protocols are in excellent agreement with simulations. © 2014 Author(s). All article content, except where otherwise noted, is licensed under a Creative Commons Attribution 3.0 Unported License. [<http://dx.doi.org/10.1063/1.4879799>]



Photon-correlation measurements of atomic-cloud temperature using an optical nanofiber

J. A. Grover, P. Solano, L. A. Orozco, and S. L. Rolston*

*Joint Quantum Institute, Department of Physics, University of Maryland and National Institute of Standards and Technology,
College Park, Maryland 20742, USA*

(Received 25 June 2015; published 28 July 2015)

We develop a temperature measurement of an atomic cloud based on the temporal correlations of fluorescence photons evanescently coupled into an optical nanofiber. We measure the temporal width of the intensity-intensity correlation function due to atomic transit time and use it to determine the most probable atomic velocity, hence the temperature. This technique agrees well with standard time-of-flight temperature measurements. We confirm our results with trajectory simulations.

DOI: [10.1103/PhysRevA.92.013850](https://doi.org/10.1103/PhysRevA.92.013850)

Self-organization of atoms coupled to a chiral reservoir

Zachary Eldredge,^{1,2} Pablo Solano,¹ Darrick Chang,³ and Alexey V. Gorshkov^{1,2}

¹*Joint Quantum Institute, NIST/University of Maryland, College Park, Maryland 20742, USA*

²*Joint Center for Quantum Information and Computer Science, NIST/University of Maryland, College Park, Maryland 20742, USA*

³*ICFO–Institut de Ciències Fotoniques, The Barcelona Institute of Science and Technology, 08860 Castelldefels (Barcelona), Spain*

(Received 31 May 2016; published 29 November 2016)

Tightly confined modes of light, as in optical nanofibers or photonic crystal waveguides, can lead to large optical coupling in atomic systems, which mediates long-range interactions between atoms. These one-dimensional systems can naturally possess couplings that are asymmetric between modes propagating in different directions. Strong long-range interaction among atoms via these modes can drive them to a self-organized periodic distribution. In this paper, we examine the self-organizing behavior of atoms in one dimension coupled to a chiral reservoir. We determine the solution to the equations of motion in different parameter regimes, relative to both the detuning of the pump laser that initializes the atomic dipole-dipole interactions and the degree of reservoir chirality. In addition, we calculate possible experimental signatures such as reflectivity from self-organized atoms and motional sidebands.

DOI: [10.1103/PhysRevA.94.053855](https://doi.org/10.1103/PhysRevA.94.053855)

Modal interference in optical nanofibers for sub-Angstrom radius sensitivity

FREDRIK K. FATEMI,^{1,*} JONATHAN E. HOFFMAN,² PABLO SOLANO,² ELIOT F. FENTON,² GUY BEADIE,³ STEVEN L. ROLSTON,² AND LUIS A. OROZCO²

¹Army Research Laboratory, Adelphi, Maryland 20783, USA

²Joint Quantum Institute, Department of Physics, University of Maryland and National Institute of Standards and Technology, College Park, Maryland 20742, USA

³Naval Research Laboratory, Washington, DC 20375, USA

*Corresponding author: fredrik.k.fatemi.civ@mail.mil

Received 30 September 2016; revised 23 November 2016; accepted 26 November 2016 (Doc. ID 277963); published 19 January 2017

Optical nanofibers (ONFs) of sub-wavelength dimensions confine light in modes with a strong evanescent field that can trap, probe, and manipulate nearby quantum systems. To measure the evanescent field and propagating modes and to optimize ONF performance, a surface probe is desirable during fabrication. We demonstrate a nondestructive near-field measurement of light propagation in ONFs by sampling the local evanescent field with a microfiber. This approach reveals the behavior of all propagating modes, and because the modal beat lengths in cylindrical waveguides depend strongly on the radius, it simultaneously provides exquisite sensitivity to the ONF radius. We show that our measured spatial frequencies provide a map of the average ONF radius (over a 600 μm window) along the 10 mm ONF waist with a 40 pm resolution and a high signal-to-noise ratio. The measurements agree with scanning electron microscopy (SEM) to within SEM instrument resolutions. This fast method is immune to polarization, intrinsic birefringence, mechanical vibrations, and scattered light and provides a set of constraints to protect from systematic errors in the measurements. © 2017 Optical Society of America

OCIS codes: (060.2310) Fiber optics; (350.4238) Nanophotonics and photonic crystals; (060.2270) Fiber characterization.

<https://doi.org/10.1364/OPTICA.4.000157>

Optical Nanofibers: a new platform for quantum optics

Pablo Solano^a, Jeffrey A. Grover^a, Jonathan E. Hoffman^a, Sylvain Ravets^{a,b}, Fredrik K. Fatemi^c, Luis A. Orozco^a, Steven L. Rolston^a

^a*Joint Quantum Institute, Department of Physics, University of Maryland and NIST, College Park, MD 20742, USA.*

^b*Laboratoire Charles Fabry, Institut d'Optique, CNRS, Univ Paris Sud, 2 Avenue Augustin Fresnel, 91127 Palaiseau cedex, France*

^c*Army Research Laboratory, Adelphi, MD 20783, USA.*

Abstract

The development of optical nanofibers (ONF) and the study and control of their optical properties when coupling atoms to their electromagnetic modes has opened new possibilities for their use in quantum optics and quantum information science. These ONFs offer tight optical mode confinement (less than the wavelength of light) and diffraction-free propagation. The small cross section of the transverse field allows probing of linear and non-linear spectroscopic features of atoms with exquisitely low power. The cooperativity – the figure of merit in many quantum optics and quantum information systems – tends to be large even for a single atom in the mode of an ONF, as it is proportional to the ratio of the atomic cross section to the electromagnetic mode cross section. ONFs offer a natural bus for information and for inter-atomic coupling through the tightly-confined modes, which opens the possibility of one-dimensional many-body physics and interesting quantum interconnection applications. The presence of the ONF modifies the vacuum field, affecting the spontaneous emission rates of atoms in its vicinity. The high gradients in the radial intensity naturally provide the potential for trapping atoms around the ONF, allowing the creation of one-dimensional arrays of atoms. The same radial gradient in the transverse direction of the field is responsible for the existence of a large longitudinal component that introduces the possibility of spin-orbit coupling of the light and the atom, enabling the exploration of chiral quantum optics.

Keywords: nanofibers, atomic traps, quantum optics, chiral quantum optics, quantum information

Contents

Bibliography

- [1] S. Haroche and J.-M. Raimond. *Exploring the Quantum: Atoms, Cavities, and Photons*. Oxford University Press, 2006.
- [2] H. J. Kimble. Strong Interactions of Single Atoms and Photons in Cavity QED. *Phys. Scr.*, T76(1):127, January 1998. ISSN 0031-8949. doi: 10.1238/Physica.Topical.076a00127. URL <http://iopscience.iop.org/1402-4896/1998/T76/019>.
- [3] E. A. Hinds. *Advances in Atomic, Molecular, and Optical Physics, Supplement 2, Cavity Quantum Electrodynamics*, chapter Perturbative Cavity Quantum Electrodynamics, pages 1–56. Academic Press, Boston, 1994.
- [4] S. Haroche. Nobel Lecture: Controlling photons in a box and exploring the quantum to classical boundary. *Rev. Mod. Phys.*, 85(3):1083–1102, July 2013. ISSN 0034-6861. doi: 10.1103/RevModPhys.85.1083. URL <http://link.aps.org/doi/10.1103/RevModPhys.85.1083>.
- [5] A. Wallraff, D. I. Schuster, A. Blais, L. Frunzio, R.-S. Huang, J. Majer, S. Kumar, S. M. Girvin, and R. J. Schoelkopf. Strong coupling of a single photon to a superconducting qubit using circuit quantum electrodynamics. *Nature*, 431(7005):162–7, September 2004. ISSN 1476-4687. doi: 10.1038/nature02851. URL <http://dx.doi.org/10.1038/nature02851>.
- [6] H. J. Kimble. *Advances in Atomic, Molecular, and Optical Physics, Supplement 2, Cavity Quantum Electrodynamics*, chapter Structure and Dynamics in Cavity Quantum Electrodynamics, pages 203–267. Academic Press, Boston, 1994.
- [7] A. Reiserer and G. Rempe. Cavity-based quantum networks with single atoms and optical photons. *Rev. Mod. Phys.*, 87:1379–1418, Dec 2015. doi: 10.1103/RevModPhys.87.1379. URL <http://link.aps.org/doi/10.1103/RevModPhys.87.1379>.
- [8] G. Calajó, F. Ciccarello, D. Chang, and P. Rabl. Atom-field dressed states in slow-light waveguide QED. *Phys. Rev. A*, 93:033833, Mar 2016. doi: 10.1103/

- PhysRevA.93.033833. URL <http://link.aps.org/doi/10.1103/PhysRevA.93.033833>.
- [9] Y.-L. L. Fang and H. U. Baranger. Waveguide qed: Power spectra and correlations of two photons scattered off multiple distant qubits and a mirror. *Phys. Rev. A*, 91:053845, May 2015. doi: 10.1103/PhysRevA.91.053845. URL <http://link.aps.org/doi/10.1103/PhysRevA.91.053845>.
 - [10] V. Paulisch, H. J. Kimble, and A. González-Tudela. Universal quantum computation in waveguide qed using decoherence free subspaces. *New Journal of Physics*, 18(4):043041, 2016. URL <http://stacks.iop.org/1367-2630/18/i=4/a=043041>.
 - [11] P. Lodahl, S. Mahmoodian, and S. Stobbe. Interfacing single photons and single quantum dots with photonic nanostructures. *Rev. Mod. Phys.*, 87:347–400, May 2015. doi: 10.1103/RevModPhys.87.347. URL <http://link.aps.org/doi/10.1103/RevModPhys.87.347>.
 - [12] J. J. Sanchez-Mondragon, N. B. Narozhny, and J. H. Eberly. Theory of spontaneous-emission line shape in an ideal cavity. *Phys. Rev. Lett.*, 51:550–553, Aug 1983. doi: 10.1103/PhysRevLett.51.550. URL <http://link.aps.org/doi/10.1103/PhysRevLett.51.550>.
 - [13] D. J. Wineland. Nobel Lecture: Superposition, entanglement, and raising Schrödinger’s cat. *Rev. Mod. Phys.*, 85(3):1103–1114, July 2013. ISSN 0034-6861. doi: 10.1103/RevModPhys.85.1103. URL <http://link.aps.org/doi/10.1103/RevModPhys.85.1103>.
 - [14] H. M. Gibbs, G. Khitrova, and S. W. Koch. Exciton-polariton light-semiconductor coupling effects. *Nat Photon*, 5(5):273–273, 05 2011. URL <http://dx.doi.org/10.1038/nphoton.2011.15>.
 - [15] S. Groblacher, K. Hammerer, M. R. Vanner, and M. Aspelmeyer. Observation of strong coupling between a micromechanical resonator and an optical cavity field. *Nature*, 460(7256):724–727, August 2009. ISSN 0028-0836. doi: 10.1038/nature08171. URL <http://dx.doi.org/10.1038/nature08171>.
 - [16] A. Blais, R. Huang, A. Wallraff, S. Girvin, and R. Schoelkopf. Cavity quantum electrodynamics for superconducting electrical circuits: An architecture for quantum computation. *Phys. Rev. A*, 69(6):062320, June 2004. URL <http://journals.aps.org/prabSTRACT/10.1103/PhysRevA.69.062320>.
 - [17] L. A. Lugiato. Theory of optical bistability. In E. Wolf, editor, *Progress in Optics*, volume XXI, pages 69–216. North-Holland, Amsterdam, 1984.
 - [18] R. Bonifacio and L. A. Lugiato, editors. *Dissipative Systems in Quantum Optics*, volume 27 of *Springer Series Topics in Current Physics*. Springer Verlag, Berlin, Heidelberg, New York, 1982.

- [19] M. S. Safronova, C. J. Williams, and C. W. Clark. Relativistic many-body calculations of electric-dipole matrix elements, lifetimes, and polarizabilities in rubidium. *Phys. Rev. A*, 69:022509, Feb 2004. doi: 10.1103/PhysRevA.69.022509. URL <http://link.aps.org/doi/10.1103/PhysRevA.69.022509>.
- [20] H. Tanji-Suzuki, I. D. Leroux, M. H. Schleier-Smith, M. Cetina, A. T. Grier, J. Simon, and V. Vuletić. Interaction between Atomic Ensembles and Optical Resonators: Classical Description. In *Adv. At. Mol. Opt. Phys.*, volume 60, pages 201–237. Elsevier, 2011. ISBN 9780123855084. doi: 10.1016/B978-0-12-385508-4.00004-8. URL <http://www.sciencedirect.com/science/article/pii/B9780123855084000048>.
- [21] M. Fleischhauer, A. Imamoglu, and J. P. Marangos. Electromagnetically induced transparency: Optics in coherent media. *Rev. Mod. Phys.*, 77:633–673, Jul 2005. doi: 10.1103/RevModPhys.77.633. URL <http://link.aps.org/doi/10.1103/RevModPhys.77.633>.
- [22] Y. Makhlin, G. Schön, and A. Shnirman. Quantum-state engineering with Josephson-junction devices. *Rev. Mod. Phys.*, 73(2):357–400, May 2001. ISSN 0034-6861. doi: 10.1103/RevModPhys.73.357. URL <http://link.aps.org/doi/10.1103/RevModPhys.73.357>.
- [23] M. K. Tey, Z. Chen, S. A. Aljunid, B. Chng, F. Huber, G. Maslennikov, and C. Kurtsiefer. Strong interaction between light and a single trapped atom without the need for a cavity. *Nat. Phys.*, 4(12):924–927, October 2008. ISSN 1745-2473. doi: 10.1038/nphys1096. URL <http://dx.doi.org/10.1038/nphys1096>.
- [24] G. Hétet, L. Slodička, M. Hennrich, and R. Blatt. Single Atom as a Mirror of an Optical Cavity. *Phys. Rev. Lett.*, 107(13):133002, September 2011. ISSN 0031-9007. doi: 10.1103/PhysRevLett.107.133002. URL <http://link.aps.org/doi/10.1103/PhysRevLett.107.133002>.
- [25] E. W. Streed, A. Jechow, B. G. Norton, and D. Kielpinski. Absorption imaging of a single atom. *Nat. Commun.*, 3:933, January 2012. ISSN 2041-1723. doi: 10.1038/ncomms1944. URL <http://dx.doi.org/10.1038/ncomms1944>.
- [26] M. Stobińska, G. Alber, and G. Leuchs. Perfect excitation of a matter qubit by a single photon in free space. *Europhysics Letters*, 86:14007, January 2009. URL <http://iopscience.iop.org/0295-5075/86/1/14007>.
- [27] A. Golla, B. Chalopin, M. Bader, I. Harder, K. Mantel, R. Maiwald, N. Lindlein, M. Sondermann, and G. Leuchs. Generation of a wave packet tailored to efficient free space excitation of a single atom. *Eur. Phys. J. D*, 66(7):190, July 2012. ISSN 1434-6060. doi: 10.1140/epjd/e2012-30293-y. URL <http://www.springerlink.com/index/10.1140/epjd/e2012-30293-y>.

- [28] S. Heugel, B. Chalopin, M. Sondermann, and G. Leuchs. Collecting more than half the fluorescence photons from a single ion. *Phys. Rev. A*, 86:043431, January 2012. ISSN 1094-1622. URL <http://pra.aps.org/abstract/PRA/v86/i4/e043431>.
- [29] J. D. Thompson, T. G. Tiecke, N. P. de Leon, J. Feist, A. V. Akimov, M. Gullans, A. S. Zibrov, V. Vuletić, and M. D. Lukin. Coupling a Single Trapped Atom to a Nanoscale Optical Cavity. *Science*, 340(6137):1202, January 2013. ISSN 1095-9203. doi: 10.1126/science.1237125. URL <http://www.sciencemag.org/content/340/6137/1202.short>.
- [30] A. Goban, C.-L. Hung, S.-P. Yu, J. Hood, J. Muniz, J. Lee, M. Martin, A. McClung, K. Choi, D. Chang, O. Painter, and H. Kimble. Atom–light interactions in photonic crystals. *Nat. Commun.*, 5, May 2014. ISSN 2041-1723. doi: 10.1038/ncomms4808. URL <http://www.nature.com/ncomms/2014/140508/ncomms4808/full/ncomms4808.html>.
- [31] A. Goban, C.-L. Hung, J. D. Hood, S.-P. Yu, J. A. Muniz, O. Painter, and H. J. Kimble. Superradiance for atoms trapped along a photonic crystal waveguide. *Phys. Rev. Lett.*, 115:063601, Aug 2015. doi: 10.1103/PhysRevLett.115.063601. URL <http://link.aps.org/doi/10.1103/PhysRevLett.115.063601>.
- [32] J. D. Hood, A. Goban, A. Asenjo-Garcia, M. Lu, S.-P. Yu, D. E. Chang, and H. J. Kimble. Atom–atom interactions around the band edge of a photonic crystal waveguide. *Proceedings of the National Academy of Sciences*, 113(38):10507–10512, 2016. doi: 10.1073/pnas.1603788113. URL <http://www.pnas.org/content/113/38/10507.abstract>.
- [33] S. Ghosh, A. R. Bhagwat, C. K. Renshaw, S. Goh, A. L. Gaeta, and B. J. Kirby. Low-light-level optical interactions with rubidium vapor in a photonic band-gap fiber. *Phys. Rev. Lett.*, 97:023603, Jul 2006. doi: 10.1103/PhysRevLett.97.023603. URL <http://link.aps.org/doi/10.1103/PhysRevLett.97.023603>.
- [34] M. Bajcsy, S. Hofferberth, V. Balic, T. Peyronel, M. Hafezi, A. S. Zibrov, V. Vuletic, and M. D. Lukin. Efficient all-optical switching using slow light within a hollow fiber. *Phys. Rev. Lett.*, 102:203902, May 2009. doi: 10.1103/PhysRevLett.102.203902. URL <http://link.aps.org/doi/10.1103/PhysRevLett.102.203902>.
- [35] V. Venkataraman, K. Saha, P. Londero, and A. L. Gaeta. Few-photon all-optical modulation in a photonic band-gap fiber. *Phys. Rev. Lett.*, 107:193902, Nov 2011. doi: 10.1103/PhysRevLett.107.193902. URL <http://link.aps.org/doi/10.1103/PhysRevLett.107.193902>.
- [36] M. R. Sprague, P. S. Michelberger, T. F. M. Champion, D. G. England, J. Nunn, X. M. Jin, W. S. Kolthammer, A. Abdolvand, P. S. J. Russell,

- and I. A. Walmsley. Broadband single-photon-level memory in a hollow-core photonic crystal fibre. *Nat Photon*, 8(4):287–291, 04 2014. URL <http://dx.doi.org/10.1038/nphoton.2014.45>.
- [37] E. Vetsch, D. Reitz, G. Sagué, R. Schmidt, S. T. Dawkins, and A. Rauschenbeutel. Optical interface created by laser-cooled atoms trapped in the evanescent field surrounding an optical nanofiber. *Phys. Rev. Lett.*, 104(20):203603, May 2010. doi: 10.1103/PhysRevLett.104.203603. URL <http://link.aps.org/doi/10.1103/PhysRevLett.104.203603>.
- [38] A. Goban, K. S. Choi, D. J. Alton, D. Ding, C. Lacroûte, M. Pototschnig, T. Thiele, N. P. Stern, and H. J. Kimble. Demonstration of a state-insensitive, compensated nanofiber trap. *Phys. Rev. Lett.*, 109:033603, Jul 2012. doi: 10.1103/PhysRevLett.109.033603. URL <http://link.aps.org/doi/10.1103/PhysRevLett.109.033603>.
- [39] J.-B. Béguin, E. Bookjans, S. Christensen, H. Sørensen, J. Müller, E. Polzik, and J. Appel. Generation and Detection of a Sub-Poissonian Atom Number Distribution in a One-Dimensional Optical Lattice. *Phys. Rev. Lett.*, 113(26):263603, December 2014. ISSN 0031-9007. doi: 10.1103/PhysRevLett.113.263603. URL <http://link.aps.org/doi/10.1103/PhysRevLett.113.263603>.
- [40] J. Lee, J. A. Grover, J. E. Hoffman, L. A. Orozco, and S. L. Rolston. Inhomogeneous broadening of optical transitions of ^{87}rb atoms in an optical nanofiber trap. *Journal of Physics B: Atomic, Molecular and Optical Physics*, 48(16):165004, 2015. URL <http://stacks.iop.org/0953-4075/48/i=16/a=165004>.
- [41] S. Kato and T. Aoki. Strong coupling between a trapped single atom and an all-fiber cavity. *Phys. Rev. Lett.*, 115:093603, Aug 2015. doi: 10.1103/PhysRevLett.115.093603. URL <http://link.aps.org/doi/10.1103/PhysRevLett.115.093603>.
- [42] N. V. Corzo, B. Gouraud, A. Chandra, A. Goban, A. S. Sheremet, D. Kupriyanov, and J. Laurat. Large bragg reflection from one-dimensional chains of trapped atoms near a nanoscale waveguide. *Phys. Rev. Lett.*, 117:133603, Sep 2016. doi: 10.1103/PhysRevLett.117.133603. URL <http://link.aps.org/doi/10.1103/PhysRevLett.117.133603>.
- [43] J. A. Grover. *Atom-trapping and photon-counting experiments with optical nanofibers*. PhD thesis, University of Maryland College Park, 2015. URL <http://drum.lib.umd.edu/handle/1903/16638>.
- [44] J. E. Hoffman, S. Ravets, J. A. Grover, P. Solano, P. R. Kordell, J. D. Wong-Campos, L. A. Orozco, and S. L. Rolston. Ultrahigh transmission optical nanofibers. *AIP Adv.*, 4(6):067124, June 2014. ISSN 2158-3226. doi: 10.1063/

- 1.4879799. URL <http://scitation.aip.org/content/aip/journal/adva/4/6/10.1063/1.4879799>.
- [45] J. M. Ward, A. Maimaiti, V. H. Le, and S. Nic Chormaic. Contributed Review: Optical micro- and nanofiber pulling rig. *Rev. Sci. Instrum.*, 85(11):111501, November 2014. ISSN 0034-6748. doi: 10.1063/1.4901098. URL <http://scitation.aip.org/content/aip/journal/rsi/85/11/10.1063/1.4901098>.
- [46] H. J. Kimble. The quantum internet. *Nature*, 453(7198):1023–30, June 2008. ISSN 1476-4687. doi: 10.1038/nature07127. URL <http://dx.doi.org/10.1038/nature07127>.
- [47] G. Kurizki, P. Bertet, Y. Kubo, K. Mlmer, D. Petrosyan, P. Rabl, and J. Schmiedmayer. Quantum technologies with hybrid systems. *Proceedings of the National Academy of Sciences*, 112(13):3866–3873, 2015. doi: 10.1073/pnas.1419326112. URL <http://www.pnas.org/content/112/13/3866.abstract>.
- [48] Z.-L. Xiang, S. Ashhab, J. Q. You, and F. Nori. Hybrid quantum circuits: Superconducting circuits interacting with other quantum systems. *Rev. Mod. Phys.*, 85:623–653, Apr 2013. doi: 10.1103/RevModPhys.85.623. URL <http://link.aps.org/doi/10.1103/RevModPhys.85.623>.
- [49] J. E. Hoffman, J. A. Grover, Z. Kim, A. K. Wood, J. R. Anderson, A. J. Dragt, M. Hafezi, C. J. Lobb, L. A. Orozco, S. L. Rolston, J. M. Taylor, C. P. Vlahacos, and F. C. Wellstood. Atoms Talking to SQUIDs. *Rev. Mex. Fís. S.*, 57:1, August 2011. URL <http://arxiv.org/abs/1108.4153v2>.
- [50] Z. Kim, C. P. Vlahacos, J. E. Hoffman, J. A. Grover, K. D. Voigt, B. K. Cooper, C. J. Ballard, B. S. Palmer, M. Hafezi, J. M. Taylor, J. R. Anderson, A. J. Dragt, C. J. Lobb, L. A. Orozco, S. L. Rolston, and F. C. Wellstood. Thin-film superconducting resonator tunable to the ground-state hyperfine splitting of ^{87}Rb . *AIP Adv.*, 1(4):042107, October 2011. ISSN 21583226. doi: 10.1063/1.3651466. URL <http://scitation.aip.org/content/aip/journal/adva/1/4/10.1063/1.3651466>.
- [51] M. Hafezi, Z. Kim, S. L. Rolston, L. A. Orozco, B. L. Lev, and J. M. Taylor. Atomic interface between microwave and optical photons. *Phys. Rev. A*, 85(2): 020302, February 2012. ISSN 1050-2947. doi: 10.1103/PhysRevA.85.020302. URL <http://link.aps.org/doi/10.1103/PhysRevA.85.020302>.
- [52] P. Lodahl, S. Mahmoodian, S. Stobbe, P. Schneeweiss, J. Volz, A. Rauschenbeutel, H. Pichler, and P. Zoller. Chiral quantum optics. *Nature*, 541(7638):473–480, January 2017. ISSN 0028-0836. doi: 10.1038/nature21037. URL <http://www.nature.com/nature/journal/v541/n7638/full/nature21037.html>.

- [53] S. Yu, J. D. Hood, J. A. Muniz, M. J. Martin, R. Norte, C.-L. Hung, S. M. Meenehan, J. D. Cohen, O. Painter, and H. J. Kimble. Nanowire photonic crystal waveguides for single-atom trapping and strong light-matter interactions. *Applied Physics Letters*, 104(11):111103, 2014. doi: 10.1063/1.4868975. URL <http://aip.scitation.org/doi/abs/10.1063/1.4868975>.
- [54] Q. Quan, I. Bulu, and M. Lončar. Broadband waveguide qed system on a chip. *Phys. Rev. A*, 80:011810, Jul 2009. doi: 10.1103/PhysRevA.80.011810. URL <http://link.aps.org/doi/10.1103/PhysRevA.80.011810>.
- [55] R. K. Chang and A. J. Campillo, editors. *Optical Processes in Microcavities*, volume 3 of *Advanced Series in Applied Physics*. World Scientific, Singapore, 1996. URL <http://www.worldscientific.com/worldscibooks/10.1142/2828#t=aboutBook>.
- [56] D. E. Chang, L. Jiang, A. V. Gorshkov, and K. H. J. Cavity QED with atomic mirrors. *New J. Phys.*, 14:063003, January 2012. URL <http://iopscience.iop.org/1367-2630/14/6/063003>.
- [57] K. J. Blow, R. Loudon, S. J. D. Phoenix, and T. J. Shepherd. Continuum fields in quantum optics. *Phys. Rev. A*, 42:4102–4114, Oct 1990. doi: 10.1103/PhysRevA.42.4102. URL <http://link.aps.org/doi/10.1103/PhysRevA.42.4102>.
- [58] K. C. Kao and G. A. Hockham. Dielectric-fibre surface waveguides for optical frequencies. *Proc. IET*, 113(7):1151–1158, 1966. URL <https://doi.org/10.1049/piee.1966.0189>.
- [59] C. K. Kao. Nobel lecture: Sand from centuries past: Send future voices fast*. *Rev. Mod. Phys.*, 82:2299–2303, Aug 2010. doi: 10.1103/RevModPhys.82.2299. URL <http://link.aps.org/doi/10.1103/RevModPhys.82.2299>.
- [60] G. Brambilla. Optical fibre nanowires and microwires: a review. *J. Opt.*, 12(4):043001, April 2010. ISSN 2040-8978. doi: 10.1088/2040-8978/12/4/043001. URL <http://iopscience.iop.org/2040-8986/12/4/043001>.
- [61] G. Y. Chen, M. Ding, T. P. Newson, and G. Brambilla. A review of microfiber and nanofiber based optical sensors. *The Open Optics Journal*, 7: (Suppl-1, M3) 32–57, 2013. URL <https://benthamopen.com/ABSTRACT/TOOPTSJ-7-32>.
- [62] M. J. Morrissey, K. Deasy, M. Frawley, R. Kumar, E. Prel, L. Russell, V. G. Truong, and S. Nic Chormaic. Spectroscopy, manipulation and trapping of neutral atoms, molecules, and other particles using optical nanofibers: a review. *Sensors (Basel)*, 13(8):10449–81, January 2013. ISSN 1424-8220. doi: 10.3390/s130810449. URL <http://www.mdpi.com/1424-8220/13/8/10449/htm>.

- [63] F. Le Kien, J. Liang, K. Hakuta, and V. Balykin. Field intensity distributions and polarization orientations in a vacuum-clad subwavelength-diameter optical fiber. *Optics Communications*, 242(4–6):445 – 455, 2004. ISSN 0030-4018. doi: <http://dx.doi.org/10.1016/j.optcom.2004.08.044>. URL <http://www.sciencedirect.com/science/article/pii/S0030401804008739>.
- [64] G. Sagué, A. Baade, and A. Rauschenbeutel. Blue-detuned evanescent field surface traps for neutral atoms based on mode interference in ultrathin optical fibres. *New J. Phys.*, 10:113008, 2008. URL <http://stacks.iop.org/1367-2630/10/i=11/a=113008>.
- [65] F. Le Kien, V. I. Balykin, and K. Hakuta. Atom trap and waveguide using a two-color evanescent light field around a subwavelength-diameter optical fiber. *Phys. Rev. A*, 70:063403, Dec 2004. doi: 10.1103/PhysRevA.70.063403. URL <http://link.aps.org/doi/10.1103/PhysRevA.70.063403>.
- [66] D. Reitz and A. Rauschenbeutel. Nanofiber-based double-helix dipole trap for cold neutral atoms. *Opt. Commun.*, 285:4705–4708, 2012. URL <http://dx.doi.org/10.1016/j.optcom.2012.06.034>.
- [67] D. J. Alton, N. P. Stern, T. Aoki, H. Lee, E. Ostby, K. J. Vahala, and H. J. Kimble. Strong interactions of single atoms and photons near a dielectric boundary. *Nat. Phys.*, 7(2):159–165, November 2011. ISSN 1745-2473. doi: 10.1038/nphys1837. URL <http://dx.doi.org/10.1038/nphys1837>.
- [68] F. Le Kien, S. Dutta Gupta, V. Balykin, and K. Hakuta. Spontaneous emission of a cesium atom near a nanofiber: Efficient coupling of light to guided modes. *Phys. Rev. A*, 72(3):32509, September 2005. ISSN 1094-1622. URL <http://journals.aps.org/prabSTRACT/10.1103/PhysRevA.72.032509>.
- [69] C. Wuttke, M. Becker, S. Brückner, M. Rothhardt, and A. Rauschenbeutel. Nanofiber fabry–perot microresonator for nonlinear optics and cavity quantum electrodynamics. *Opt. Lett.*, 37(11):1949–1951, Jun 2012. doi: 10.1364/OL.37.001949. URL <http://ol.osa.org/abstract.cfm?URI=ol-37-11-1949>.
- [70] J. C. Knight, G. Cheung, F. Jacques, and T. A. Birks. Phase-matched excitation of whispering-gallery-mode resonances by a fiber taper. *Opt. Lett.*, 22: 1129–1131, 1997. URL <https://doi.org/10.1364/OL.22.001129>.
- [71] K. P. Nayak, P. N. Melentiev, M. Morinaga, F. L. Kien, V. I. Balykin, and K. Hakuta. Optical nanofiber as an efficient tool for manipulating and probing atomic fluorescence. *Opt. Express*, 15(9):5431–5438, Apr 2007. doi: 10.1364/OE.15.005431. URL <http://www.opticsexpress.org/abstract.cfm?URI=oe-15-9-5431>.
- [72] G. Kakarantzas, T. A. Birks, and P. S. J. Russell. Structural long-period gratings in photonic crystal fibers. *Opt. Lett.*, 27:1013–1015, 2002. URL <https://doi.org/10.1364/OL.27.001013>.

- [73] S. M. Spillane, T. J. Kippenberg, O. J. Painter, and K. J. Vahala. Ideality in a fiber-taper-coupled microresonator system for application to cavity quantum electrodynamics. *Phys. Rev. Lett.*, 91:043902, Jul 2003. doi: 10.1103/PhysRevLett.91.043902. URL <http://link.aps.org/doi/10.1103/PhysRevLett.91.043902>.
- [74] Y. Louyer, D. Meschede, and A. Rauschenbeutel. Tunable whispering-gallery-mode resonators for cavity quantum electrodynamics. *Phys. Rev. A*, 72: 031801, 2005. URL <http://journals.aps.org/prabSTRACT/10.1103/PhysRevA.72.031801>.
- [75] M. J. Morrissey, K. Deasy, S. Chakrabarti, and S. Nic Chormaic. Tapered optical fibers as tools for probing magneto-optical trap characteristics. *Review of Scientific Instruments*, 80(5):053102, 2009. doi: 10.1063/1.3117201. URL <http://dx.doi.org/10.1063/1.3117201>.
- [76] M. Fujiwara, T. Noda, A. Tanaka, K. Toubaru, H. Q. Zhao, and S. Takeuchi. Coupling of ultrathin tapered fibers with high-q microsphere resonators at cryogenic temperatures and observation of phase-shift transition from undercoupling to overcoupling. *Opt. Express*, 20:19545–19553, 2012. URL <https://www.osapublishing.org/oe/abstract.cfm?URI=oe-20-17-19545>.
- [77] T. Schröder, M. Fujiwara, T. Noda, H.-Q. Zhao, O. Benson, and S. Takeuchi. A nanodiamond-tapered fiber system with high single-mode coupling efficiency. *Opt. Express*, 20(10):10490–10497, May 2012. doi: 10.1364/OE.20.010490. URL <http://www.opticsexpress.org/abstract.cfm?URI=oe-20-10-10490>.
- [78] M. Sadgrove, R. Yalla, K. P. Nayak, and K. Hakuta. Photonic crystal nanofiber using an external grating. *Opt. Lett.*, 38(14):2542–2545, June 2013. URL <https://doi.org/10.1364/OL.38.002542>.
- [79] L. Tong, R. R. Gattass, J. B. Ashcom, S. He, J. Lou, M. Shen, I. Maxwell, and E. Mazur. Subwavelength-diameter silica wires for low-loss optical wave guiding. *Nature*, 426(6968):816–819, 12 2003. URL <http://dx.doi.org/10.1038/nature02193>.
- [80] R. Grimm, M. Weidemuller, and Y. B. Ovchinnikov. Optical dipole traps for neutral atoms. volume 42 of *Advances In Atomic, Molecular, and Optical Physics*, pages 95 – 170. Academic Press, 2000. doi: 10.1016/S1049-250X(08)60186-X. URL <http://www.sciencedirect.com/science/article/pii/S1049250X0860186X>.
- [81] D. Reitz, C. Sayrin, R. Mitsch, P. Schneeweiss, and A. Rauschenbeutel. Coherence Properties of Nanofiber-Trapped Cesium Atoms. *Phys. Rev. Lett.*, 110(24):243603, June 2013. ISSN 0031-9007. doi: 10.1103/PhysRevLett.110.243603. URL <http://link.aps.org/doi/10.1103/PhysRevLett.110.243603>.

- [82] C. Lacroûte, K. S. Choi, A. Goban, D. J. Alton, D. Ding, N. P. Stern, and H. J. Kimble. A state-insensitive, compensated nanofiber trap. *New J. Phys.*, 14:023056, 2012. URL <http://iopscience.iop.org/article/10.1088/1367-2630/14/2/023056/pdf>.
- [83] B. Albrecht, Y. Meng, C. Clausen, A. Dareau, P. Schneeweiss, and A. Rauschenbeutel. Fictitious magnetic-field gradients in optical microtraps as an experimental tool for interrogating and manipulating cold atoms. *Phys. Rev. A*, 94:061401, Dec 2016. doi: 10.1103/PhysRevA.94.061401. URL <http://link.aps.org/doi/10.1103/PhysRevA.94.061401>.
- [84] P. Solano, F. K. Fatemi, and L. A. Orozco. Dynamics of trapped atoms around an optical nanofiber probed through polarimetry. *To be published*, :, 2017.
- [85] N. Schlosser, G. Reymond, and P. Grangier. Collisional blockade in microscopic optical dipole traps. *Phys. Rev. Lett.*, 89(2):023005, Jun 2002. doi: 10.1103/PhysRevLett.89.023005. URL <http://link.aps.org/doi/10.1103/PhysRevLett.89.023005>.
- [86] E. Vetsch, S. T. Dawkins, R. Mitsch, D. Reitz, P. Schneeweiss, and A. Rauschenbeutel. Nanofiber-based optical trapping of cold neutral atoms. *IEEE Journal of Selected Topics in Quantum Electronics*, 18(6):1763–1770, Nov 2012. ISSN 1077-260X. doi: 10.1109/JSTQE.2012.2196025. URL <http://dx.doi.org/10.1109/JSTQE.2012.2196025>.
- [87] P. Solano, J. A. Grover, J. E. Hoffman, S. Ravets, F. K. Fatemi, and L. A. O. ans S. L. Rolston. Optical nanofibers: a new platform for quantum optics polarimetry. *To be published*, :, 2017.
- [88] C. J. Foot. *Atomic Physics*. Oxford University Press, 2005.
- [89] X. Qi, B. Q. Baragiola, P. S. Jessen, and I. H. Deutsch. Dispersive response of atoms trapped near the surface of an optical nanofiber with applications to quantum nondemolition measurement and spin squeezing. *Phys. Rev. A*, 93:023817, Feb 2016. doi: 10.1103/PhysRevA.93.023817. URL <http://link.aps.org/doi/10.1103/PhysRevA.93.023817>.
- [90] S. Dawkins, R. Mitsch, D. Reitz, E. Vetsch, and A. Rauschenbeutel. Dispersive Optical Interface Based on Nanofiber-Trapped Atoms. *Phys. Rev. Lett.*, 107:243601, August 2011. URL <http://link.aps.org/doi/10.1103/PhysRevLett.107.243601>.
- [91] D. Cho. Analogous Zeeman effect from the tensor polarizability in alkali atoms. *J. Korean Phys. Soc.*, 30:373, 1997. URL http://old.kps.or.kr/jkps/abstract_view.asp?articleuid=A7132FDE-8732-42EA-9C20-907094FA6BEC&globalmenu=3&localmenu=10.

- [92] J. Ye, H. J. Kimble, and H. Katori. Quantum state engineering and precision metrology using state-insensitive light traps. *Science*, 320(5884):1734–1738, 2008. ISSN 0036-8075. doi: 10.1126/science.1148259. URL <http://science.sciencemag.org/content/320/5884/1734>.
- [93] B. Arora and B. K. Sahoo. State-insensitive trapping of Rb atoms: linearly versus circularly polarized lights. *Phys. Rev. A*, 86(3):033416, September 2012. ISSN 1050-2947. doi: 10.1103/PhysRevA.86.033416. URL <http://link.aps.org/doi/10.1103/PhysRevA.86.033416>.
- [94] F. Le Kien, V. Balykin, and K. Hakuta. State-Insensitive Trapping and Guiding of Cesium Atoms Using a Two-Color Evanescent Field around a Subwavelength-Diameter Fiber. *J. Phys. Soc. Japan*, 74(3):910–917, March 2005. ISSN 0031-9015. doi: 10.1143/JPSJ.74.910. URL <http://dx.doi.org/10.1143/JPSJ.74.910>.
- [95] D. Ding, A. Goban, K. S. Choi, and H. J. Kimble. Corrections to our results for optical nanofiber traps in Cesium. *arXiv:1212.4941 [physics, physics:quant-ph]*, December 2012. URL <http://arxiv.org/abs/1212.4941>. arXiv: 1212.4941.
- [96] F. Le Kien, P. Schneeweiss, and A. Rauschenbeutel. Dynamical polarizability of atoms in arbitrary light fields: general theory and application to cesium. *Eur. Phys. J. D*, 67(5):92, November 2013. ISSN 1434-6079. doi: 10.1140/epjd/e2013-30729-x. URL <http://dx.doi.org/10.1140/epjd/e2013-30729-x>.
- [97] P. Schneeweiss, F. L. Kien, and A. Rauschenbeutel. Nanofiber-based atom trap created by combining fictitious and real magnetic fields. *New J. Phys.*, 16(1):013014, January 2014. ISSN 1367-2630. doi: 10.1088/1367-2630/16/1/013014. URL <http://stacks.iop.org/1367-2630/16/i=1/a=013014>.
- [98] C. Wuttke, G. Cole, and A. Rauschenbeutel. Optically active mechanical modes of tapered optical fibers. *Phys. Rev. A*, 88(6):061801, November 2013. ISSN 1050-2947. doi: 10.1103/PhysRevA.88.061801. URL <http://arxiv.org/abs/1311.0916v1> <http://link.aps.org/doi/10.1103/PhysRevA.88.061801>.
- [99] F. K. Fatemi, P. Solano, L. A. Orozco, and S. L. Rolston. Polarimetric measurement of the motion of trapped atoms around a nanofiber. In APS, editor, *Bull. Am. Phys. Soc.*, volume 61 of *47th Annual Meeting of the APS Division of Atomic, Molecular and Optical Physics*, page G6.00009 , 2016. URL <http://meetings.aps.org/Meeting/DAMOP16/Session/G6.9>.
- [100] E. Fenton, A. Khan, B. Patterson, P. Solano, S. L. Rolston, L. A. Orozco, and F. K. Fatemi. Torsional modes of a nanofiber: polarimetric excitation and read out. In *Frontiers in Optics 2016*, page FTu3I.6. Optical Society of America,

2016. doi: 10.1364/FIO.2016.FTu3I.6. URL <http://www.osapublishing.org/abstract.cfm?URI=FiO-2016-FTu3I.6>.
- [101] G. A. Smith, S. Chaudhury, and P. S. Jessen. Faraday spectroscopy in an optical lattice: a continuous probe of atom dynamics. *J. Opt. B: Quantum Semiclass. Opt.*, 5:323–329, 2003. URL <http://iopscience.iop.org/article/10.1088/1464-4266/5/4/301>.
 - [102] V. V. Klimov and M. Ducloy. Spontaneous emission rate of an excited atom placed near a nanofiber. *Phys. Rev. A*, 69:013812, Jan 2004. doi: 10.1103/PhysRevA.69.013812. URL <http://link.aps.org/doi/10.1103/PhysRevA.69.013812>.
 - [103] F. Le Kien and K. Hakuta. Cooperative enhancement of channeling of emission from atoms into a nanofiber. *Adv. Nat. Sci.: Nanosci. Nanotechnol.*, 3:035001, 2012. URL <http://iopscience.iop.org/article/10.1088/2043-6262/3/3/035001/pdf>.
 - [104] F. Le Kien and K. Hakuta. Effect of the orientation of a weak magnetic field on the radiative decay of a cesium atom near a nanofiber. *Phys. Rev. A*, 78:063803, Dec 2008. doi: 10.1103/PhysRevA.78.063803. URL <http://link.aps.org/doi/10.1103/PhysRevA.78.063803>.
 - [105] N. R. Verhart, G. Lepert, A. L. Billing, J. Hwang, and E. A. Hinds. Single dipole evanescently coupled to a multimode waveguide. *Optics Express*, 22(16):19633, August 2014. ISSN 1094-4087. doi: 10.1364/OE.22.019633. URL <https://www.osapublishing.org/oe/abstract.cfm?uri=oe-22-16-19633>.
 - [106] E. M. Purcell. Spontaneous emission probabilities at radio frequencies. *Phys. Rev.*, 69:681, 1946. URL <http://journals.aps.org/pr/abstract/10.1103/PhysRev.69.674.2>.
 - [107] A. Taflove and S. C. Hagness. *Computational Electrodynamics: The Finite-Difference Time-Domain Method, Third Edition*. Artech House, 3 edition, 2005. ISBN 1580538320. URL <http://www.amazon.com/exec/obidos/redirect?tag=citeulike07-20&path=ASIN/1580538320>.
 - [108] L. Novotny and B. Hecht. *Principles of Nano-Optics*. Cambridge University Press, 2012. ISBN 978-1107005464.
 - [109] D. E. Chang, J. I. Cirac, and H. J. Kimble. Self-organization of atoms along a nanophotonic waveguide. *Phys. Rev. Lett.*, 110:113606, January 2013. URL <http://journals.aps.org/prl/abstract/10.1103/PhysRevLett.110.113606>.
 - [110] T. Caneva, M. T. Manzoni, T. Shi, J. S. Douglas, J. I. Cirac, and D. E. Chang. Quantum dynamics of propagating photons with strong interactions:

- a generalized inputoutput formalism. *New Journal of Physics*, 17(11):113001, 2015. URL <http://stacks.iop.org/1367-2630/17/i=11/a=113001>.
- [111] T. Grießer and H. Ritsch. Light-induced crystallization of cold atoms in a 1d optical trap. *Phys. Rev. Lett.*, 111:055702, Aug 2013. doi: 10.1103/PhysRevLett.111.055702. URL <http://link.aps.org/doi/10.1103/PhysRevLett.111.055702>.
 - [112] P. Domokos and H. Ritsch. Collective cooling and self-organization of atoms in a cavity. *Phys. Rev. Lett.*, 89:253003, Dec 2002. doi: 10.1103/PhysRevLett.89.253003. URL <http://link.aps.org/doi/10.1103/PhysRevLett.89.253003>.
 - [113] D. Holzmann, M. Sonnleitner, and H. Ritsch. Self-ordering and collective dynamics of transversely illuminated point-scatterers in a 1D trap. September 2014. URL <http://arxiv.org/abs/1409.5307>.
 - [114] Z. Eldredge, P. Solano, D. Chang, and A. V. Gorshkov. Self-organization of atoms coupled to a chiral reservoir. *Phys. Rev. A*, 94:053855, Nov 2016. doi: 10.1103/PhysRevA.94.053855. URL <http://link.aps.org/doi/10.1103/PhysRevA.94.053855>.
 - [115] H. Ritsch, P. Domokos, F. Brennecke, and T. Esslinger. Cold atoms in cavity-generated dynamical optical potentials. *Rev. Mod. Phys.*, 85:553–601, Apr 2013. doi: 10.1103/RevModPhys.85.553. URL <http://link.aps.org/doi/10.1103/RevModPhys.85.553>.
 - [116] J. P. Clemens, L. Horvath, B. C. Sanders, and H. J. Carmichael. Collective spontaneous emission from a line of atoms. *Phys. Rev. A*, 68:023809, Aug 2003. doi: 10.1103/PhysRevA.68.023809. URL <http://link.aps.org/doi/10.1103/PhysRevA.68.023809>.
 - [117] M. Gross and S. Haroche. Superradiance: An essay on the theory of collective spontaneous emission. *Physics Reports*, 93(5):301 – 396, 1982. ISSN 0370-1573. doi: [http://dx.doi.org/10.1016/0370-1573\(82\)90102-8](http://dx.doi.org/10.1016/0370-1573(82)90102-8). URL <http://www.sciencedirect.com/science/article/pii/0370157382901028>.
 - [118] A. Svidzinsky and J.-T. Chang. Cooperative spontaneous emission as a many-body eigenvalue problem. *Phys. Rev. A*, 77:043833, Apr 2008. doi: 10.1103/PhysRevA.77.043833. URL <http://link.aps.org/doi/10.1103/PhysRevA.77.043833>.
 - [119] R. G. DeVoe and R. G. Brewer. Observation of Superradiant and Subradiant Spontaneous Emission of Two Trapped Ions. *Physical Review Letters*, 76(12): 2049–2052, 1996. doi: 10.1103/PhysRevLett.76.2049. URL <http://link.aps.org/doi/10.1103/PhysRevLett.76.2049>.

- [120] W. Guerin, M. O. Araújo, and R. Kaiser. Subradiance in a large cloud of cold atoms. *Phys. Rev. Lett.*, 116:083601, Feb 2016. doi: 10.1103/PhysRevLett.116.083601. URL <http://link.aps.org/doi/10.1103/PhysRevLett.116.083601>.
- [121] D. Marcuse. *Principles of optical fiber measurement*. Academic Press, Boston, 1981.
- [122] A. W. Snyder and J. D. Love. *Optical Waveguide Theory*. Chapman and Hall, 1983.
- [123] A. Yariv. *Optical Electronics*. Oxford University Press, 1990.
- [124] D. Marcuse. *Theory of Dielectric Optical Waveguides (Second Edition)*. Academic Press, Boston, 1991.
- [125] G. Sagué. *Cold atom physics using ultra-thin optical fibres*. PhD thesis, University of Mainz, 2008.
- [126] E. Vetsch. *Optical Interface Based on a Nanofiber*. PhD thesis, University of Mainz, 2010.
- [127] J. E. Hoffman. *Optical nanofiber fabrication and analysis towards coupling atoms to superconducting qubits*. PhD thesis, University of Maryland College Park, 2014. URL <http://drum.lib.umd.edu/handle/1903/16078>.
- [128] M. Lax, W. H. Louisell, and W. B. McKnight. From maxwell to paraxial wave optics. *Phys. Rev. A*, 11:1365–1370, Apr 1975. doi: 10.1103/PhysRevA.11.1365. URL <http://link.aps.org/doi/10.1103/PhysRevA.11.1365>.
- [129] W. L. Erikson and S. Singh. Polarization properties of maxwell-gaussian laser beams. *Phys. Rev. E*, 49:5778–5786, Jun 1994. doi: 10.1103/PhysRevE.49.5778. URL <http://link.aps.org/doi/10.1103/PhysRevE.49.5778>.
- [130] J. A. Grover, P. Solano, L. A. Orozco, and S. L. Rolston. Photon-correlation measurements of atomic-cloud temperature using an optical nanofiber. *Phys. Rev. A*, 92:013850, Jul 2015. doi: 10.1103/PhysRevA.92.013850. URL <http://link.aps.org/doi/10.1103/PhysRevA.92.013850>.
- [131] F. K. Fatemi, J. E. Hoffman, P. Solano, E. F. Fenton, G. Beadie, S. L. Rolston, and L. A. Orozco. Modal interference in optical nanofibers for sub-angstrom radius sensitivity. *Optica*, 4(1):157–162, Jan 2017. doi: 10.1364/OPTICA.4.000157. URL <http://www.osapublishing.org/optica/abstract.cfm?URI=optica-4-1-157>.